ABSORPTION AND ORAL BIOAVAILABILITY OF NANOENCAPSULATED CURCUMIN

by

HAILONG YU

A dissertation submitted to the

Graduate School-New Brunswick

Rutgers, the State University of New Jersey

In partial fulfillment of the requirements

For the degree of

Doctor of Philosophy

Graduate Program in Food Science

Written under the direction of

Dr. Qingrong Huang

And approved by

_____

_____

_____

_____

New Brunswick, New Jersey

MAY, 2012

ABSTRACT OF THE DISSERTATION

ABSORPTION AND ORAL BIOAVAILABILITY OF NANOENCAPSULATED CURCUMIN

By **HAILONG YU**

Dissertation Director:

Dr. Qingrong Huang

Many natural bioactive compounds bear various health-promoting benefits and are incorporated in functional foods. The utilization of the compounds in human body, or the bioavailability is usually not taken into consideration in the process of food formulation. In this Ph.D. study, the problem of the poor bioavailability of polyphenols, such as curcumin, was addressed by development of two nanoscale delivery systems, namely biopolymer micelles and nanoemulsions.

It is known that solubilization and metabolism are two limiting factors for curcumin oral bioavailability. Using Caco-2 cell monolayers model, it was revealed that the permeation of solubilized curcumin was fast and by passive diffusion and that solubilization, not permeation of curcumin limited the absorption and the oral bioavailability. Subsequently, the solubilization of curcumin was improved by encapsulation of curcumin in biopolymer-based micelles and organogel-based

formulations. Polymer micelles were generated from modified starch and self-synthesized modified epsilon polylysine. Upon encapsulation, the water solubility of curcumin was greatly increased and curcumin was stabilized against alkaline degradation. Moreover, the *in vitro* anti-cancer and cellular antioxidant activities of curcumin were also enhanced.

On the other hand, food-grade curcumin organogel with high loading and *in vitro* bioaccessibility was developed. Based on the organogel, nanoemulsions were further generated to achieve faster and more complete digestion. The absorption mechanism of the nanoemulsion was examined using Caco-2 cell monolayer permeation assay and was suggested as the classic digestion-permeation route. It was further revealed that the oral bioavailability increased by 9-fold compared with unformulated curcumin on mice.

Moreover, the toxicity of nanoemulsions was examined *in vitro*. Three tested food-grade nanoemulsions did not show significant toxicity on Caco-2 cell monolayers, which suggested that nanoemulsions may not affect the integrity of the small intestine epithelium.

The biopolymer micelles and nanoemulsion formulations can be applied for oral delivery of other water-insoluble compounds for functional food application. And the formulation development method driven by absorption mechanisms also provides an example for future formulation studies.

ACKNOWLEDGEMNET

I am deeply indebted to my major advisor, Dr. Qingrong Huang for his guidance and support throughout the course of my studies at Food Science in Rutgers University. His support makes me explore the topics that truly interesting to me. Meanwhile, his experience and knowledge in chemistry, especially in physicochemistry broadens my research horizon. Dr. Huang is also very supportive and helpful with my career development and provides me many insightful suggestions on my career plans. With a busy schedule, Dr. Huang always prioritizes our meetings and manuscript revision. Without his effort, I cannot have such an attractive publication list, and finish my Ph.D. study within three years. Dr. Huang also helps greatly with my wife Ke and is very understanding after my twins Sophia and Sam were born. I feel very lucky to have Dr. Huang as my advisor of Ph.D. study.

I would like to thank Dr. Tung Ching Lee, Dr. Chi-Tang Ho and Dr. Mou-Tuan Huang for their willingness to be my committee members, and for their valuable suggestions and help with my research. I am very grateful for Dr. Lee and Dr. Ho for their time and effort on writing the recommendation letters for me for various scholarships. They also give me the precious opportunities for academic service, and suggestion on my career plans. Meanwhile, Dr. Huang provided me the strongest support with my mouse work and pharmacokinetics studies.

I am grateful for all my previous and current lab mates for their help and support to my work.

I also want to express my gratitude to Dr. Diana Martin, my teaching advisor for her support with my teaching and career development, and her care of Ke and my twins. I am also grateful for the teaching assistantship from Office of Undergraduate Instruction, Division of Life Sciences.

I am indebted to my wife Ke Shi, who provides greatest support with my decision of pursuing this Ph.D. and with every aspect of my life. I also would like to express my gratitude to my parents and parents-in-law for their love and support.

Specially, I am grateful to my twins Sophia and Samuel for all the joys they bring to me.

CONTENTS

LIST OF TABLES

LIST OF ILLUSTRATIONS

RATIONALE AND HYPOTHESIS

Curcumin is a bioactive compound in the spice turmeric. It processes many health-promoting benefits, such as anti-cancer, anti-inflammatory, anti-oxidation and anti-microbial activities. These health-promoting benefits of curcumin, however, are curtailed by its low oral bioavailability, which represents the rate and the extent to which orally consumed curcumin reaches systemic circulation.

Generally speaking, solubilization, absorption, and metabolisms are among the most important factors affecting the bioavailability. It has been already known that curcumin is water insoluble, and undergoes rapid metabolism in the body. The absorption rate of curcumin, on the other hand, still remains elusive.

Solubilization of water-insoluble compounds, such as curcumin, in small intestine lumen before absorption is accomplished by incorporation in micelles and mixed micelles formed by endogenous emulsifiers, such as bile salts and phospholipids, and exogenous emulsifiers (or precursors) provided in formulations. Metabolism occurs primarily in liver and may also occur in the small intestines. In the scope of food science, solubilization may be the primary target.

Based on the analysis of the limiting factors for the oral bioavailability of curcumin, it is hypothesized that **based on the mechanisms of solubilization and absorption, proper formulations are able to improve the solubilization and the oral bioavailability of curcumin**.

Lipids in emulsions, after orally consumed, are digested mainly by pancreatic lipase, in the small intestine lumen. Under the catalysis of lipase, one molecule of triglyceride turns into two molecules of free fatty acid and one molecule of 2-monoacylglycerol. All those digestion products are amphiphilic and able to provide ***extra*** components to form the mixed micelle system and thus maximize the solubilization of curcumin. Meanwhile, in the O/W emulsions, curcumin is readily dissolved and is in molecularly dispersed status. During digestion, it is expected that in a well-designed formulation, curcumin gradually partitions from the oil phase into the core of micelles, with no precipitation or re-dissolution. This is advantageous compared with other formulations, such as dispersion, which requires time and energy consuming dissolution.

Therefore, encapsulation of curcumin in nanoemulsion systems is expected to increase the solubilization of curcumin and thus to enhance its oral bioavailability.

CHAPTER 1. INTRODUCTION

Functional foods

Functional foods now are a trend in food industry and food science research. With the advance of molecular biology and chemical biology, many chemicals enriched in traditional foods are found to provide healthy benefit. With this knowledge, food industry incorporates these bioactive compounds (now usually called nutraceuticals or bioactives) into foods and called those products functional foods.

Definition

The term "functional foods" was initiated in 1980s in Japan. However, there is so far no official definition from United States Department of Agriculture (USDA) or US Food and Drugs Administration (FDA). Institute of Food Technologists (IFT) gave its own definition of functional food in one of its expert reports. It states that functional foods are "foods and food components that provide a health benefit beyond basic nutrition"(*2*). Other agencies in the world have similar definitions. Health Canada, for instance, defines functional foods as "similar in appearance to a conventional food, consumed as part of the usual diet, with demonstrated physiological benefits, and/or to reduce the risk of chronic disease beyond basic nutritional functions", while in the Report on Functional Foods from Food and Agriculture Organization of United Nations (FAO), functional foods are general considered as "those foods which are intended to be consumed as part of the normal diet and that contain biologically active components which offer the potential of enhanced health or reduced risk of disease"(*3*).

Comparing these definitions, it is not difficult to find out that the essential element of functional foods is the "health benefit BEYOND basic nutrition", with the traditional view of food to provide basic nutrition. Another noteworthy aspect is that according to these definitions, many natural produces, such as apple and orange, are included as functional foods, while food scientists and food industry usually focus more on processed foods with added-in bioactive compounds found in natural products.

Market value

In food industry, functional foods have been a trend for more than two decades. The current market value in United States is over six billions (2009, estimated). The forecasted market value in the year of 2014 will be greater than eight billion US dollars (*4*). As noted above, only processed foods with added in nutraceuticals were counted.

Nutraceuticals

Similar to the regulation status of functional foods, nutraceuticals so far has no official definition, although it is widely used in academic field and as well as in food industry. Generally speaking, nutraceuticals refer to bioactive compounds found in natural products, esp. in phytochemicals. Basic vitamins and minerals might be excluded from nutraceuticals, as those are thought to provide basic nutrition.

Actually, before the development of modern pharmaceutics industry, herbs have been used in ancient civilizations for thousands of years, when there is no strict and clear boundary between food and drug. (The boundary nowadays is actually set by the governmental regulations). However, at that time, the herbs were used as a whole or at

best as extracts. No single compound was identified to be responsible for the bioactive activities.

With the development of modern biology and chemistry, esp. molecular biology and chemical biology, the bioactive compounds are isolated from natural products and their interaction with human body are discovered. Many bioactive compounds are able to function as cell signaling molecules to regulate gene expression and thus may have health benefit, such as anti-cancer and anti-inflammatory activity (*5*).

In the food science field and also food industry, the anti-oxidant properties of nutraceuticals are usually publicized most. However, it is more reasonable to consider many, if not all, nutraceuticals as signaling molecules, given the fact that the bioavailability of many nutraceuticals is far lower than the effective anti-oxidant concentration (*6*). Moreover, xenophormesis theory further proposes that nutraceuticals, especially polyphenols, are synthesized in autotrophs in response to various stresses, and, when heterotrophs, such as human and other mammals, eat these polyphenols, they are able to sense the clue of stress through molecular signaling and may adapt accordingly (*7*).

Bioavailability

Definition

Bioavailability (F) represents "The relative amount of an administered dose that reaches the general circulation and the rate at which this occurs" (American Pharmaceutical Association,1972) (*8*). In food science, nutraceuticals are exclusively consumed orally along with food, so the oral bioavailability is what is focused on

throughout this dissertation. The amount of bioactive compounds that enter into systemic circulation over time after administration can be measured from pharmacokinetics studies, which generates the concentration in plasma over time curve. From the curve, the Area-under-the-curve (AUC) can be obtained, and the bioavailability of different formulations can be compared.

The **absolute bioavailability** is define as the ratio of AUC from oral administration to the AUC from intravenous (i.v.) injection (*9*). By definition, the bioavailability of i.v. administrated dose equals to 1 (100%). Meanwhile, the relative (or called comparative) bioavailability measures the differences between two dosage forms (such as tablet and suspension) (*8*).

$$Bioavailability\ (F) = \frac{AUC\ (oral\ dose)\ /\ Mass\ (oral\ dose)}{AUC\ (i.v.dose)\ /Mass\ (i.v.\ dose)} \times 100\ \%$$

There are majorly two classes of factors that influence the bioavailability: (1) formulation factors, such as the existence of excipients, particle size, crystalline or amorphose states, and (2) physiology factors, such as gastric emptying, pH in the lumen of small intestine and changes of the intestine walls.

Three steps to be bioavailable

For nutraceuticals consumed with food, they need to accomplish three tasks to enter systemic circulation to be bioavailable: There are generally three steps for nutraceuticals to enter systemic circulation. **(A). Solubilization**. Nutraceuticals in food become solubilized in the small intestine lumen. **(B) Absorption**. Nutraceuticals are absorbed by the small intestine through different routes across the small intestine epithelium. **(C)**

Transport to systemic circulation. Absorbed nutraceuticals either enter intestinal lymph and then directly systemic circulation or pass through liver via portal vein, and then enter the systemic circulation.

Solubilization. Nutraceuticals can be water-soluble or water-insoluble by its nature. For water-soluble nutraceuticals, they are readily solubilized in the aqueous solution in the small intestine lumen. For water-insoluble nutraceuticals, they have to get help from amphiphilc compounds (emulsifiers or surfactants) in the lumen fluid. These compounds include bile salts and phospholipids and may all include exogenous emulsifiers from the food. In the lumen, these amphiphiles form micelles or mixed micelles, and these micelles have lipophilic core and may solubilize water-insoluble compounds inside.

Lipids in the food are also able to contribute to the micelle formation after digestion by lipase. Triglycerides turn to free fatty acids, monoglycerides and diglycerides. Phospholipids turn to free fatty acids and lysophospholipids. All these lipase-digestion products are amphiphiles and contribute to mixed micelles and solubilize water-insoluble nutraceuticals.

Absorption. Major organs that consist of the digestive tract are mouth, pharynx, esophagus, stomach, small intestine (duodenum, jejunum, ileum) and large intestine (including colon) (*10*). Major site of nutrients and nutraceuticals absorption is the small intestine, specifically through the enterocytes (absorption epithelial cells) lining the lumen of the jejunum. Solubilized nutraceuticals, by definition, are molecularly dispersed in the aqueous solution in the small intestine lumen. They are able to pass the epithelial layers by different mechanisms. *A. Diffusion*. Diffusion is driven by thermal movement

and a concentration difference is required across the epithelium layer. (1) *diffusion*: Water soluble compounds tends to diffuse paracellularly. Although there are tight junctions and the inter-epithelial gaps are only a few angstroms wide, water soluble compounds are still able to diffuse through the inter-epithelial gaps (tight junction) between adjacent cells. (2) *Transcellular diffusion*: lipophilic compounds, molecularly dispersed in micelles and mixed micelles, tend to diffuse through the phospholipid membrane and cytosol of epithelial cells. In another scenario, mediated transport occurs: molecules are carried by specific protein and cross the epitheliums. This process could require no metabolic energy but require a positive concentration gradient (*facilitated transport*), or require the input of energy (*active transport*).

Specifically for some nutraceuticals, they are *effluxed* out of epithelial layers and back to the intestinal lumen, by proteins on the cell membranes, such as P-glycoproteins.

Transport to systemic circulation. There are two routes for absorbed compounds to enter systemic circulations. For most polar and water-soluble compounds, they diffuse into blood vessels and are carried into liver through hepatic portal vein. In the liver, they may undergo possible metabolism. For highly lipophilic compounds, they may be incorporated into chylomicrons, which are too big to enter blood vessels but follow lymphatic transport to systemic circulation directly (*11*).

Metabolism refers to biochemical modification or degradation. It usually involves conjugation, reduction, and oxidation and so on. Throughout the journey of nutraceuticals from digestion to entry into the systemic circulation, there are two major sites where

nutraceuticals possibly undergo metabolism: the epithelial walls along the digestive tract (intestinal metabolism), and the liver (hepatic metabolism).

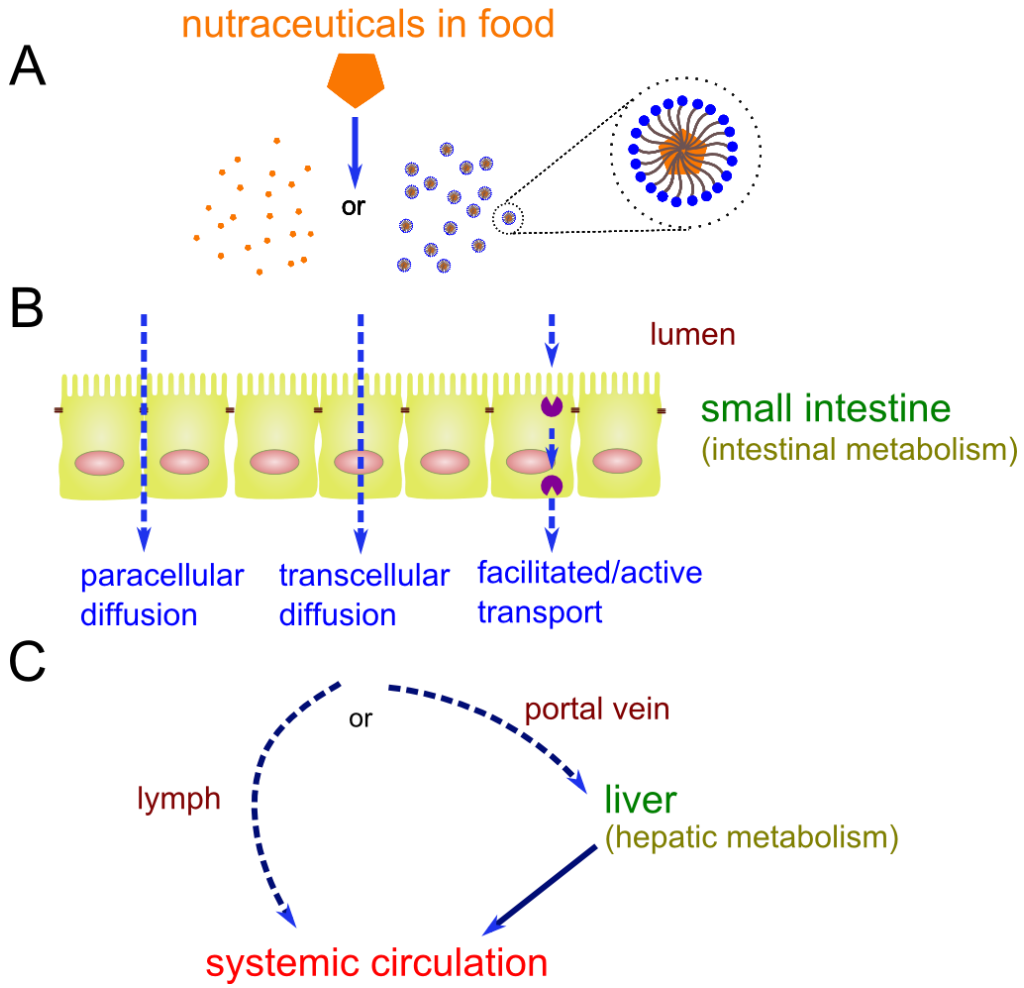

Figure 1. Schematic view of the process in which nutraceuticals become oral bioavailable. There are generally three steps for nutraceuticals to enter systemic circulation. (A) Solubilization. Nutraceuticals in food become solubilized in the small intestine lumen. (B) Absorption. Nutraceuticals are absorbed by the small intestine through different routes across the small intestine epithelium. (C) Transport to systemic circulation. Absorbed nutraceuticals either enter intestinal lymph and then directly systemic circulation or pass through liver via portal vein, and then enter systemic circulation. Metabolism could occur at small intestine epithelium (intestinal metabolism) and/or at liver (hepatic metabolism).

Methods/Formulations to improve the bioavailability

To improve the bioavailability of nutraceuticals, there are generally three aspects to be focused on: 1. increase of dissolution rate, 2. Enhancement of absorption, and 3. avoidance or minimizing metabolism.

Increase of dissolution rate

Formulation scientists focus most of their efforts on methods and formulations to improve the dissolution rate of nutraceuticals. In the simplest dissolution process, nutraceuticals, mostly in the crystalline form, are initially in the lowest thermodynamic status and thus may need high energy input to be dissolved in aqueous solution. Generally, various formulations pre-disrupt the crystalline lattice of nutraceuticals, and thus cause more rapid dissolution rate. Meanwhile, it is important to note that the dissolution occurs in bio-relevant aqueous solutions, with specific ionic strength and pH and containing certain amount of emulsifiers, such as phospholipids and bile salts.

In the field of food science, there are basically kinds of formulations used to increase dissolution rate: 1. Emulsions, 2. Micelles, 3. Complex with cyclodextrin and proteins, and 4. Suspensions and dispersions. In emulsion system, lipophilic compounds are already dissolved in oil phase. After lipase digestion, nutraceuticals are partitioned in the core of micelles. In micelles and complexes, nutraceuticals are readily dissolved (molecularly dispersed). Compared with untreated nutraceuticals in large crystalline lattice, suspension and dispersions, either as crystals or amorphous, have much larger surface areas and may be dissolved more rapidly.

Enhancement of absorption

In pharmaceutical science, absorption enhancer function to increase the gaps between adjacent epitheliums, interact with mucus layers or inhibit the activities of efflux transporters. These findings should be carefully evaluated before applying to food science, since some of these absorption enhancers are not Generally-Regarded-As-Safe (GRAS) grade, may have some adverse effects associated with the absorption enhancement function.

Avoidance or minimizing metabolism

So far, formulations may not manipulate too much about metabolism, but only a few methods are known to inhibit or avoid metabolism: lipophilic compounds, when treated along with long-chain triglycerides, may bypass the hepatic metabolism (see above and Figure 1.C.). Some compounds, such as piperine in peppers, are able to inhibit enzymes responsible for intestinal and hepatic glucuronidation (*12-14*).

Caco-2 cell monolayers as an *in vitro* tool to predict intestinal absorption.

Caco-2 cell line (ATCC number: HTB-37) is from human colorectal adenocarcinoma. After three weeks of confluent culture on porous inserts of cell culture plates, Caco-2 monolayer spontaneously differentiate and reveal many phenotypes of small intestine enterocytes: tight junctions between adjacent cells, microvilli on the apical surface, expression of multiple drug transport proteins and metabolic enzymes (Figure 2). It has been already well established that Caco-2 cell monolayers are a very good model to predict bioactives' permeation and absorptions. Different studies demonstrate that *in vivo*

absorption is well predicted from the apparent permeation rate (P_{app}) across Caco-2 cell monolayers (*15*-*17*). Although the P_{app} obtained from different labs are different, there is a general trend that high P_{app} implies high absorption. General speaking, $P_{app} > 1 \times 10^{-6}$ cm/s means high permeation while $P_{app} < 1 \times 10^{-7}$ cm/s implies low permeation(*15*, *18*).

At the same time, the absorption mechanisms can also be examined. By performing two-way (apical to basolateral and basolateral to apical) permeation experiments and calculating the rate ratio, the existence of potential active efflux/uptake can be identified. In general, if P_{app}(B-A)/P_{app}(A-B) is greater than 2 or less than 0.5, the active uptake or efflux mechanisms are suggested respectively. Otherwise, the absorption mechanism may simply be passive diffusion (*16*).

Figure 2. Scheme of differentiation of Caco-2 monolayers after three weeks of confluent culture. Microvilli and tight junction are shown.

Curcumin

Curcumin is the major curcuminoid compound found in the rhizome of plant turmeric (*Curcuma longa*). It is estimated that it consists of 2 – 5 % of the rhizome. Also in the turmeric are demethoxycurcumin, bisdemethoxycurcumin (Figure 3). The commercial grade curcumin usually contains 70-90% curcumin, 10-15% demethoxycurcumin and less than 5% of bisdemethoxycurcumin (Figure 2), and maybe trace amount of curcumin glucuronide and curcumin sulfate (Figure 4, (*19*)).

In everyday food consumption, turmeric, instead of the extracted curcumin, is the major form. There are basically two usage of turmeric in food: spice and colorant. Tumeric has been used as a spice for thousands of years. It is an important ingredient of curry powder. Meanwhile, because of its brightly yellow color, it is also a food colorant. In US, turmeric belongs to colorants exempt from certification, with E number E100 (*20*).

Health benefit of curcumin has been noticed and used for a long time in East and South Asia. It is used as antiseptic agent to paste on wounds and as anti-inflammatory agent to cure throat sour. The mechanisms underlining these health-promoting properties of curcumin were not discovered until the era of molecular biology.

Molecular Mechanisms of curcumin's bioactivity

Generally speaking, there are four major properties of curcumin which entitle curcumin as a nutraceuticals: anti-oxidation, anti-cancer, anti-inflammatory and anti-microbial activities (*21-24*). The anti-oxidation property of curcumin derives from its two phenol group and the conjugated double bond. Anti-cancer and anti-inflammatory properties of curcumin are demonstrated by its functioning as a ligand in many signaling

transduction pathways. Every year, there are new downstream genes are found to be regulated by curcumin. A few key players are listed here: COX gene family, Ahr, IL1β and PKD are responsible for curcumin's anti-inflammatory property (*7*). Inhibition of NF-κB and AP-1 signaling pathways may be the major mechanisms for curcumin's anticancer activity (*21*). In addition, curcumin is also reported to inhibit Gram-positive and Gram-negative bacterial growth (*25-32*). The mechanisms include inhibition of cytokinesis and phototoxicity (*25, 31*).

Animal models demonstrating cucumin's health benefit

Many animal studies also suggests health benefits (e.g. anti-cancer effect) of curcumin (*33*). Topically administrated curcumin inhibits TPA-induced mouse ear inflammation (*34*) and epidermis inflammation (*35, 36*). More importantly, dietary curcumin showed inhibitory effect on chemical-induced and genetically engineered carcinogenesis in animal model (*21*). For instance, dietary curcumin inhibit carcinogenesis in digestive tract (*37-40*), in liver (*41, 42*), maybe in lung (with controversy) (*43, 44*). It also suppresses metastasis of breast cancer (*45*), leukemia and ovary cancer (*46*). Injected and dietary curcumin alleviates the pathology of Alzheimer transgenic mouse (*47, 48*).

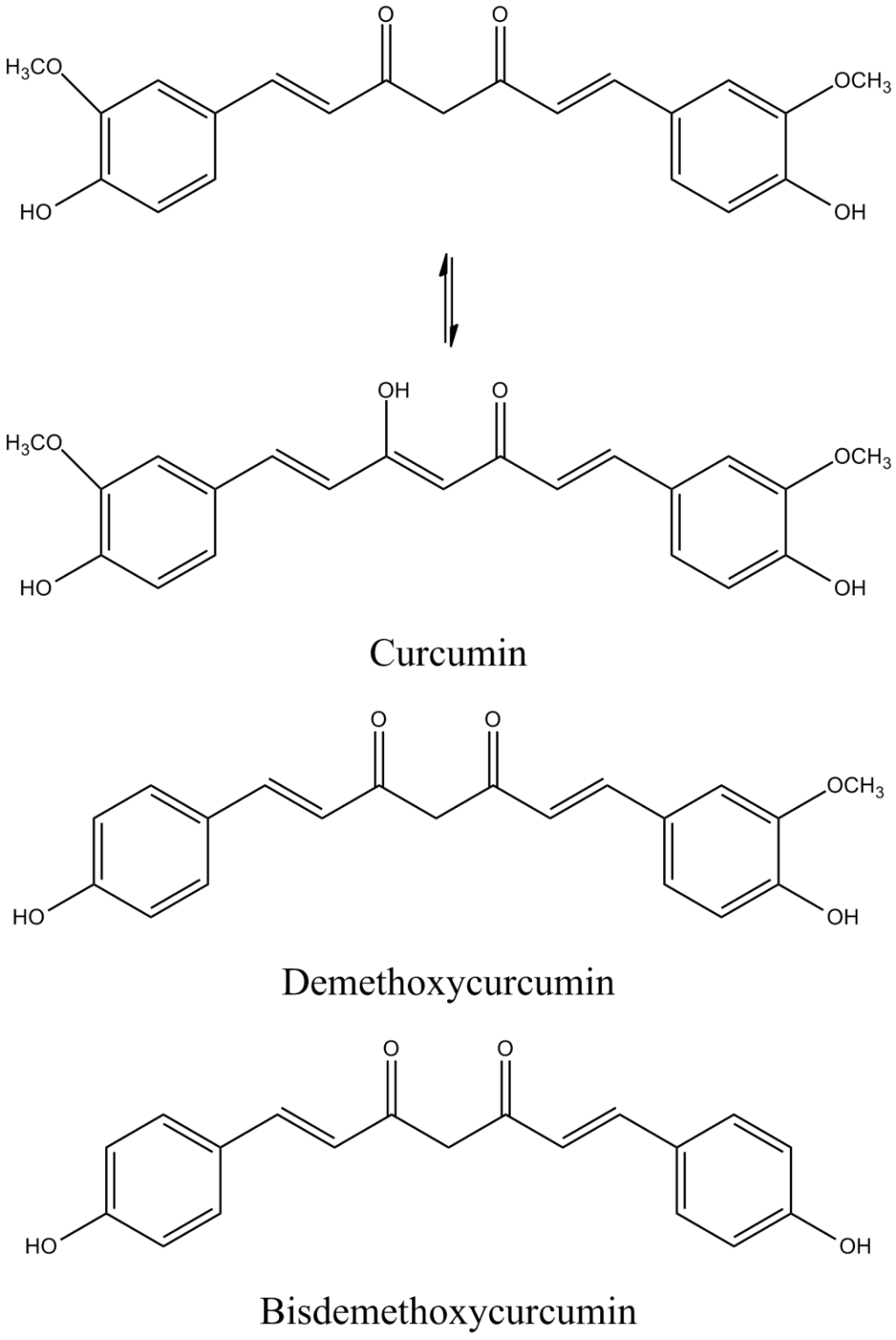

Figure 3. Chemical structures of curcumin in equilibrium of keto- and enol-forms, demethoxycurcumin and bisdemethoxycurcumin, in keto form.

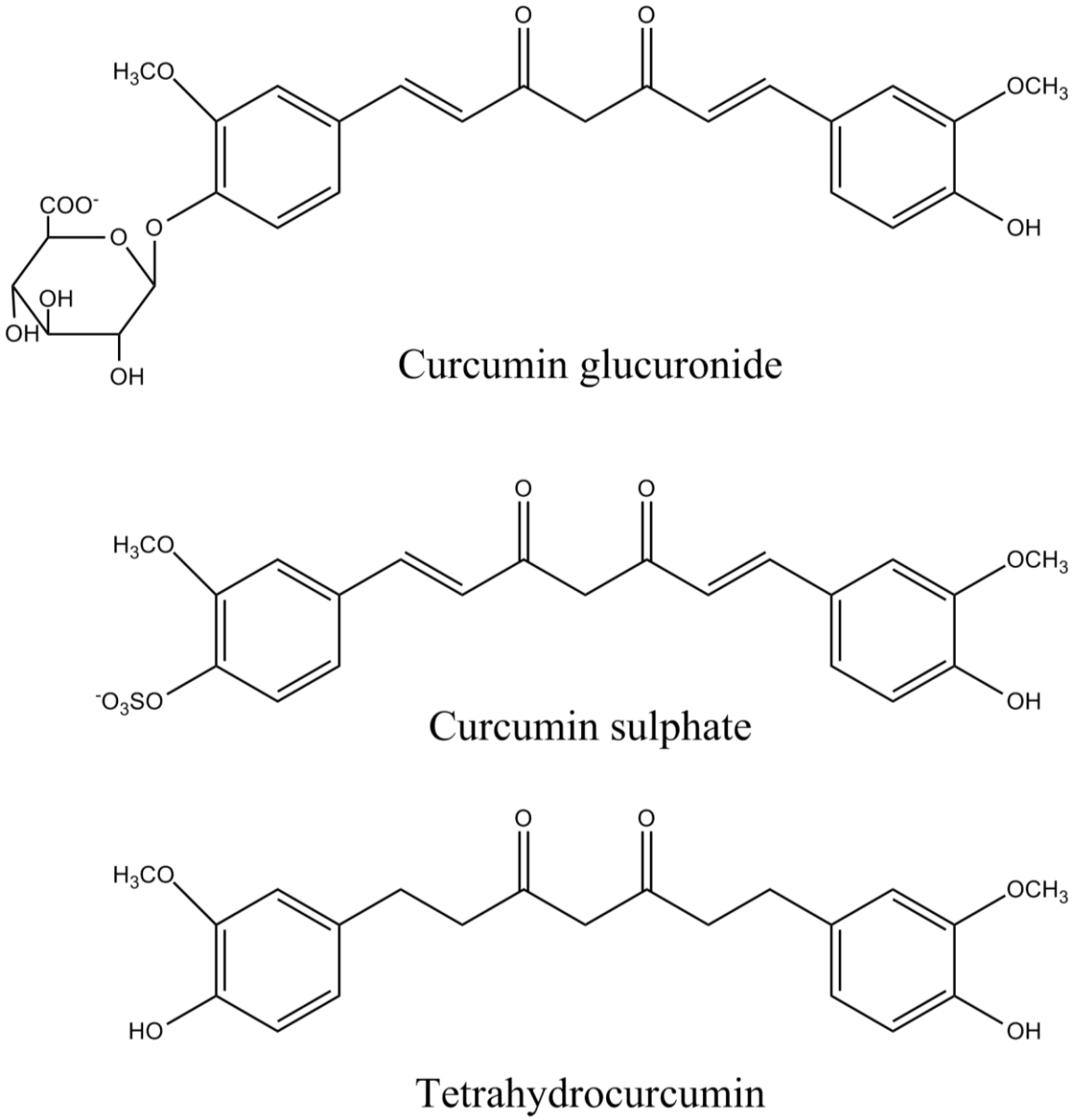

Figure 4. Three major metabolites of curcumin, curcumin glucuronide, curcumin sulphate and tetrahydrocurcumin.

Clinical studies

Multiple clinical studies demonstrate that curcumin shows no toxicity at several grams per day for months (*49, 50*). Oral treatment of curcumin has shown to improve biomarkers' expression in digestive tract, especially in colon (*50-52*). Curcumin also showed comparable effect with corticosteroid therapy to treat chronic anterior uveitis, with no apparent side effect. In a phase I trial of pancreatic cancer, safety of curcumin was confirmed and some patients showed improved biomarker expression (*53*). Additionally, studies also suggest that a large sample size, higher dose studies are needed to make solid conclusions (*54, 55*).

In the clinicaltrial.gov website, there are 44 records about curcumin, demonstrating very active clinical studies of curcumin (*56*).

Bioavailability

Curcumin is well-known as a nutraceuticals with low bioavailability (*57*). Numerous studies focus on the pharmacokinetics of curcumin in experiment animals and human. The highest serum concentrations reported are listed here: in human, 51ng/ml from 12 g curcumin (*58*); and in rat, 1.35 ± 0.23 μg/mL from 2g/kg curcumin (*59*); in mouse, 0.22 μg/mL from 1g/kg curcumin(*60*).

Absorbed curcumin undergoes rapid metabolism. The major metabolites of oral treatment are curcumin sulfate and curcumin glucuronide (Figure 2), probably generated by phase-II enzymes in the liver and intestines, while the major metabolite of i.p. injection is tetrahydrocurcumin, which also undergoes conjugation to form glucuronide and sulfate (*60, 61*).

Curcumin is water insoluble. It was estimated that the water solubility of curcumin was at most 11ng/mL (*62*). Most of unformulated curcumin treated orally is usually found in facet. This may be largely due to the insolubility of curcumin in water and slow dissolution of curcumin in lumen fluid. It is also likely that absorbed curcumin (or its metabolites) is excreted from the bile, which has not been investigated yet. Meanwhile, the solubility and rate of dissolution of curcumin in lumen fluid or bio-relevant solution also remains elusive.

It is surprisingly to find out that there is no study focusing on the permeation rate of curcumin through any cell monolayers, such as Caco-2, in order to illuminate the absorption rate and mechanism. An *in vitro* everted rat intestinal sac assay showed that after 3 hours, 48% of curcumin was absorbed in the sac tissue. Moreover, when curcumin at the same concentration was firstly dissolved in micellar solutions, the absorption fraction increased to 56%, suggesting that dissolution/solubilization is one of the limiting factors affecting absorption (*63*).

To sum up the problem of curcumin's low bioavailability: solubilization, absorption, and metabolism are among the key factors influencing nutraceuticals' bioavailability; curcumin is insoluble in water; it is metabolized rapidly in small intestine and liver; the permeation rate across small intestine epithelium is unknown.

Formulations

Considering the potential health benefit of curcumin and its low bioavailability, devising effective formulation may be one of the important approaches to achieve better

bioavailability and thus health promoting benefit. Specifically for curcumin, there are roughly 8 types of formulations.

Polymer and surfactant micelles. Micelles are formed from amphiphilic compounds above their critical micelle (aggregation) concentration. The shell of micelles is hydrophilic while the core is hydrophobic which is able to encapsulate lipophilic nutraceuticals. In the literature, curcumin has been encapsulated in the micelles formed from low-molecular-weight surfactant (*64-68*) and amphiphilic synthetic polymers (*69-71*). Upon encapsulation, alkaline hydrolysis is suppressed (*64, 67*) and curcumin's release from the polymeric micelles is in a controlled fashion (*70*). Strictly speaking, curcumin in micelles is in the molecular dispersed form (solubilized) and the whole structure is thermodynamic stable.

Dispersion. Since it is not water soluble, when curcumin dissolved in water-miscible organic solvent is added in water, curcumin will form dispersion or precipitation, either in crystalline or amorphous form (*72, 73*). With surfactants added in the water, this curcumin dispersion can be in micrometer or nanometer size(*73-75*). Curcumin dispersion has much larger surface than unformulated curcumin powder (crystal usually in micron or sub-milliliter size). Larger surface increases curcumin's dissolution, explained by Ostwald-Freundlich equation:

$$ln\ (C_S/C_{S0}) = \frac{2Mw\ \times\ \Upsilon}{\rho\ \times\ R\ \times\ T} \times \frac{1}{r}$$

where C_S is the solubility of the nutraceuticals compound of a given particle size,C_{S0} is the solubility of the nutraceuticals with a flat interface with water, Mw is the molecular weight of the nutraceuticals, γ is the interfacial tension between the nutraceutical and water, ρ is the density of the compound, R is the Universal Gas Constant, T is the absolute temperature of the system, and r is the radius of the droplet/particle.

With smaller particle size (r), the solubility (Cs) increased exponentially.

Emulsion. Emulsion is a common formulation in food science and food industry. Specifically for curcumin, the solubility of curcumin in different triglyceride ranges from a few to tens of mg/mL (*76*), much higher than that in water. Therefore curcumin is well suited in a variety of emulsion systems, including regular O/W emulsion (*77, 78*), self-microemulsifying system (*4*), microemulsion (*76, 79*), solid lipid particle (*56, 80-82*). Study also shows upon encapsulation in emulsions, curcumin has improved oral bioavailability or *in vivo* bioactivity (*4, 77*) .

Molecular complex. Proteins in general have hydrophilic surface and hydrophobic core. Thus a variety of proteins, such as albumin (*83-88*), collagen (*89*), casein (*87, 90*), and fibrinogen (*88*) were used to form molecular complex with curcumin. Using fluorescence method, the binding constant of curcumin and proteins are usually in the scale of 10^{-4}M. After binding, the protein conformation changes. Similarly, cyclodextrins are able to trap curcumin inside (*91-96*). It is also found that lecithin (contained various amount of phospholipids) is also be able to form complex with curcumin and the complex can enhance curcumin's oral bioavailability (*83, 97-99*).

Liposome. Above a certain concentration, phospholipid is able to form liposomes, a lipid bi-layer structure, as the cell membrane. Curcumin is able to locate in the membrane (*83, 100-104*). It is noteworthy that the composition of liposome affects the loading capacity of liposome (*103, 104*). Liposome with higher percentage of phosphatidylcholine (PC) is able to encapsulate more curcumin (*103*).

Nano- or Micro- particles. Micro-sized or nano-sized particles with entrapped curcumin are generated by adding curcumin and water-insoluble polymers dissolved in water-miscible co-solvent into water (with or without surfactant). In this process, polymer condenses and aggregates during which some of the curcumin is trapped inside the polymer (*105-112*). A commonly used polymer is poly(lactic-co-glycolic acid) or PLGA (*66, 105, 107, 108, 112*), which is biodegradable and biocompatible and is approved by US FDA for therapeutic usage (not food usage). In addition to the dripping method, electrospinning, for instance is also able to generate nanofibers, from poly(epsilon-caprolactone) and cellulose acetate, with curcumin encapsulated (*100, 113*).

Conjugation. Strictly speaking, conjugation is not a real method of formulation, since it changes nutraceuticals' chemical identity, through chemical/biochemical reactions. After conjugation, the solubility of curcumin changes greatly and may still possess many of the original bioactivities (*62, 76, 114-116*). From a pharmaceutical viewpoint, these conjugates may be prodrugs, while it may not be accepted in food science before careful toxicity evaluation.

With the aid of adjuvants. It is found that certain phytochemicals are able to affect the activity / expression of proteins responsible for metabolism or xenobiotics cellular

transport (*14*, *117, 118*). Piperine, for example, is a compound found in black peppers and long peppers, and is able to inhibit the activity of a variety of metabolizing enzymes (*12*). It has already been found that adding piperine in curcumin formulation is able to increase curcumin's bioavailability (*59, 112*).

Table 1. Representative studies of curcumin formulations with increased oral bioavailability (or in vivo bioactivity or absorption after oral treatment). N.D. not determined.

	Formulation	Maximum Loading	Bioavailability	ref.
Molecular Complex	Patented Mariva, Containing lecithin (30% PC)	~ 18%	5 folds increase in curcumin, 24 fold in curcumin glucuronide	(*99*)
Molecular Complex	Curcumin and phospholipids Co-dissolved and dried	~32%	~ 5 folds increase	(*98*)
SMEDDS	57.5% surfactant 30.0% co-surfactant and 12.5% oil	2.1%	3.86 folds increase in absorption	(*4*)
Solid lipid nanoparticle	Tween-80 stabilized Glyceryl behenate	N.D.	39 fold at 50mg/Kg dose in rat	(*119*)
Liposome	Homogenized curcumin in water + 5% lecithin in water	~1.7%	more than 5 folds	(*103*)
Nanoparticle	PLGA and curcumin co-dispersion	~11.6%	Oral , 9 folds in rat	(*112*)
Nanoparticle	PLGA solvent co-dispersion	Estimated ~ 8%	Oral 21 folds in rat	(*120*)
Dispersion	HPC-ML, SDS, wet-milling	N.D.	16 folds in rat	(*73*)
Dispersion	HPMC-AS co-solvent, freeze drying	N.D.	12 folds in rat	(*73*)
Dispersion (emulsion)	PEG, propyleneglycol, ethanol, dispersion	N.D.	9 folds in rat	(*73*)

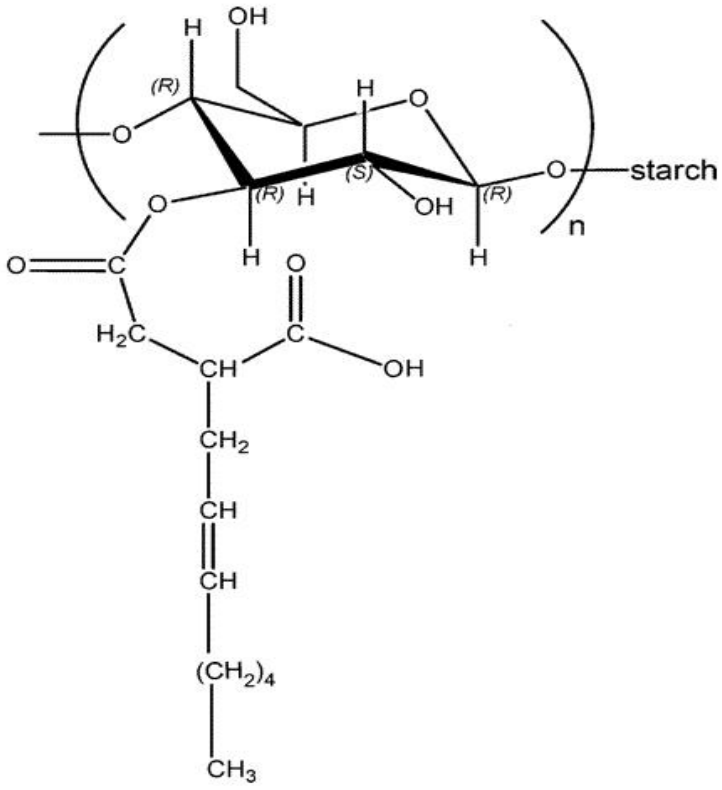

Figure 5 Chemical structure of hydrophobically modified starch

Hydrophobically modified starch

Hydrophobically modified starch (HMS), which was synthesized with waxy maize and n-octenyl succinic anhydride (n-OSA) (*121*). HMS is widely used as wall material to encapsulate flavors in spray drying process (*121-125*).

Epsilon polylysine

ε-Polylysine (EPL) is a homo-polymer of L-lysine through isopeptide bond between ε-amino and α-carboxyl groups (Figure 6). In contrast with poly-L-lysine, which is synthesized by chemists, EPL is generated by bacterium *Streptomyces albulus* (*126, 127*). The biogenic EPL usually has 25-35 lysine monomers. The polydispersity is dependent on specific bacteria strains and culture conditions (*128*).

Because of its primary amine groups, EPL is cationic in neutral aqueous solutions. Like chitosan, another cationic biopolymer, EPL also has antimicrobial activities. It has been shown that EPL is able to be absorbed onto bacterial surface, causing stripping of the outer membrane, abnormal distribution of the cytoplasm, and finally death of the bacteria (*129*).

The antimicrobial spectrum of EPL is wide. EPL is able to inhibit the growth of both gram positive (such *as Listeria monocyogenes*) and gram negative bacteria (such as *Escherichia coli*). The minimum inhibitory concentrations of EPL against common food pathogens are in the range of 5-100 μg/mL (*129, 130*). Based on absorption, distribution, metabolism, excretion and toxicity (ADMET) studies, EPL is proved to be safe for consumption (*131, 132*). It has been approved as a natural food preservative used in rice and in traditional Japanese food in Japan and USA (GRAS No. 000135) (*133*).

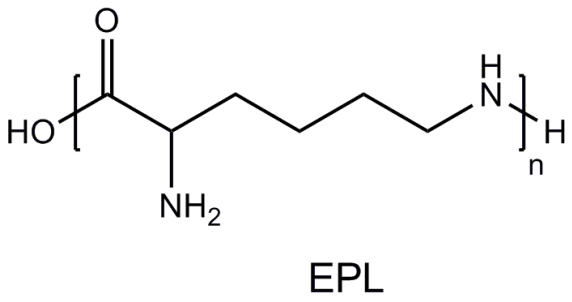

EPL

Figure 6. Chemical structure of epsilon polylysine.

EPL could also be used as a dietary agent. It has been shown that EPL is able to inhibit the enzymatic activity of pancreatic lipase *in vitro* (*134*) and that oral consumption of EPL lowered the triglyceride level in rats' blood plasma, which further suggested that EPL could function to suppress dietary fat intake (*134*).

Chemical modification is an effective way to impart novel properties and functions to existing materials. EPL has been modified chemically in previous studies. Shima *et al.* found that conjugation of derivatives of benzoic acids to EPL caused significant decrease in its antimicrobial activity (*129*). EPL was also modified by conjugating with glucose and dextran through Maillard reaction (*135, 136*). It was found that the antimicrobial activity of EPL was almost retained. Furthermore, the dextran-EPL conjugate was able to stabilize emulsions. The emulsifying capacity of synthesized conjugates was not affected by high ionic strength but was sensitive to extreme acidic condition (*136*). The modified EPL was hydrophilic but not amphiphilic, and the mechanism of stabilizing emulsions was thought to be the increase of viscosity caused by the high-molecular-weight dextran-EPL conjugate.

In vitro digestion to evaluate solubilization of compounds formulated in lipid-based formulations

Overview

In vitro lipid digestion (lipolysis) is an *in vitro* assay to predict the *in vivo* solubilization of lipophilic compounds in the lipid-based formulations during digestion (*137-140*). Catalyzed by lipase, triglyceride is hydrolyzed into 2-monoglycerides and fatty acids. These lipolysis products, as well as the phospholipids and bile salts in the

digestion media form micelles and mixed micelles, both of which solubilize the lipophilic compounds and make them possible to be absorbed (*139*).

For compounds whose bioavailability is limited by solubilization, but not absorption, lipid digestion method has been demonstrated to be able to evaluate different lipid based emulsions and have a good *in vitro-in vivo* correlation (IVIVC) (*141, 142*). Lipid digestion was also used to evaluate the bioaccessibility of tocopherol from sunflower seed oil bodies (*143*).

Effects of components in the formulation.

Due to the physicochemical difference of the compounds of interest, the optimal lipid-based formulations need to be examined experimentally (*144*). Either long-chain triglyceride or middle-chain triglyceride may provide the maximum solubilization capacity after digestion for a specific compound.

Effect of different emulsifiers on the digestion rate was investigated. B-lactoglobulin and lysophosphotidylcholine were shown to accelerate the lipid hydrolysis in a model gastro-intestinal system, while 2-monopalmitin decreased the rate (*145*). Additives in emulsion systems also affect the lipolysis rate. Dietary fibers and tea extract slowed down the lipid digestion (*146-148*). Chitosan on the surface of emulsion inhibited the lipase activity because of the cationic charge of chitosan and flocculation of emulsions, while another coating of pectin restored the lipase activity, maybe due to the neutralization of the positive charge (*149*).

Experimentation procedure

Lipid-based formulations, such as O/W emulsions, are added to the digestion medium (pH 7.4-7.5), at 37^{o}C and stirred for a certain period of time. Subsequently, pancreatin, containing protease, amylase and most importantly lipase, is added in to initiate the digestion. To ensure total dissolution of fatty acids, pH is maintained at 7.4-7.5, by adding NaOH. After 30 minutes, digestion medium is ultracentrifuged, so that compounds solubilized in micelles are in the middle aqueous phase, undigested lipids are on the top layer, and fatty acid calcium salts and undissolved compounds are precipitated in the pellets (Figure 8).

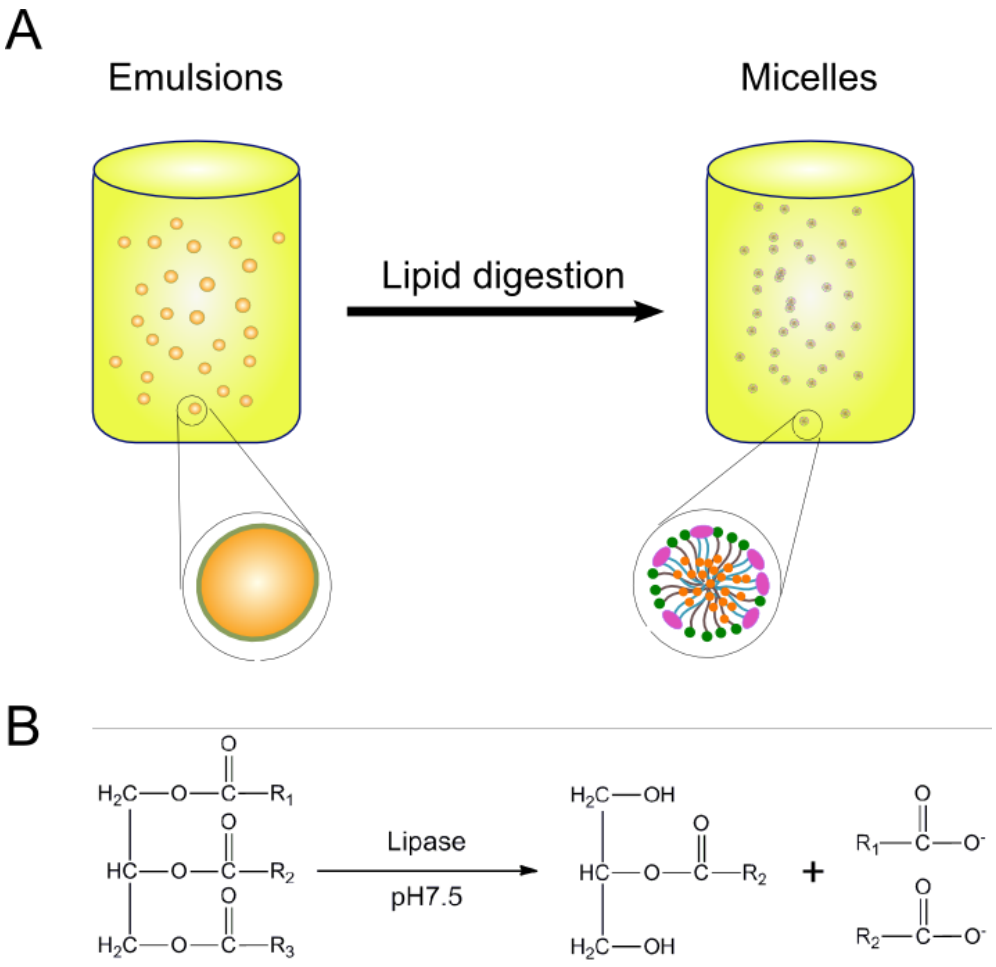

Figure 7. Scheme of *in vitro* lipid digestion. (A) Lipophilic compounds are dissolved in the O/W emulsion. After lipase digestion, the compounds partition in the core of (mixed) micelles. (B) Under the catalysis of lipase, triglyceride is hydrolyzed into 2-monoglyceride and 2 fatty acids. At pH7.5, fatty acids ionize as salts.

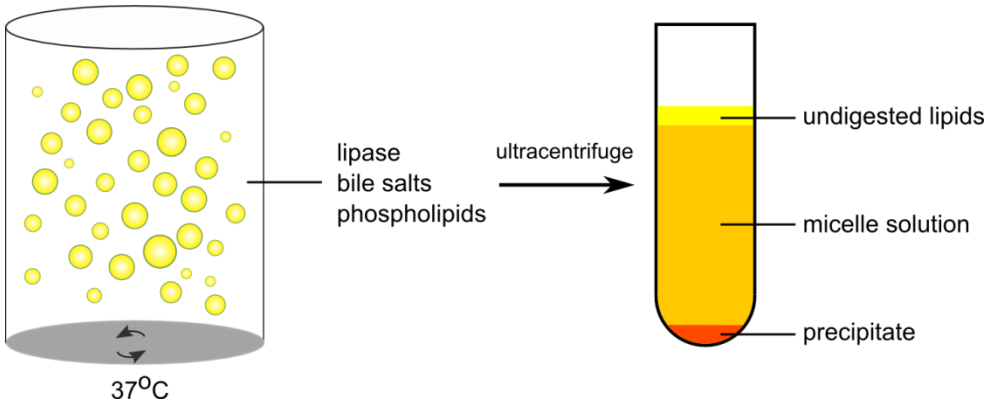

Figure 8 Scheme of the three layers after ultracentrifuge of digested formulation.

CHAPTER 2. ENCAPSULATION OF CURCUMIN IN MICELLES FORMED BY MODIFIED STARCH

In searching food-grade amphiphilic materials to encapsulate curcumin, I focused on hydrophobically modified starch (HMS), an abundant and low cost food ingredient synthesized with waxy maize and n-octenyl succinic anhydride (n-OSA) (*121*). My finding was that, following the polymeric micellar encapsulation strategy, HMS is also able to form polymer micelles and to encapsulate curcumin. In this study, I demonstrated that HMS micelles greatly increased the water solubility of curcumin. Moreover, curcumin encapsulated in HMS micellar cores exhibited increased anti-cancer activity in vitro.

Materials and Methods

Materials. Curcumin was a generous gift from Sabinsa Corporation (Piscataway, NJ), which contains 85% curcumin, with 11% of demethoxycurcumin and 4% of bisdemethoxycurcumin (*77*). It was used without further purification. Hydrophobically modified starch (HMS) was obtained from National Starch and Chemical Company (Bridgewater, NJ) with a brand name of Hi-Cap 100. Pyrene, acetone and chloroform were purchased from Sigma-Aldrich (St. Louis, MO).

Determination of the Critical Aggregation Concentration of HMS. The critical aggregation concentration (CAC) of HMS was determined by measuring the fluorescence spectrum of 6×10^{-7} M pyrene in 1X phosphate buffered saline (1X PBS) containing different concentrations of HMS (0.01% - 5%). The excitation fluorescence spectrum from 300 to 350nm was obtained using Cary Eclipse fluorescence spectrophotometer

(Varian Instruments, Walnut Creek, CA). The emission wavelength was set at 390nm and the slit openings were set at 5 nm for both excitation and emission. The ratio of the intensity at 337nm (I_{337}) to that at 334nm (I_{334}) was calculated and plotted against the common logarithm of HMS concentration. The CAC of HMS was determined as the corresponding concentration of HMS at the turning point in the plot.

Loading of Curcumin in HMS Solution. Excessive amount of curcumin was mixed with 1X PBS with 1% HMS and homogenized at 24000 rpm for 10 min with High Speed Homogenizer (ULTRA–TURRAX T-25 basic, IKA Works, Wilmington, NC) and stirred on a magnetic stirrer over night at room temperature. On the next day, free curcumin was removed by high-speed centrifugation and filtration through 0.45μm filter.

Quantification of Curcumin Extracted from HMS Micelles. Equal volume of chloroform was added to curcumin HMS solution and subsequently vortexed for 10 min and then stirred on a magnetic stirrer over night. After complete phase separation, the chloroform phase was diluted 10 times, and the UV-Vis absorbance at 419 nm was measured with a Cary UV-Vis spectrophotometer (Varian Instruments, Walnut Creek, CA). The quantity of curcumin was determined according to the calibration curve of curcumin in chloroform in the concentration range of 1-5 μg/mL.

Lyophilization and Reconstitution. Curcumin HMS solution was frozen at –20 ℃ over night and then lyophilized using a Freezone4.5 freeze–dry system (Labconco, Kansas City, MO). Deionized H_2O was used to reconstitute the curcumin HMS solution.

Infrared Spectrum and Fluorescence Spectrum of HMS Encapsulated Curcumin. The infrared spectrum of lyophilized curcumin HMS was measured by using a Thermo

Nicolet Nexus 670 FT-IR system with attenuated total reflectance (ATR) accessory (Thermo Fisher Scientific, Waltham, MA). The fluorescence emission spectra of curcumin water solution and curcumin HMS solution were determined using a Cary Eclipse fluorescence spectrophotometer (Varian Instruments, Walnut Creek, CA). The excitation wavelength was set at 319 nm, and the emission spectra were ranged from 450 nm to 650 nm. The slit openings were set at 10 nm for both excitation and emission.

Synchrotron Small-Angle X-ray Scattering (SAXS). SAXS datasets were collected from solutions of 10 mg/mL HMS with and without the addition of curcumin at the BIOCAT undulator beamline 18-ID of APS, Argonne National Laboratory. To minimize radiation damage during data collection, samples were continuously pumped through a 1.5 mm-wide quartz capillary at 12.5 μl/s for an average exposure time of 0.6 s. The scattering intensity profiles were obtained by subtracting the average of 15 water-only profiles from the average of 15 starch-water or curcumin-starch-water profiles, which were performed with the program IGOR Pro (WaveMatrics), and macros written by the BIOCAT staff.

Cell Culture and *In Vitro* Anti-Cancer Activity Assay. Human hepatocellular carcinoma cell line HepG2 was obtained from American Type Culture Collection (HB-8065, Manassas, Virginia, USA) and were cultured in minimum essential medium (Invitrogen, Carlsbad, California, USA) containing 10% fetal bovine serum (Invitrogen, Carlsbad, California, USA), 100 units/mL penicillin (Invitrogen, Carlsbad, California, USA) and 100 μg/mL streptomycin (Invitrogen, Carlsbad, California, USA). Cells were maintained in incubators at 37 ℃ under 95% relative humidity and 5% CO_2.

Anti-cancer activity of curcumin was examined by methyl thiazol tetrazolium bromide (MTT) assay. Briefly, HepG2 cells were seeded in 96-well microtiter plates at a density of 10,000 cells per well in a final volume of 100 µl medium. After 24 hours, the cells were treated with a medium containing DMSO-dissolved or HMS encapsulated curcumin of different concentrations. Other cells were untreated as negative control, or treated only with DMSO or HMS at the maximum concentration used to dissolve and encapsulate curcumin, respectively. After 24 hours, cell culture media were aspirated and cells were incubated with 100 µl MTT solution (0.5 mg/mL in RPMI 1640 medium) for 2 h at 37 ℃. Subsequently, MTT solution was carefully aspirated and the formazan crystals formed were dissolved in 100 µl DMSO per well. Light absorbance at 560 and 670nm was recorded with Absorbance Microplate Reader (Molecular Devices, Sunnyvale, California, USA). Relative cell viability was expressed as A560-A670 normalized to that of the untreated wells. Data were presented as mean ± standard deviation with 8 well repeats.

Statistical Analysis. Anti-cancer effect of DMSO-dissolved and HMS-encapsulated curcumin was compared with t-test using SigmaPlot 10.0 software (Systat Software, San Jose, CA).

Results

Capability of HMS to form polymer micelles.

To demonstrate the ability of hydrophobically modified starch (HMS) to form micelles, the pyrene fluorescent method was first used to determine the possible critical aggregation concentration (CAC) of HMS. The fluorescent spectrum of pyrene is

sensitively affected by its microenvironment. When pyrene is in hydrophilic environment, one of its excitation peaks is at 334 nm. Once pyrene migrates into hydrophobic environment, such as the core portion of polymer micelles, this peak shifts from 334 to about 337 nm Figure 9. By plotting the ratio of the fluorescence intensity at 337 nm to that at 334 nm (I_{337}/I_{334}) versus polymer concentrations, the CAC of amphiphilic polymers can be determined(*150*). As shown in Figure 10, I_{337}/I_{334} increased with the increase of HMS concentration. At 0.36%, a turning point appeared, indicating the onset of the self-assembly of HMS and the CAC of HMS.

Compared with other surfactants and synthetic amphiphilic polymer micelles, HMS has a relatively high CAC. This may be due to its big portion of hydrophilic polysaccharide group and low degree of substitution (typically less than 3%) limited by the food industry regulation.

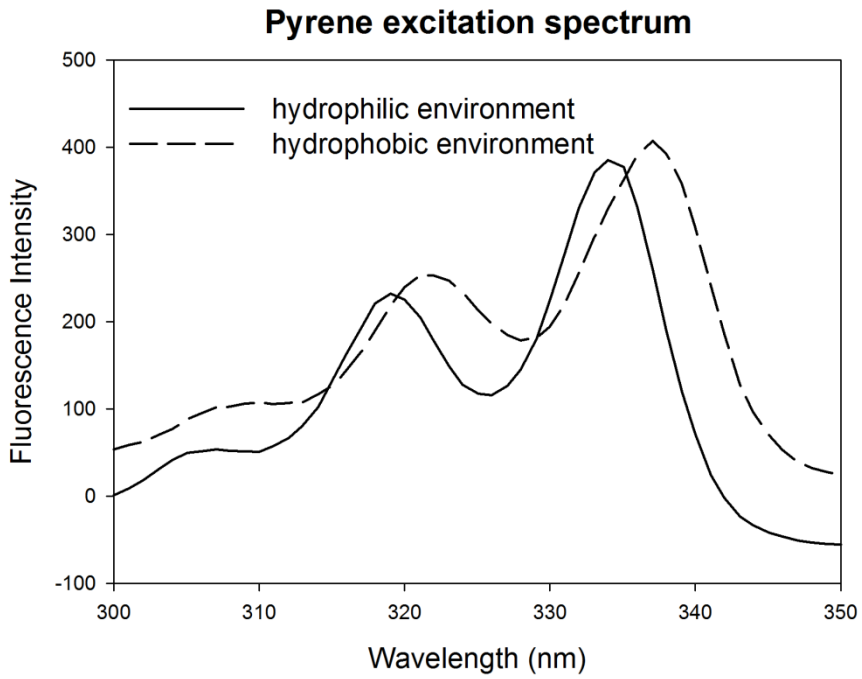

Figure 9. Comparison of the excitation fluorescence spectra of pyrene in hydrophilic and hydrophobic environment

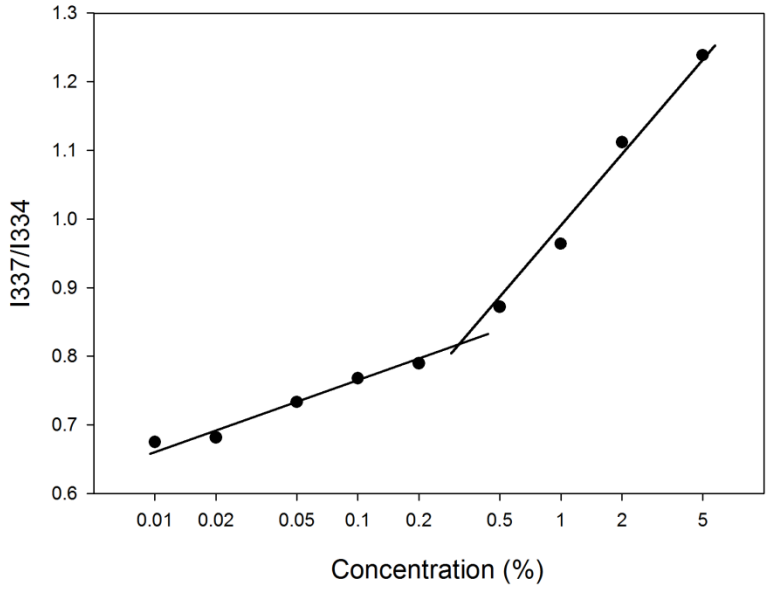

Figure 10. Determination of the critical aggregation concentration (CAC) of modified starch

Encapsulation of Curcumin in HMS Solution

HSM solution 1% was prepared to encapsulate curcumin in HSM micelles. Curcumin powder was loaded under high-speed homogenization and stirred on a magnetic stirrer overnight. After removal of free curcumin, curcumin HMS solution was clear and yellowish (Figure 11), compared with curcumin water solution as a control (Figure 12). To quantify the amount of curcumin in the HMS micelles, curcumin was extracted with chloroform. The concentration of curcumin was calculated using the calibration curve of curcumin chloroform solution. It is determined that the absolute concentration of curcumin in filtered HMS solution is 18.4 μg/mL. Compared with the estimated water solubility of 11 ng/mL (*62*), HMS can at least increase the solubility by 1670 folds.

Curcumin HMS solution was subsequently lyophilized and reconstituted with water. Lyophilized curcumin HMS solution afforded a yellowish powder with no noticeable free curcumin powder. After being reconstituted with water, this powder dissolved back to clear solution very quickly and easily, with no noticeable curcumin precipitates (Figure 2C). Our results suggested that curcumin was indeed trapped in the HMS micelles and the complex of HMS and curcumin could resist against freeze-drying.

The structure of HMS with or without the addition of curcumin has been studied by synchrotron small-angle X-ray scattering. The small-angle scattering cross section per unit volume, *I(q)*, for a starch solution can be written as:

$$I(q) = \phi V_p (\Delta\rho)^2 P(q) S(q) \qquad (1)$$

where ϕ and V_p are the volume fraction and the molecular volume of HMS molecules respectively; $\Delta\rho$ is the X-ray electron density contrast between HMS and water; *P(q)* is the form factor; and *S*(*q*) is the structure factor. At current HMS concentration, *S(q)*=1. HMS is a flexible polymer chain, thus the form factor can be fitted by Debye function (Higgins & Benoit, 1994), which is written as:

$$P(q) = \frac{2}{(qR_g)^4}\left[\exp(-q^2R_g^2) + q^2R_g^2 - 1\right] \quad (2)$$

where R_g is the radius of gyration fitted from the Debye function. Figure 3 show the X-ray scattering intensity profiles of 10 mg/mL HMS water solutions with or without the addition of curcumin. Our results showed that 10 mg/mL HMS solution has a slightly higher intensity at low *q* than 10mg/mL HMS-curcumin solution. From the fits of scattering intensity profiles to equation 2, we conclude that, no matter whether there is curcumin in the 10 mg/mL HMS solutions, the radius of gyration of HMS remained at 14.1 ± 0.1 nm, further suggesting that the addition of curcumin did not perturb the micellar structure of HMS (Figure 13).

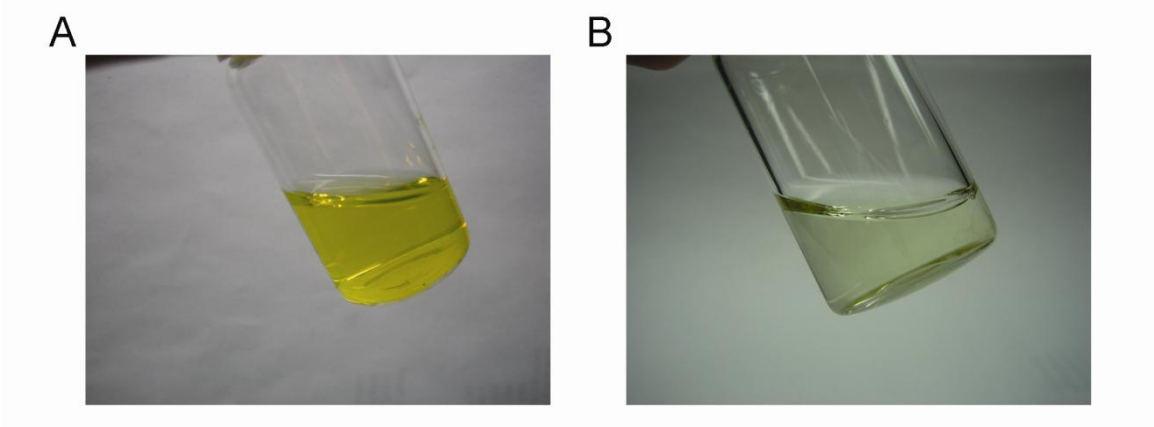

Figure 11. Photographic images of curcumin in HMS solution (A) and water loaded with curcumin (B).

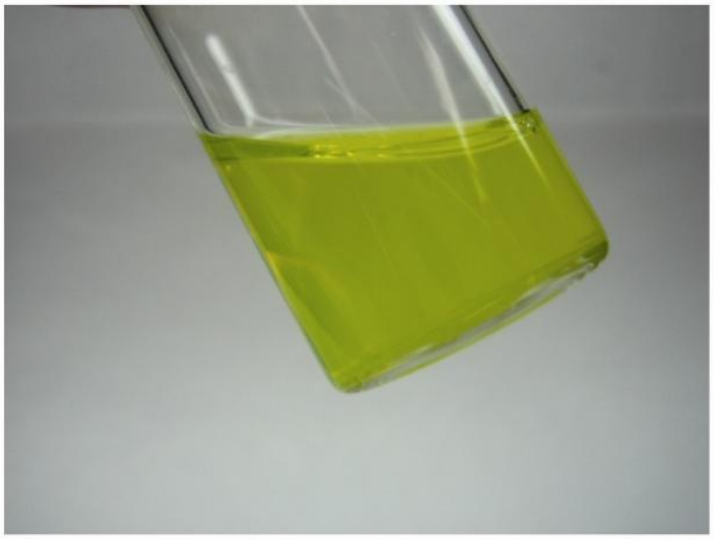

Figure 12. Reconstitution solution from lyophilized HMS-curcumin encapsulation.

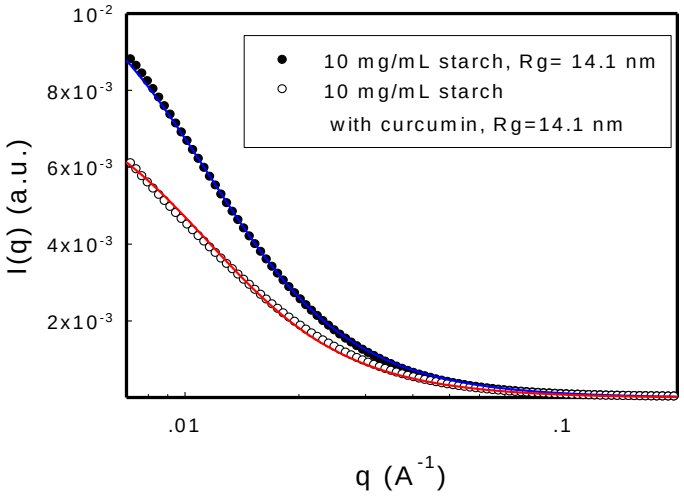

Figure 13. Small-angle X-ray scattering intensity profiles of 10 mg/mL HMS water solution with (empty circles) or without (solid circles) the addition of curcumin. The solid lines are fits to equation 2.

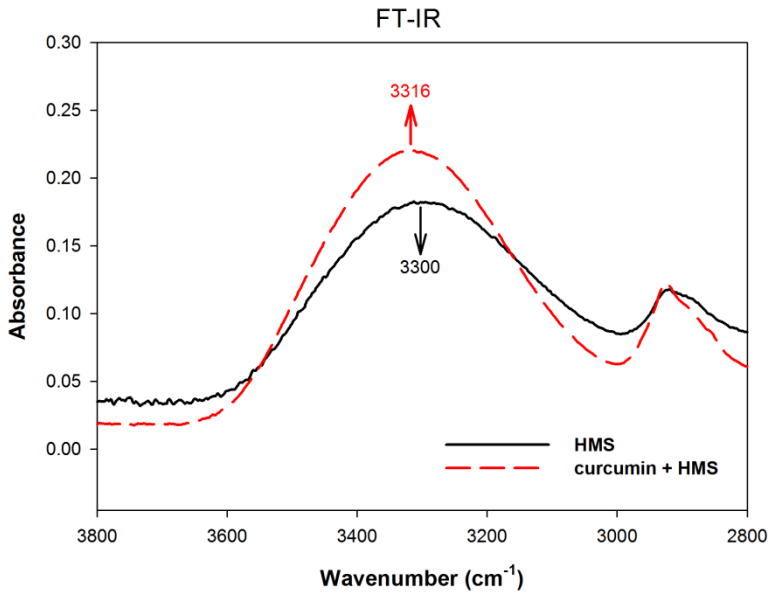

Figure 14. FT-IR spectra of HMS (solid line) and HMS loaded with curcumin (dashed line) in the wavenumber range from 3800cm^{-1} to 2800 cm^{-1}.

Interaction between curcumin and HMS

To investigate the interaction between HMS and curcumin, the infrared (IR) spectra of lyophilized curcumin HMS powder and HMS powder alone were measured. Compared with that of pure HMS, the IR spectrum of curcumin HMS powder showed a band shift from 3300 to 3316 cm^{-1} as evidenced in Figure 14, which was assigned to the vibrational band of the hydroxyl (-OH) group of HMS. The band shift in the IR is mostly likely due to the formation of intermolecular hydrogen bonding between HMS and curcumin Considering that curcumin itself is a fluorescent compound, and the fact that the fluorescence spectrum of a compound is usually affected by its microenvironment, we compared the emission spectrum of curcumin in HSM solution with that of curcumin in water. As shown in Figure 15, the emission peak of curcumin in water was at 542 nm, while the peak shifted to 531 nm when curcumin was encapsulated in HMS solution. This result further confirmed that the microenvironment of curcumin was changed upon HMS encapsulation.

Enhanced in vitro anti-cancer activity of curcumin encapsulated in HMS

By inducing apoptosis, curcumin is demonstrated as a potent anti-cancer agent (*151*). To investigate the in vitro anti-cancer activity of curcumin encapsulated in HMS, HepG2 cells were treated, respectively, with DMSO-dissolved curcumin and HMS-encapsulated curcumin of the same concentrations. After treatment for 24 hours, the cell viability was determined with MTT assay. As shown in Fig. 6, HepG2 cells treated with DMSO or HMS alone reveals comparable cell viability to untreated cells, suggesting that at the concentration used, DMSO and HMS have no cytotoxicity. Furthermore, HMS-encapsulated curcumin was more effective than DMSO-dissolved curcumin in anti-

carcinogenesis. At the concentrations of 0.4, 2, and 10 μg/mL, the anti-cancer activity of HMS-encapsulated curcumin was significantly higher than that of DMSO-dissolved curcumin ($P<0.001$), suggesting that HMS encapsulation is more effective to deliver curcumin to cancer cells

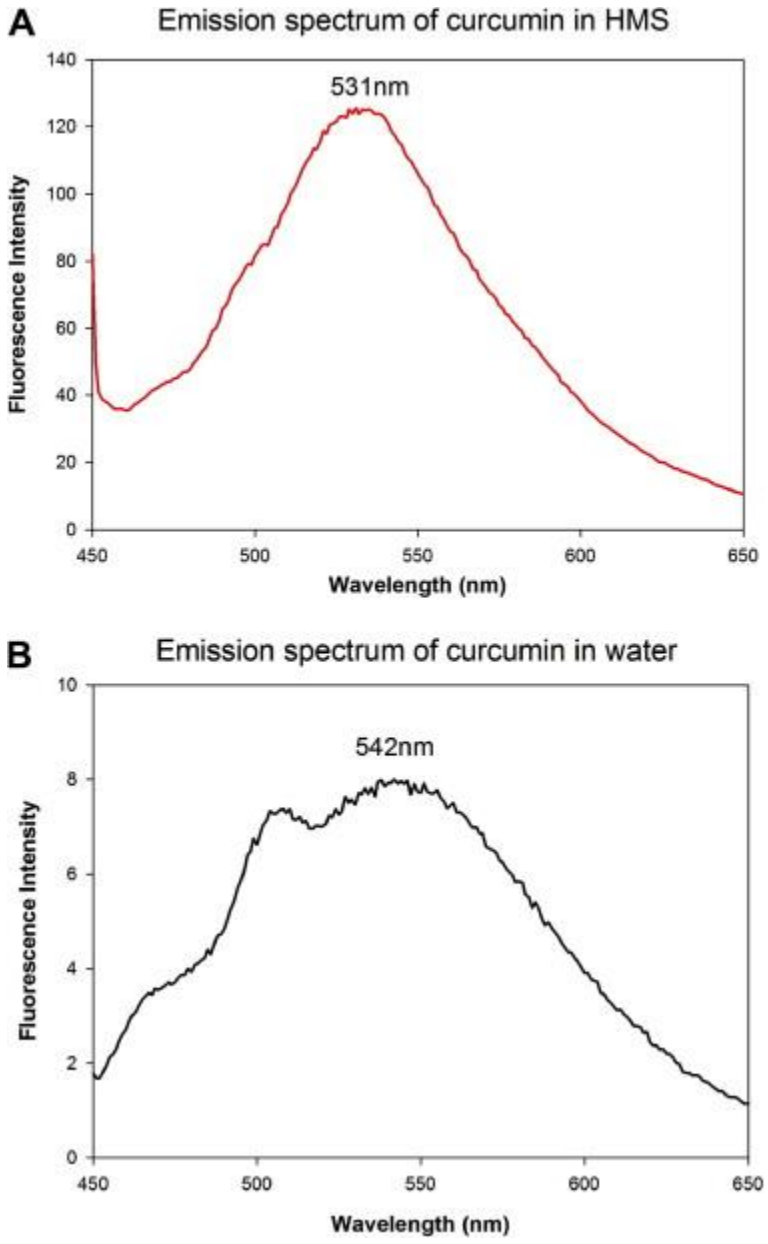

Figure 15. Comparison of fluorescence emission spectra of curcumin in HMS solution (A) and in water (B).

.

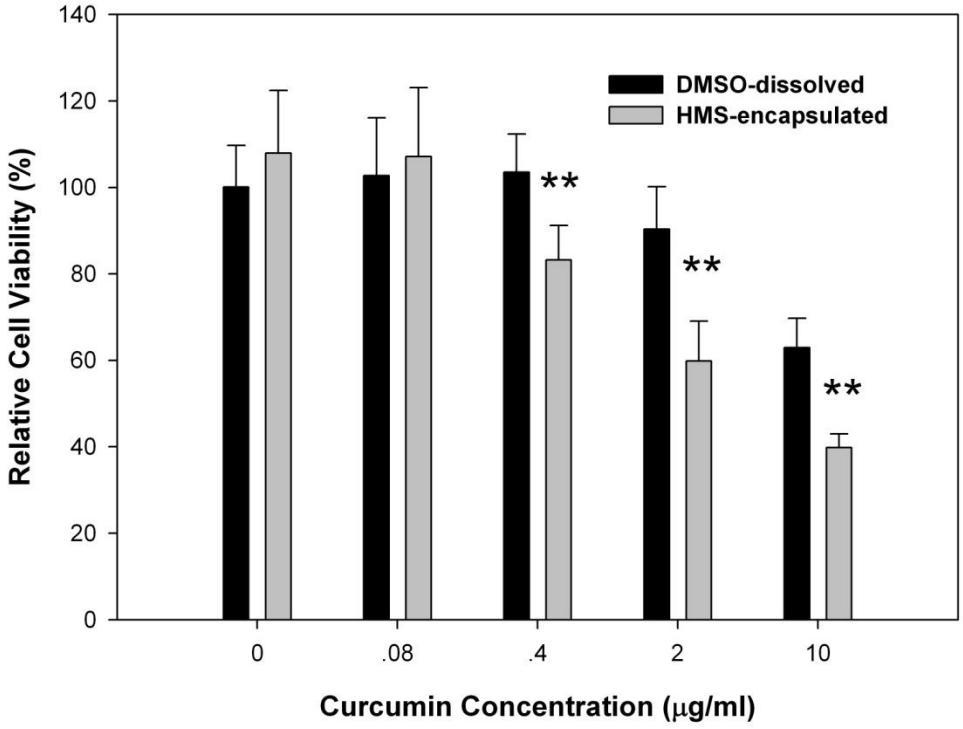

Figure 16. The plot of relative cell viability versus curcumin concentration for free curcumin (dissolved in DMSO, black bars) and HMS-encapsulated curcumin (grey bars). Conditions of DMSO **alone and HMS alone were expressed as** curcumin **at zero concentration. Data was presented as mean ± standard deviation, *n* = 8. **Denotes that the differences are statistically significant.**

Discussion and Conclusion

In this study, curcumin was encapsulated into polymer micelles formed by hydrophobically modified starch. Upon encapsulation, curcumin showed increased water solubility. As the peak position shifted in either infrared or fluorescence spectra, it was suggested that the microenvironment of curcumin was changed upon encapsulation, and there may be a hydrogen bonding interaction between curcumin and HMS.

Compared with other polymeric micelles used to encapsulate curcumin, the critical aggregation concentration of HMS is relatively high and the encapsulation capacity of HMS is relatively low. This may be due to the low degree of substitution (DS) of HMS. The DS of HMS does not exceed 3%, which is quite different from amphiphilic block co-polymers, such as PEO-b-PCL (*152*). On the other hand, we showed that freeze-dried HMS encapsulated curcumin could be easily reconstituted. It suggests the structural stability of HMS-curcumin micelles, which is further evidenced by the constant HMS R_g with and without curcumin. To the best of our knowledge, this is the first report regarding this property.

From our results, an increase in curcumin solubility may be due to the combination of hydrophobic microenvironment of curcumin and hydrogen bonding between modified starch and curcumin. This hydrogen bond interaction has also been conceived between curcumin and some of other molecules studied, such as phosphatidylcholine (*97*). Using thermodynamic analysis, Began et al. (1999) found that the thermodynamic parameters for the binding of curcumin to phosphatidylcholine is driven by both entropy and enthalpy, suggesting that curcumin forms hydrogen bond with phosphatidycholine in addition to hydrophobic interaction. On the other hand, the extensive research on the

interaction between curcumin and human serum albumin only suggested the hydrophobic interaction but no hydrogen bonding (*85, 86*).

In the literature, different micelle encapsulation formulations of curcumin revealed variations in *in vitro* anti-cancer/cytotoxicity activity. Micelles formed by PEO-b-PCL showed less anti-cancer activity, probably due to the prolonged release profile and the lack of direct interaction between curcumin and cells (*70*). Curcumin encapsulated in mPEG-palmitate nanocarriers, on the other hand, had comparable activities to DMSO-dissolved curcumin (*75*). In contrast, our results suggested the enhanced activity of encapsulated curcumin. Since HMS is a slightly-modified biomolecule, the interaction between HMS and HepG2 cells could be the reason of enhanced anti-cancer activity. As a matter of fact, curcumin – casein micelle complex also revealed a stronger activity than free curcumin (*87*).

In summary, I have demonstrated that hydrophobically modified starch is able to self assemble to form micelles and to encapsulate curcumin into its hydrophobic core. Upon encapsulation, the water solubility of curcumin increased about 1670 folds and the anti-cancer activity was also greatly increased. This study suggested that hydrophobically modified starch could be used as a self assembled biopolymer to encapsulate water-insoluble bioactives in functional food.

CHAPTER 3. SYNTHESIS AND CHARACTERIZATION OF MODIFIED EPSILON POLYLYSINE

The aim of this study is to synthesize and characterize hydrophobically modified EPL, which is expected to be a surface active amphiphile and is able to be used as an emulsifier. This study demonstrated that hydrophobically modified EPL(s) are bi-functional molecule: they are amphiphilic and also antimicrobial.

Materials and Methods

Materials. ε-Polylyine (EPL) was purchased from Zhejiang Silver-Elephant Bio-engineering Co., Ltd, China and used without further purification, unless noted specifically. Dimethyl sulfoxide (DMSO), octenyl succinic anhydride (OSA), deuterium oxide (D_2O), sodium bicarbonate ($NaHCO_3$), methanol and agar were purchased from Sigma-Aldrich (St. Louis, MO). Pyrene was obtained from Alfa Aesar (Ward Hill, MA). Dialysis membranes (MWCO 1,000Da) were purchased from Spectrum Laboratories, Inc. (Rancho Dominguez, CA). *Escherichia coli* (*E.coli*) O157:H7 (ATCC 43888) was purchased from MicroBioLogics, Inc. (Saint Cloud, MN). Nutrient broth and 96-well microtiter plates were obtained from BD Biosciences (San Jose, CA).

Synthesis of hydrophobically modified EPL. 1.5 g EPL was dissolved in 30 ml DMSO, and different concentrations of OSA were added dropwise under stirring at 35-40 ^{o}C. After 18 h, the whole reaction was dialyzed in 1000 Da molecular weight cut-off (MWCO) dialysis membrane against 95% EtOH, 0.01% $NaHCO_3$, and deionized water sequentially, and then lyophilized with a Freezone4.5 freeze–dry system (Labconco, Kansas City, MO) to obtain the final products.

Infrared and ^{1}H NMR spectroscopy. The Fourier transform infrared (FT-IR) spectra of original EPL and modified EPL were measured using Thermo Nicolet Nexus 670 FT-IR system with a Smart MIRacle^{TM} horizontal Attenuated Total Reflectance (ATR) accessory (Thermo Electron Corp., Madison, WI). Each spectrum was averaged over 512 scans with 4 cm^{-1} resolution.

^{1}H NMR spectroscopy was taken on a Varian 500 MHz NMR spectrometer (Palo Alto, CA). All of the samples were dissolved in D_2O.

Determination of the degree of substitution. The degree of substitution (DS) was defined as the percentage of the reacted α-amine groups on the lysine monomer in the EPL molecule. It was calculated as the peak area at 4.0 ppm divided by the total peak areas at 3.82 ppm and 4.0 ppm from the ^{1}H NMR spectra.

$$DS = \frac{A_{\delta 4.0}}{A_{\delta 3.82} + A_{\delta 4.0}} \times 100\% \quad (1)$$

Determination of the critical aggregation concentration (CAC). The critical aggregation concentrations (CACs) of modified EPL were determined by measuring the fluorescence excitation spectra of pyrene in modified EPL solutions (*150, 153-155*). Modified EPL was dissolved in deionized water at different concentrations (0.01, 0.02, 0.05, 0.1, 0.2, 0.5, 1, 2, 5, and 10 mg/mL). 1.0 mM pyrene stock solution was prepared in methanol. 4 μL of this solution was added to glass tubes, and methanol was removed by purging with nitrogen. Subsequently, 4.0 mL of modified EPL solutions of different concentrations were respectively transferred to each tube. All tubes were sonicated for 30 min to facilitate pyrene dissolution. Subsequently, the fluorescence excitation spectra of pyrene from 300nm to 350nm were obtained using Cary Eclipse fluorescence

spectrophotometer (Varian Instruments, Walnut Creek, CA). The emission wavelength was set at 390 nm and the excitation and emission slit openings were both set at 5 nm. The ratio of the intensity at 337nm (I_{337}) to that at 334nm (I_{334}) was calculated and plotted against the common logarithm of the concentrations of modified EPL. A major change in the slope indicated the onset of micelle formation and the corresponding concentrations of modified EPL(s) were determined as the CACs of EPL(s).

Dynamic light scattering (DLS). The mean hydrodynamic diameters and the corresponding polydispersity of the polymer micelles were determined using DLS-based BIC 90plus particle size analyzer equipped with a Brookhaven BI-9000AT digital correlator (Brookhaven Instrument, New York, NY) at a fixed scattering angle of 90^o at 25 ^{o}C. The light source of the particle size analyzer is a solid state laser operating at 658 nm with 30 mW power, and the signals were detected by a high sensitivity avalanche photodiode detector. The normalized field-field autocorrelation function *g(q,t)* is obtained from the intensity-intensity autocorrelation function, *G(q,t)*, via the Sigert relation:

$$\alpha g(q,t) = [G(q,t)/A - 1]^{1/2} \quad (1)$$

where *A* is the experimentally determined baseline, α is the contrast factor which is less than 1, due to the fact that only a fraction of dynamic scattering intensity falls within the correlator window and also the fact that a finite size pinhole is used in the experiment. For all micelle size measurements, the measured baseline A is in agreement with the theoretically calculated baseline to 0.01%.

The diffusion coefficient *D* was calculated according to $D=\tau^{-1}q^{-2}$, where q is the amplitude of scattering vector defined as $q=(4\pi n/\lambda)\sin(\theta/2)$, n is the solution refractive

index, λ is the laser wavelength and θ is the scattering angle. The diffusion coefficient *D* can be converted into mean emulsion droplet diameter *d* using the Stokes-Einstein equation:

$$d = \frac{kT}{3\pi\eta D} \quad (2)$$

where *k* is the Boltzmann constant, *T* is the absolute temperature, and η is the solvent viscosity.

Cumulant analysis method was used in our size measurements, where *g(q,t)* was decomposed into a distribution of decay rate Γ(= 1/τ) given by

$$g(q,t) = \int G(\Gamma) e^{-\Gamma t} d\Gamma \quad (3)$$

The first two moments of the distribution *G(Γ)* are as follows:

$$\Gamma = Dq^2 \quad (4)$$

$$\mu^2 = (D^2 - D^{*2})q^4 \quad (5)$$

Where D* is the average diffusion coefficient. The polydispersity term defined in the Cumulant analysis is:

$$polydispersity = {}^{\mu_2}/_{\Gamma^2} \quad (6)$$

Here *polydispersity* has no unit. It is close to zero for monodisperse or nearly monodisperse samples, and larger for broader distribution.

Surface tension measurement. 5 mg/mL modified EPL(s) solutions were prepared in deionized water. The surface tension was measured using the pendant drop method

with VCA optima surface analysis system (AST Products, Billerica, MA). The surface tension values were expressed as mean ± standard deviation, with 16 repeats.

Differential scanning calorimetry (DSC). The thermal properties of modified EPLs were analyzed with a DSC823e thermal analyzer (Mettler Toledo, Columbus, OH). 5.5-6.0 mg modified EPL(s) samples were sealed in aluminum crucibles and the lid of each crucible was penetrated to form a small hole. The samples were first heated from 25 to 200 ^{o}C with a heating rate of 10 ^{o}C/min, subsequently cooled to -120 ^{o}C with a cooling rate of -30 ^{o}C/min, and finally heated back to 210 ^{o}C with a heating rate of 10 ^{o}C/min. Glass transition temperatures (T_g) were determined by the STARe software associated with the thermal analyzer. Before DSC analysis, EPL was first dialyzed against deionized water using dialysis membrane with molecular weight cut-off (MWCO) of 1000 Da, and then freeze dried.

Determination of the minimum inhibitory concentration against *Escherichia coli* (*E.coli*) O157:H7. Minimum inhibitory concentrations (MIC) of different modified EPL(s) were determined by microtiter broth dilution method (*156*). Briefly, 10^5 CFU/mL *E.coli* O157:H7 was cultured in nutrient broth with EPL or modified EPL(s) of different concentrations (100, 50, 25, 12.5, 6.25, 3.13, 1.56, 0.781 and 0.391 μg/mL). Media inoculated with *E.coli* O157:H7 but without antimicrobial compounds were served as positive control. Media alone was taken as negative control. After cultured for 24 h at 37 ^{o}C, optical absorbance at 600 nm (OD_{600}) of each well was recorded using Absorbance Microplate Reader (Molecular Devices). MIC of each tested compound was defined as the lowest concentration of the compound with which bacteria had no optically prominent growth.

Preparation of Oil-in-Water Emulsion 0.1g of M-EPL (OSA-*g*-EPL8.5) was dissolved in 10 mL dH_2O and 0.1 gram of MCT with trace amount of Sudan III as indicator was added in. The mixture was first stirred for 5 minutes on a magnetic stirrer and then homogenized at 24000 RPM for 20 minutes using High Speed Homogenizer (ULTRA–TURRAXT-25basic, IKAWorks). Prepared emulsion was stored at ambient temperature.

Measurement of the particle size of oil droplets At certain time interval during homogenization and storage, the mean hydrodynamic diameters of oil droplets were determined using DLS-based BIC90 plus particle size analyzer equipped with a Brookhaven BI-9000AT digital correlator (Brookhaven Instrument) at a fixed scattering angle of 90^o at ambient temperature. Emulsions were diluted with dH_2O 20 times before the measurement. Data were shown as mean ±standard error (n=3).

Cell culture and maintenance HepG2 cell line was obtained from Dr. Mou-Tuan Huang of Department of Chemistry Biology, Rutgers, the State University of New Jersey. Cells were maintained in Minimum Essential Medium with 10% Fetal Bovine Serum and 1X penicillin and streptomycin, at 37^oC with 5% CO_2.

Caco-2 cell line was generously provided by Dr. Judith Storch of Department of Nutrition, Rutgers, the State University of New Jersey. Cells were maintained in Dulbecco's Modified Eagle Medium (DMEM) with 10% fetal bovine serum, 1X non-essential amino acids and 1X penicillin and streptomycin, at 37^oC with 5% CO2. Passage 35 to 45 were used in the studies, to keep relatively constant cellular phenotypes (*16*).

Cytotoxicity Assay. cytotoxicity assay Cytotoxicity of M-EPLs was investigated using by MTT method (*157, 158*). 10,000 HepG2 cells were plated into each well of 96-well microplate. On the second day, cells were treated with different concentrations (100, 250, 500, 750 and 1000 μg/mL) of EPL or M-EPLs in culturing medium. After 24-hour treatment, media were aspirated and cells were treated with MTT for 2 hours. Subsequently, the formazan salt formed in cells were dissolved in DMSO and optical density at 560 and 670 nm were recorded with Bio-Tek® Synergy HT Multi-Mode Microplate Reader. Relative cell viability was calculated as percentage of A560-A670 of each treatment well compared with that of untreated well. IC_{50} referred to the concentration of M-EPL which caused 50% of relative cell viability.

Cultivation of Caco-2 monolayers and transepithelial electrical resistance (TEER) measurement across Caco-2 monolayer. To generate Caco-2 monolayer in the insert filters of 12-well plates, Caco-2 cells were plated in the 0.45 μM polycarbonate filters of 12-well plate (Corning): 0.5 mL per well with cell density of 0.6×10^6 cells/mL. In the wells, 1.5 mL culture media was added. Every two days, media inside the filters and wells were changed. Cells were used after 21-29 days of culture.

On the date of experiment, cell culture media of the two sides of Caco-2 monolayers were removed carefully to keep intact of the monolayer. Cells were washed with pre-warmed Hank's balanced salt solution (HBSS) plus 25mM HEPES. 0.5mL and 1.5 mL HBSS + 25mM HEPES were added in the apical and basolateral compartments, respectively. Cells were incubated in a 37^{o}C shaker at 100 rpm for 20-30mins before OSA-g-EPL treatment. Initial TEER (t=0) was measured right before adding OSA-g-EPL to the apical compartment. Subsequently, TEER was measured every 15 minutes till 90

minutes after treatment. Treatment media were removed and cells were cultured in regular growth media overnight. On the next day, cells were again incubated in HBSS + 25 mM HEPES for 20-30 minutes, before final TEER was measured.

All the TEER values were measured using EVOM2, Epithelial Voltohmmeter (World Precision Instruments), with the unit of ohm (Ω). Background TEER was measured on filters without cells. Final TEER values were calculated and presented as:

$$TEER\ across\ cells\ (\Omega \times cm^2) = [TEER\ (\Omega) - \ background\ TEER\ (\Omega)]\ \times area\ (cm^2)$$

Results and Discussions

Synthesis of Modified ε-Polylysine

To hydrophobically modify a biopolymer containing primary amine or hydroxyl groups, fatty acid with the aid of 1-ethyl-3-(3-dimethylaminopropyl) carbodiimide hydrochloride (EDC), acid chlorides and acid anhydrides are often used. In this study, we chose octenyl succinic anhydride (OSA), because of its long history of use in food industry, especially in synthesizing the hydrophobically modified starch (*152*, *159-161*). ε-Polylysine (EPL) and OSA were reacted in DMSO through nucleophilic reaction (**Error! Reference source not found.**). The products were then dialyzed to remove nreacted OSA (and its possible hydrolysates) and lyophilized to obtain the products denoted as OSA-*g*-EPL(s).

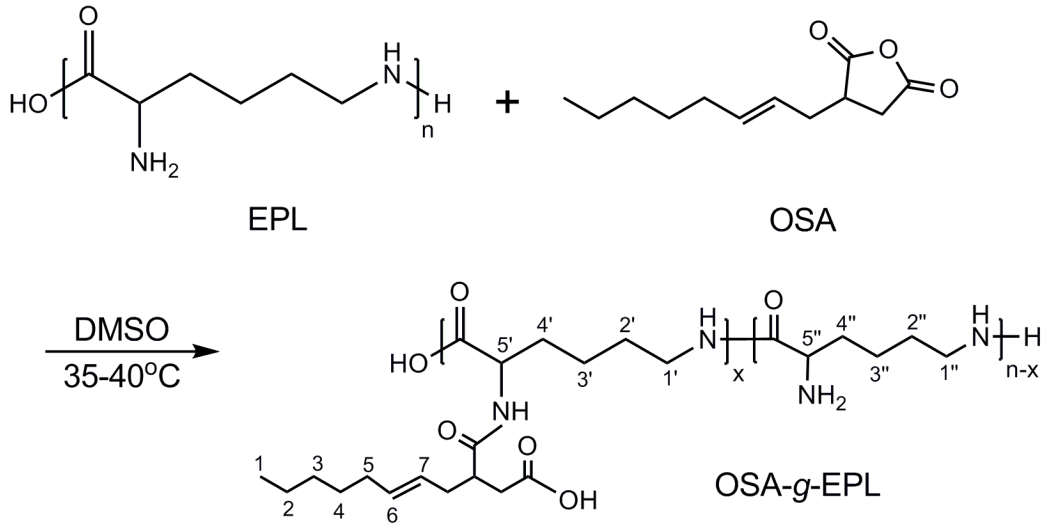

Figure 17 Synthetic scheme of hydrophobically modified ε-polylysine (EPL), or OSA-*g*-EPL(s)

The success of reaction was confirmed by ^{1}H NMR spectroscopy. As shown in Figure 18. ^{1}H NMR spectra of (a) EPL, (b) OSA-*g*-EPL6.2, (c) OSA-*g*-EPL8.5, (d) OSA-*g*-EPL12.4, and (e) OSA-*g*-EPL20.5.Figure 18, the peaks specific to EPL (Figure 18A.) appeared between 1.2 and 4.0 ppm. Peaks at about 3.82 and 3.12 ppm corresponded to terminal methine and methylene groups, respectively. In the products (OSA-*g*-EPL(s), Figure 18B-D.), peak assignments were as follows: δ 0.74 (CH3), 1.27 [CH2 (β, γ, δ) of OSA and CH_2 (γ) of EPL], 1.46 [CH_2 (β) of EPL], 1.76 [(CH_2 (α) of OSA and CH_2 (δ) of EPL], 3.12 [CH2 (α) of EPL], 3.82 [unreacted methine of EPL], 4.0 [reacted methine of EPL], 5.2 and 5.4 [H on CH=CH of OSA].

The peak of the methine group of EPL shifted partially from 3.82 to 4.0 ppm when acylation reaction occurred in the amine groups. This shift indicated the presence of major functional groups linked to EPL.

The degree of substitution (DS) of EPL can be calculated as the area ratio of the reacted methine proton (δ 4.0) to the total methine proton (δ 3.82 and δ 4.0), or proton on the double bond (δ 5.2 and 5.4) to the total methine proton (δ 3.82 and δ 4.0). In this study, the former method was used. The DS of OSA-*g*-EPL(s) at different feed ratios of OSA to EPL were listed in Table 2. One notices that the DS of OSA-*g*-EPL(s) increased with the increase of feed ratio. Once the DS values were determined, the reaction products were further denoted as OSA-*g*-EPL<n>, with n indicating the DS value. For example, in OSA-*g*-EPL6.2, 6.2% amine groups in EPL were reacted with OSA.

To further confirm the synthesis, infrared spectra of OSA-*g*-EPL(s) were collected and compared with that of EPL, as shown in Figure 19. The N–H stretching bands were

located between 3300–3200 cm^{-1}. With the increase of DS, the position of this band shifted to larger wavenumbers, i.e., from 3213 to 3224, 3234, 3263 and 3271 cm^{-1}, suggesting the existence of hydrogen bonding between the N-H group of EPL moiety and the increasing number of carbonyl (C=O) groups from OSA moieties on the products. The weak band at approximate 3070-3060 cm^{-1} corresponded to the overtone of the N-H stretch band (amide II band) at 1560–1530 cm^{-1}. The intensity of this band was stronger for OSA-*g*-EPL(s) than for EPL. The two bands at 2925 and 2859 cm^{-1} were designated as C-H stretching. With hydrophobic substitution, the two bands were naturally more prominent. The band at 1539 cm^{-1} in the spectrum of EPL corresponded to amide II band originated from N-H bending. After conjugation, it was intensified as anticipated. The band at 1390 cm^{-1} was designated as methyl C-H bending and was increasingly prominent with the increase of DS.

The results of ^{1}H NMR and ATR-FTIR spectroscopies both confirmed that OSA-*g*-EPL(s) were successfully synthesized by conjugating OSA onto EPL. Subsequently, thermal properties and self assembly behavior of OSA-*g*-EPL(s) were analyzed and compared with those of original EPL.

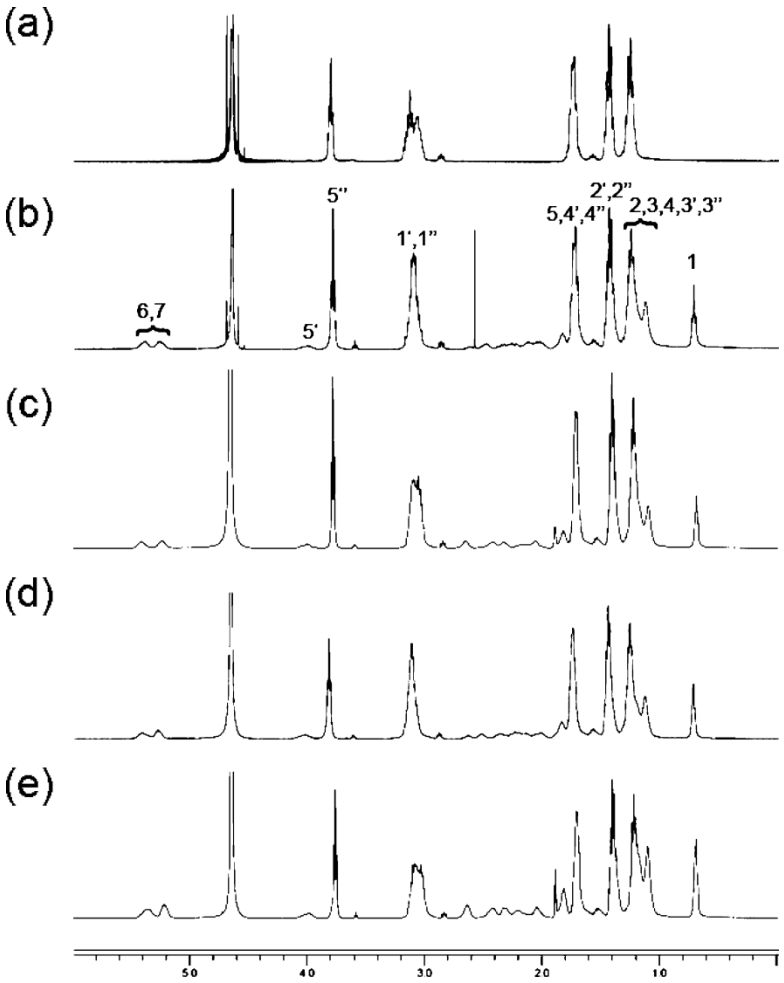

Figure 18. ^{1}H NMR spectra of (a) EPL, (b) OSA-*g*-EPL6.2, (c) OSA-*g*-EPL8.5, (d) OSA-*g*-EPL12.4, and (e) OSA-*g*-EPL20.5.

Feed ratio	DS	T_g (^oC)	CAC (mg/mL)	Surface Tension (mN/m)	MIC (μg/mL)
10-0	0	133.1	ND	72.3 ±1.0	12.5
10-1	6.2%	126.1	1.76	40.6 ±2.1	12.5
10-3	8.5%	94.0	0.64	44.8 ±2.8	12.5
10-6	12.4%	78.9	0.32	35.6 ±1.8	12.5
10-10	20.5%	60.6	0.18	39.5 ±2.2	12.5

Table 2. Summary of degree of substitution (DS), glass transition temperatures (T_g), critical aggregation concentrations (CAC), surface tension, and minimum inhibitory concentrations (MIC) of OSA-*g*-EPL(s).ND, not determined.

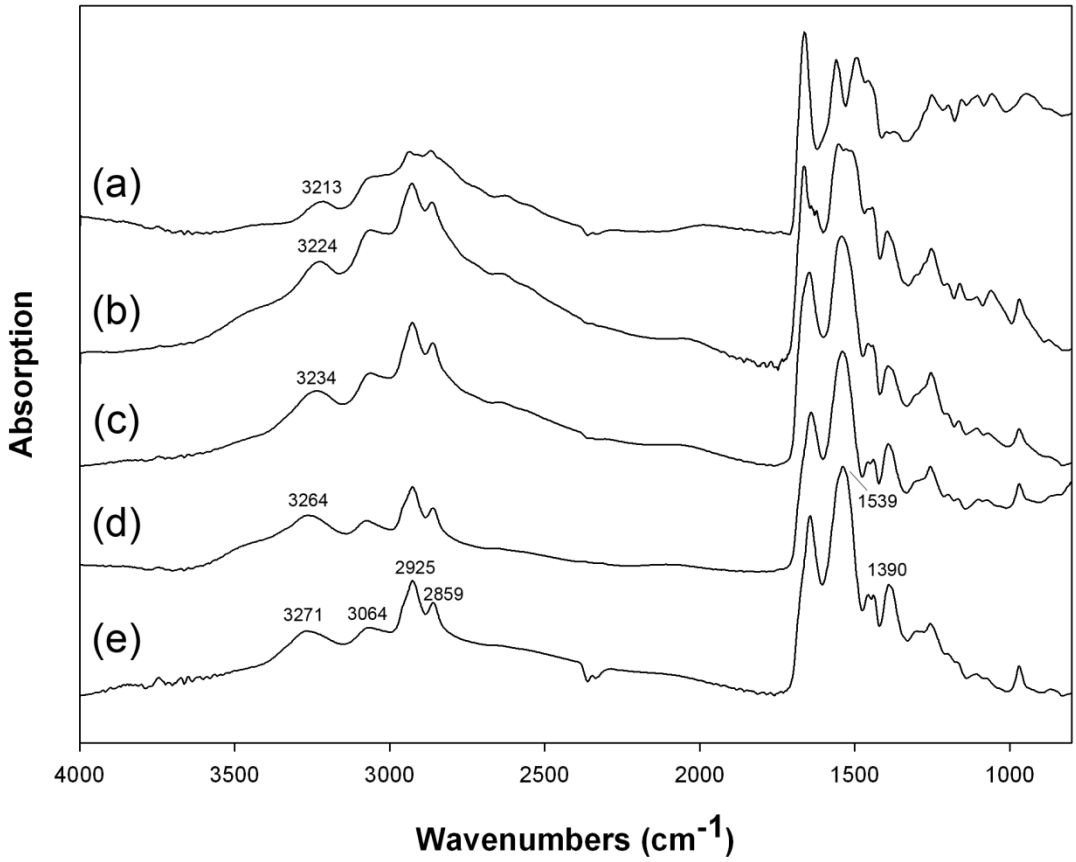

Figure 19. . ATR FT-IR spectra of (a) EPL, (b) OSA-*g*-EPL6.2, (c) OSA-*g*-EPL8.5, (d) OSA-*g*-EPL12.4, and (e) OSA-*g*-EPL20.5. Numbers on the spectra indicated the wavenumbers of the corresponding peak positions.

Thermal Properties of OSA-g-EPL(s)

The thermal properties of modified EPL(s) were analyzed by differential scanning calorimetry (DSC). For comparison, dialyzed EPL sample was also analyzed. From Figure 20, it was shown that each of the five samples gave a single glass transition temperature (T_g), and with the increase of DS, T_g decreased from 133.1 ^oC for EPL to 60.6 ^oC for OSA-*g*-EPL20.5 (Figure 20 and Table 2). The decrease of T_g was due to the plasticizing effect of OSA moieties, since OSA has a much lower melting point and glass transition temperature (*162*). It was noteworthy that the dialyzed EPL only showed a single T_g at 133.1 ^oC, which was different from what was reported (T_g at 88 ^oC and T_m at 172.8 ^oC) (*126*). This may be due to the different chemical constitutions and purification procedures from different manufacture sources. Meanwhile, it was also noted that before dialysis, the EPL sample has two T_g(s) at 92.6 ^oC and 165.1 ^oC (not shown), suggesting that the salt contents and small-molecular-weight lysine oligomers may interfere with the DSC results.

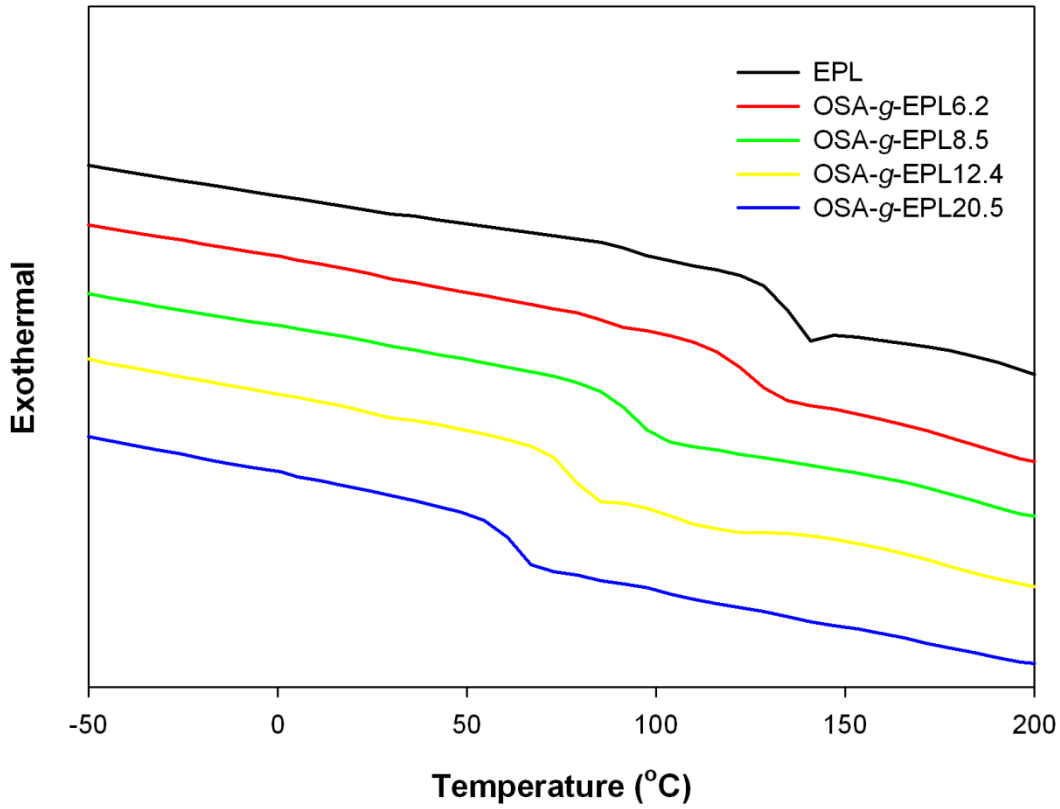

Figure 20. Differential scanning calorimetry analysis of EPL and OSA-*g*-EPL(s). Only the curves from the second heating procedure were shown.

Self-assembly of OSA-g-EPL(s) in water

It is self-evident that OSA-*g*-EPL(s) were amphiphilic and would aggregate and form polymer micelles in aqueous solutions above their critical aggregation concentrations (CACs). Considering that polymer micelles have been well applied in delivery systems (*163*, *164*), it is important to investigate whether and above what concentration the OSA-*g*-EPL(s) are able to form polymer micelles. Therefore, the CACs of OSA-*g*-EPL(s) were determined with pyrene fluorescence excitation spectra method (*154, 163*). For instance, the excitation spectra of pyrene in OSA-*g*-EPL12.4 water solution were shown in Figure 21A. At low polymer concentration, one peak in the spectrum was at 334nm. With increase of the OSA-*g*-EPL12.4 concentration, pyrene migrated into the hydrophobic micro-domains formed by the polymer aggregate, and the peak shifted gradually to 337 nm. By calculating the ratio of the fluorescence intensity at 337 to that at 334 (I337/I334), the critical aggregation concentration could be determined. As shown in Figure 21B, 0.32 mg/mL was the onset concentration where I337/I334 started to increase abruptly, and thus was the CAC of OSA-*g*-EPL12.4 in deionized water. As shown in Table 2, all of the OSA-*g*-EPL(s) molecules were able to form polymer micelles in water. The increase of the OSA substitution caused decrease of the CAC value, with the lowest CAC being 0.18mg/ml for OSA-*g*-EPL20.5.

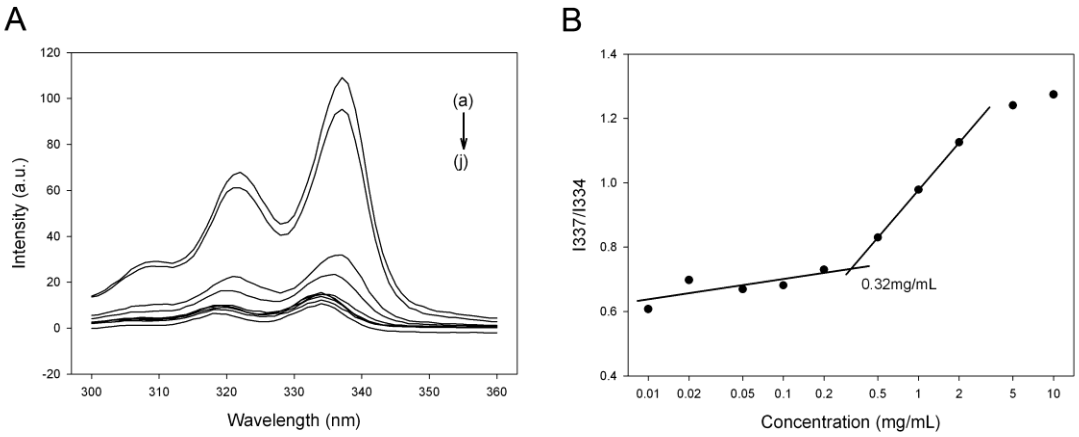

Figure 21. Determination of the critical aggregation concentrations (CACs) of OSA-*g*-EPL12.4.

Samples	Effective diameter (nm)	Polydispersity
OSA-*g*-EPL6.2	42.0 ±2.6	0.359
OSA-*g*-EPL8.5	110 ±2.0	0.080
OSA-*g*-EPL12.4	102.2 ±0.1	0.089
OSA-*g*-EPL20.5	72.2 ±4.2	0.263

Table 3. Summary of the effective hydrodynamic diameters and polydispersity of OSA-*g*-EPLs.

The particle size of the OSA-*g*-EPL(s) was determined using dynamic light scattering at the concentration of 5 mg/mL [above the CMCs of all the OSA-*g*-EPL(s)]. It was found that the hydrodynamic diameters of the polymer micelles were in the range of 40-110 nm (Table 3). The corresponding hydrodynamic radii of hydration were from 20 to 55 nm. The smaller particle size of OSA-*g*-EPL20.5 may be due to the compact packing of the hydrophobic core of the polymer micelle.

Interfacial properties of OSA-g-EPL (s)

As amphiphiles, OSA-*g*-EPL(s) could also form adsorption layers on the air/water interface and lower the interfacial tension. The air/water surface tension of the OSA-*g*-EPL(s) at the concentration of 5 mg/mL [above CACs of all the OSA-*g*-EPL(s)] was measured with pendant drop method and was in the range of 35-40 mN/m, while the surface tension of original EPL remained at the similar level as pure water (Table 2), which was consistent with a previous report (*136*). This result further confirmed the amphiphilicity of synthesized OSA-*g*-EPL(s) and suggested that OSA-*g*-EPL(s) could be used as emulsifiers in emulsion formulation.

Antimicrobial activity of OSA-g-EPL(s)

A high antimicrobial activity is essential for a bi-functional emulsifier. However, previous studies suggested that chemical modification to the α-amine groups of EPL would lower its antimicrobial activity (*129*, *136*). Therefore, to examine the antimicrobial activities of OSA-*g*-EPL(s), the minimum inhibitory concentrations (MICs) of OSA-*g*-EPL(s) against *E.coli* O157:H7 were determined and compared with that of unmodified EPL. Interestingly, the MICs of all the four OSA-*g*-EPL(s) remained the same as that of

EPL, being 12.5 μg/mL (Figure 22). This result suggested that OSA-*g*-EPL(s) retained the antimicrobial activity of EPL.

OSA-g-EPL is able to stabilize emulsions.

It was previously shown that OSA-*g*-EPL is able to lower the surface tension of water, which suggests that, in principle, it could also lower the interfacial tension between water and oil and thus stabilize emulsions. In this study, an oil-in-water (O/W) emulsion system stabilized with M-EPL was prepared and the particle size of the oil droplets during preparation and storage was monitored. As shown in Figure 23, after 20-mins high-speed homogenization, the particle size of the oil droplets decreased to about 155 nm. Actually, 5-mins homogenization is already able to make the particle size down to 175 nm. It could be due to the small fraction of oil (1%) in this system. If the oil fraction increases, more time/energy is expected to be needed to achieve the same particle size. Original EPL was not able to stabilize the emulsion systems, phase separation immediately occurred (data not shown), which corresponded to the previous observation that EPL is not surface (*158*).

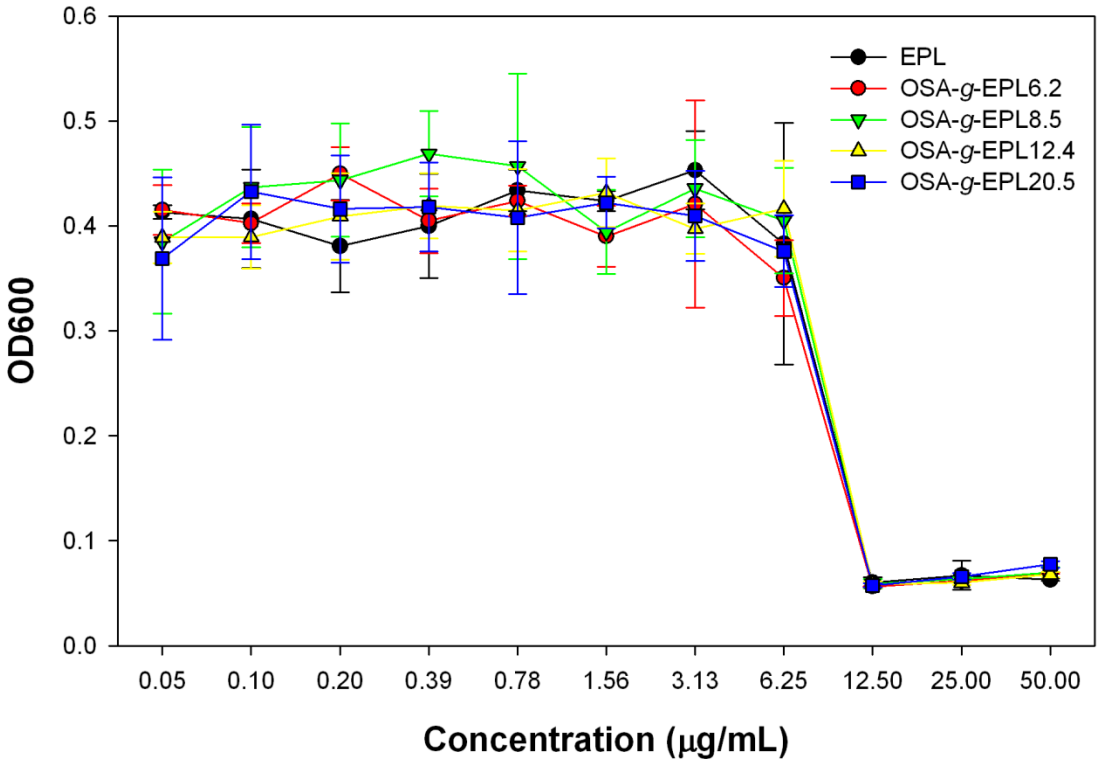

Figure 22. Optical absorption at 600nm (OD_{600}) of *E.coli* O157:H7 versus the concentrations of EPL, OSA-*g*-EPL6.2, OSA-*g*-EPL8.5, OSA-*g*-EPL12.4, and OSA-*g*-EPL20.5. The minimum inhibitory concentrations of these polymers against *E.coli* O157:H7 were all found to be 12.5 μg/ml.

This model emulsion system made with M-EPL was also stable during storage. After 32 days of storage, the size of the oil droplet increased to about 165 nm (Figure 24) and only a very thin layer of creaming was noticed on the water surface, suggesting that the emulsion was fairly stable, even in the absence of any thickeners.

Cytotoxicity of M-EPL increased with the degree of substitution

The safety issue of any synthetic or modified biopolymers is of great concern when they are proposed to use in food system. The cytotoxicity of M-EPLs with difference degrees of substitution was examined on HepG2 cells. It was shown that unmodified EPL has very weak cytotoxicity, its IC_{50} value was not detected in the tested concentration range, which is consistent with the *in vivo* toxicity study (*132*). The IC_{50} values of OSA-g-EPL8.5, OSA-g-EPL12.4 and OSA-g-EPL20.5 were 574, 443 and 335 μg/mL, respectively (Figure 25). The cytotoxicity increased along with the increase of the degree of substitution, suggesting that these cationic emulsifiers might incorporate into the cell membrane and cause cell death. As a matter of fact, many synthetic emulsifiers used in food industry have in vitro cytotoxicity (*165*). More detailed i*n vivo* examination is needed to address the safety issue

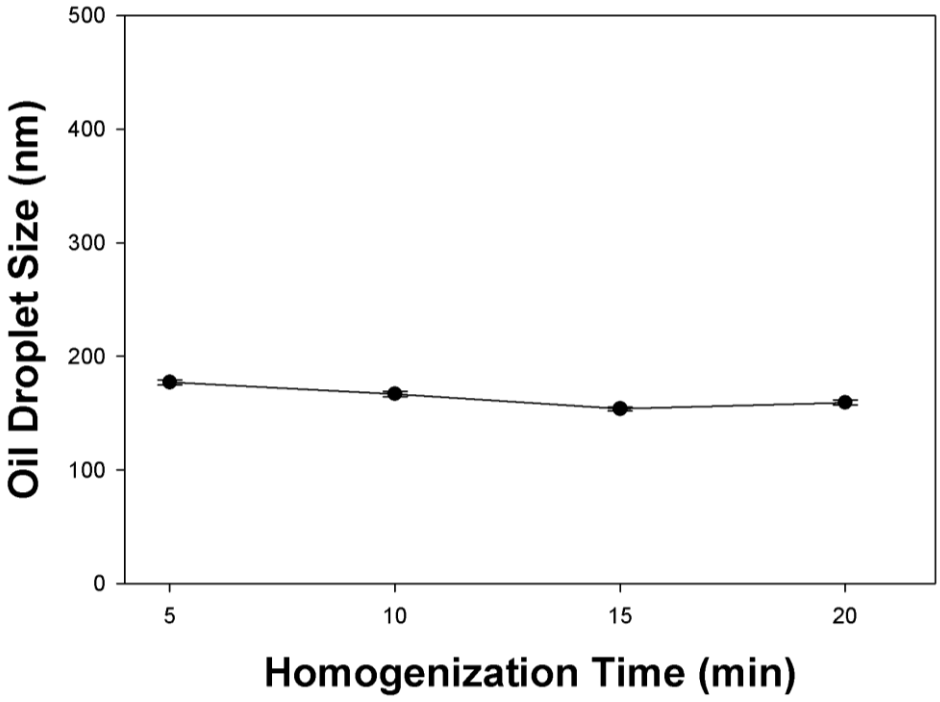

Figure 23. Formation of OSA-g-EPL stabilized O/W emulsion using high-speed homogenization. Data are shown as mean ± standard error, n=3.

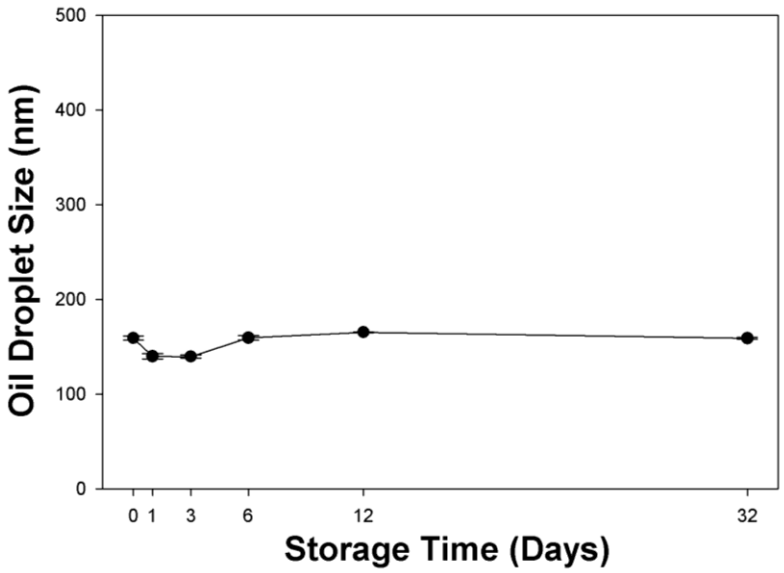

Figure 24. Stability of emulsions formed with OSA-g-EPL. Data are shown as mean ± standard error, n=3.

.

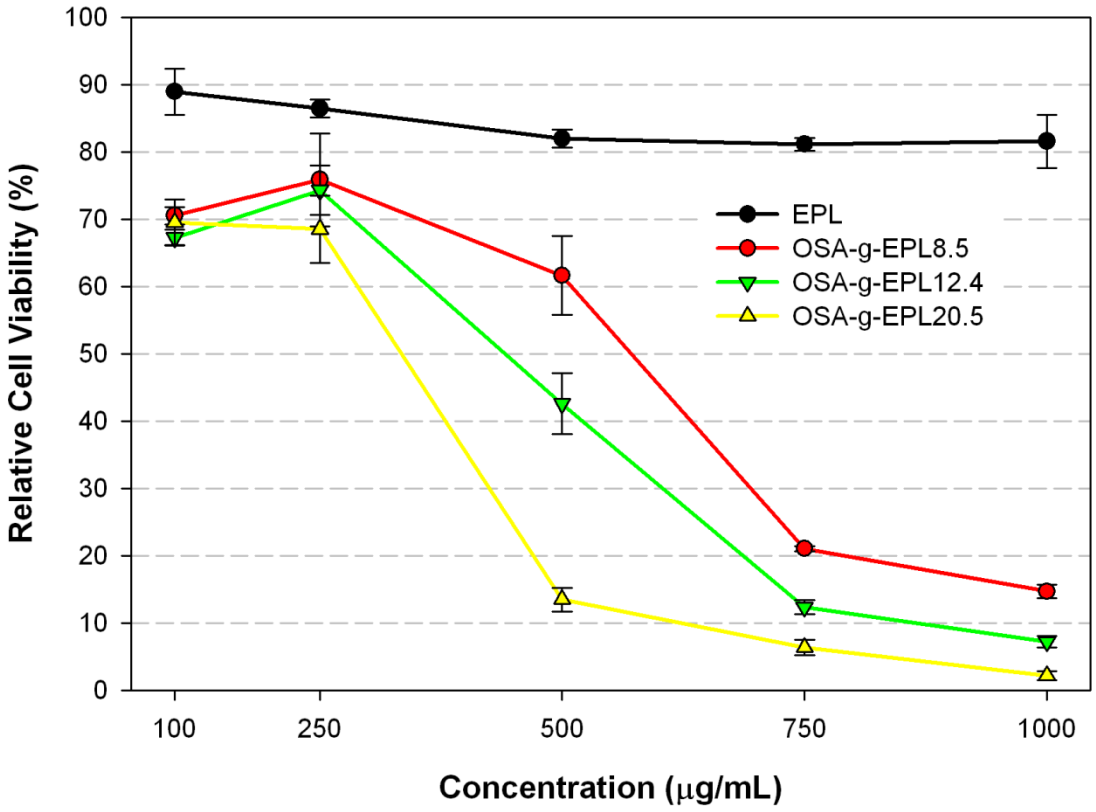

Figure 25. The cytotoxicity of EPL and M-EPLs on HepG2 cells. Data are shown as mean ± standard deviation, n=4.

OSA-g-EPL decreased TEER values through Caco-2 monolayer.

Transepithelial electrical resistance (TEER) is a rapid and convenient method to evaluate the integrity of Caco-2 cell monolayers. It also provides a prediction of the paracellular permeation rate of hydrophilic compounds across Caco-2 monolayers, and suggests a faster absorption in small intestine. Because of the tight junctions between adjacent cells, TEER value of confluent and differentiated Caco-2 monolayer is much greater than that of porous supporting polymer membrane (background TEER reading). In my studies, the background TEER reading was 119 ± 7 $\Omega \times cm^2$. After 21 days of culture, at my hand, Caco-2 cell monolayers typically had TEER reading greater than 2000 $\Omega \times cm^2$, which was higher than that of some other investigators, while was lower than others. This phenomena was well noticed in the field and was thought to be due to the different colonies, different passage numbers or different culturing conditions, such as serum (*16*).

In the literature, it has been shown that some absorption enhancers increase the absorption of hydrophilic compounds through compromising tight junctions. One type of such excipient is chitosan and its derivatives, and the positive charge of chitosan is thought to interact with the negative charged cell membrane and cause disruption of actin network and the tight junction (*166-171*).

Since the modified EPL, OSA-g-EPL still kept most of the primary amine groups of original EPL, its effect on TEER across Caco-2 monolayers was investigated. As shown in Figure 26, TEER of untreated Caco-2 monolayers maintained the same through the experiment, while OSA-g-EPL greatly decreased the TEER reading immediately after the treatment. Furthermore this decrease was dose-dependent: 10 μg/mL caused about 75%

decrease of TEER reading after 90-minute treatment, while 20 μg/mL OSA-g-EPL minimized the TEER to about only 6%.

The effect of OSA-g-EPL on the TEER was also reversible. After removal of treatment and overnight cultivation in culture media, the TEER reading returned to its original level before treatment. These results suggest that OSA-g-EPL was able to transiently and reversibly decrease TEER of Caco-2 monolayer, and may be served as an absorption enhancer for the paracellular transport of hydrophilic bioactives.

For all the absorption enhancers, toxicity is always a concern. To further investigate the cytotoxicity of OSA-g-EPL treatment on TEER, two assays were performed right after treatment and after overnight recovery of Caco-2 cells in culture media. Lactate dehydrogenase is thought to be a constitutional enzyme in cell cytoplasm. Disruption of cell membrane, an important outcome of cytotoxicity causes leakage of LDH from cytoplasm into media. Therefore the amount of LDH leakage could be used as a marker for cytotoxicity. In the case of OSA-g-EPL treatment on Caco-2 monolayers, immediately after removal of OSA-g-EPL, the lactate dehydrogenase (LDH) leakage was measured. It was clearly shown that 25 μg/mL OSA-g-EPL caused substantial leakage of lactate dehydrogenase out of cells, suggesting disruption of the intact of cell membranes. This leakage was much mitigated, equaling to about 31 % of cell lysis. On the other hand, untreated cells have little LDH leakage (Figure 27 A). The increased LDH leakage with OSA-g-EPL treatment suggests cytotoxicity of OSA-g-EPL, which may caused from its positive charge disrupting the cell membrane.

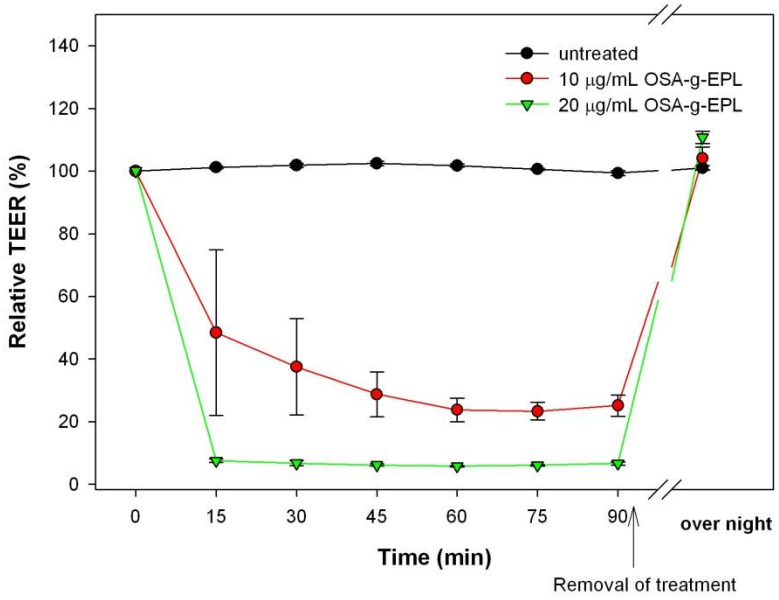

Figure 26. Effect of OSA-g-EPL treatment on the TEER of Caco-2 monolayer. After 90 minutes treatments, OSA-g-EPL was removed. The last data points were measured on the next day after cultivation in growth media over night

However, the MTT assay performed on the next day reveals no permanent cell death caused by OSA-g-EPL treatment, in that cells treated with 10 μg/mL OSA-g-EPL had about the same MTT activity with untreated cells, while cells treated with 25 μg/mL OSA-g-EPL had even higher MTT activity (Figure 27 B). Considering these two contradictory results together with the finding of recovery of TEER overnight, it may be concluded that the disruption of cells (TEER decrease caused by actin disorganization and LDH leakage caused by positive charge of OSA-g-EPL), although temporary and reversible, suggest some negative effect on Caco-2 monolayers. These results should be taken into serious account when applying OSA-g-EPL to any food or pharmaceutical applications.

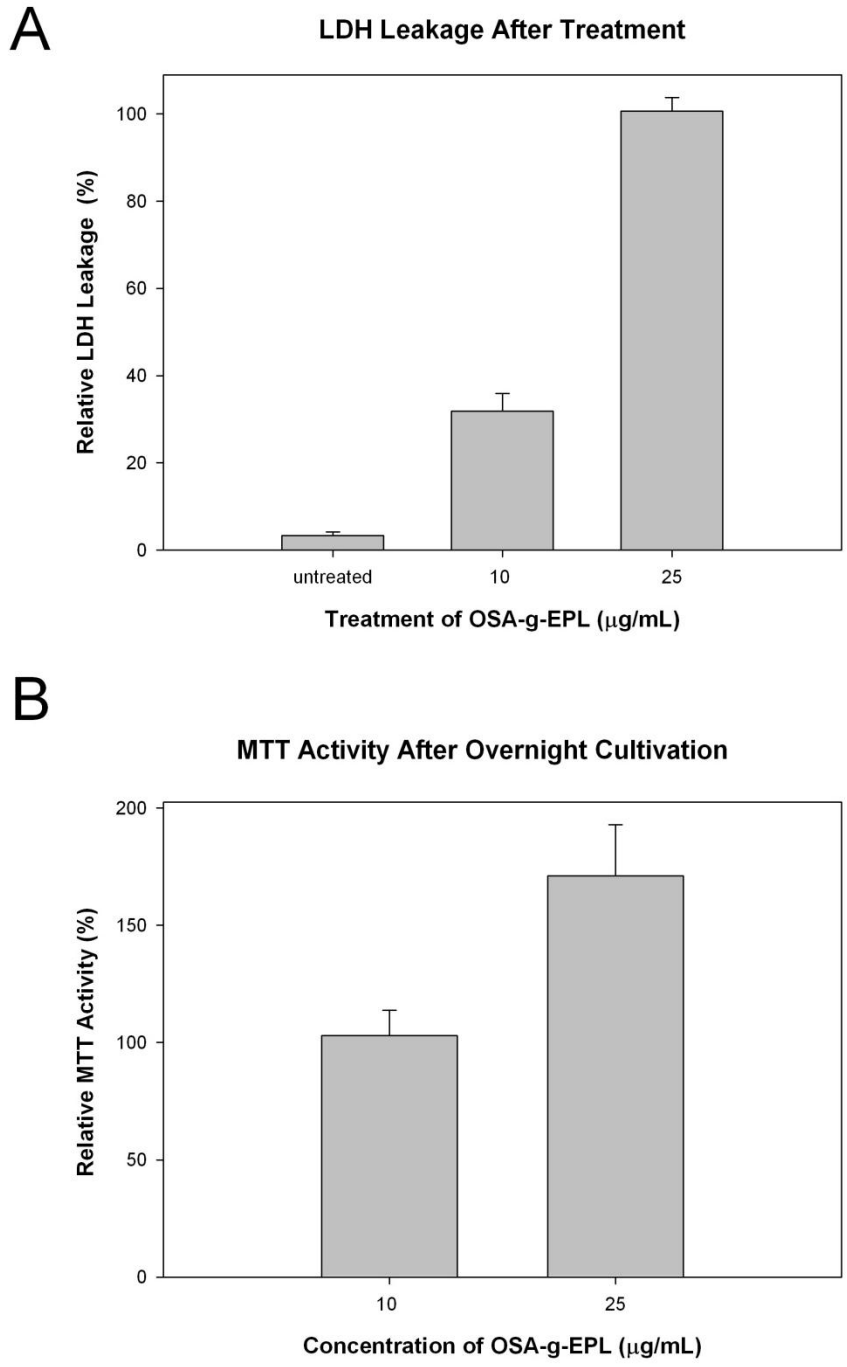

Figure 27. Examination of the Cytotoxicity of OSA-g-EPL treatment on Caco-2 monolayers. A. LDH leakage level right after removal of OSA-g-EPL. The LDH activities in the media were compared to the level of surfactant-lyzed cells. B. MTT assay measuring the viable cell number after overnight recovery.

Conclusion

In summary, OSA-*g*-EPL(s) with different degrees of OSA substitution were successfully synthesized by conjugating OSA onto the amino groups of EPL molecules, confirmed by ^{1}H NMR and ATR-FTIR spectroscopy. Furthermore, they were demonstrated as bi-functional materials: on one hand, they were amphiphiles, and able to self assemble to form micelles, lower the surface tension of water and stabilize O/W emulsions; on the other hand, they retained the antimicrobial activity of EPL. Our results suggested that OSA-EPL(s) were novel functional ingredients that could be used as antimicrobial emulsifiers in food industry. Additionally, the cytotoxicity assay of OSA-g-EPL(s) revealed that cytotoxicity increases with the increase of degree of substitution, but the IC50 values for all the compounds were greater than 300 g/mL (300ppm), suggesting they may be used as food additives.

OSA-g-EPL was also found to be able to decrease the TEER reading of Caco-2 monolayers reversibly, suggesting its potential use as an absorption enhancer of hydrophilic bioactives. On the other hand, the toxicity of OSE-g-EPL revealed by LDH leakage assay suggest a cautious use of OSA-g-EPL in food and pharmaceutical applications before further in vivo safety evaluations.

CHAPTER 4. ENCAPSULATION OF CURCUMIN IN MICELLES FORMED BY MODIFIED EPSILON POLYLYSINE

In the previous section (Section D.2.), it was shown that modified EPLs were synthesized and they were able to form polymer micelles in dH2O. In this study, the micelle structures of M-EPLs were analyzed using synchrotron small angle X-ray scattering (SAXS). Subsequently, three loading methods were compared to achieve the maximal water solubility of curcuminoids upon encapsulation in the M-EPL-based polymer micelles. Furthermore, the effects of polymer micelle encapsulation on the stability against alkaline hydrolysis and the cellular antioxidant activity of curcuminoids were also investigated.

Materials and Methods

Materials Curcuminoids powder containing about 82% curcumin, 15% demethoxycurcumin (DCur) and 3% bisdemethoxycurcumin (BDCur) was received as a gift from Sabinsa Corporation (Piscataway, NJ, United States). ε-Polylyine (EPL) was purchased from Zhejiang Silver-Elephant Bioengineering Co., Ltd., China, and used without further purification. Octenyl succinic anhydride (OSA), sodium bicarbonate ($NaHCO_3$), dimethyl sulfoxide (DMSO), and chloroform were purchased from Sigma-Aldrich. Dialysis membranes (molecular weight cutoff 1000Da) were obtained from Spectrum Laboratories. Glacial acetic acid, HPLC-grade water and acetonitrile were from J.T. Baker.

HepG2 cells were generously provided by Dr. Mou-Tuan Huang from Department of Chemical Biology, Rutgers, the State University of New Jersey. Minimum Essential Medium (MEM), Hank's buffered salt solution (HBSS), RPMI-1640 media, fetal bovine serum (FBS), phosphate buffered saline (PBS), 100X penicillin and streptomycin, and 0.25% trypsin with ethylenediaminetetraacetic acid (EDTA), L-glutamine, were all purchased from Thermo Scientific. Insulin, 2',7'-dichlorfluorescein-diacetate (*DCFH-DA*), 2,2′-azobis (2-amidinopropane) (ABAP), Williams' Medium E (WME), hydrocortisone were purchased from Sigma-Aldrich.

Synthesis of modified ε-polylysine (M-EPLs) M-EPL was synthesized according to our previous paper (*158*). Briefly, EPL was dissolved in DMSO and different amounts of octenyl succinic anhydride were added dropwise. After 18-hours' reaction at about 35-40 ^{o}C, the products were dialyzed and lyophilized. Degree of substitution was calculated from ^{1}H-NMR spectra of M-EPLs. To prepare the modified EPL for curcuminoids encapsulation, 10 g EPL and 4.3 mL OSA were used.

Small-angle X-ray scattering (SAXS) measurements SAXS intensity profiles were collected at the BioCAT, 18-ID beamline, at the Advanced Photon Source, Argonne National Laboratory. The sample-detector distance was set at 2.592 m to cover a Q range of 0.006-0.3 Å^{-1} (with a Mar165 CCD being offset laterally relative to the X-ray beam). A flow cell of 1.5mm diameter capillary equipped with a brass block (thermostatted with a water bath) was utilized for holding samples. A MICROLAB 500 Hamilton pump was applied to load samples to the flow cell at a constant rate (10 μL/s) during X-ray exposure to minimize radiation damage. The X-ray wavelength was 1.033 Å and a short exposure period of 1 second was used to acquire the scattering data. The whole experiment was

kept at room temperature. Fifteen curves were collected for each sample and their averaged curves were utilized for further analysis. The final SAXS profiles were gained after subtracting the solvent background. Pair distribution functions were acquired to obtain the dimension parameters of modified ε-polylysine of different degrees of substitution.

Encapsulation of curcuminoids into M-EPL micelles Three loading methods were compared in the aspect of the loading capacity.

(1) *Solvent evaporation*. Fifty milligrams of M-EPL were dissolved in 10mL distilled water. Ten milligrams of curcuminoids were dissolved in 5 mL chloroform. The aqueous solution and chloroform were mixed together and homogenized at 24000 rpm for 10 min using a high-speed homogenizer (ULTRA–TURRAX T-25 basic, IKA Works). The coarse emulsion was kept in a chemical hood and stirred over night to evaporate chloroform. On the next day, the solution was filtered through 0.45 μm filter to remove curcuminoids precipitate and freeze dried.

(2) *Dialysis*. Fifty milligrams of M-EPL and 10 mg curcuminoids were dissolved in 10 mL DMSO and then dialyzed against distilled water (dH_2O) in a dialysis bag with molecular-weight-cut-off (MWCO) equal to 1,000. After repeated dialysis, solutions in the dialysis bag were filtered through 0.45μm filter and freeze dried.

(3) *High-speed homogenization*. Fifty milligrams of M-EPL were dissolved in 10 mL dH_2O and 10 mg curcuminoids were added in. Subsequently, the curcuminoids suspension was homogenized at 24000 rpm for 10 minutes and then stirred overnight at room temperature. On the second day, the solution was filtered and freeze dried (*172*).

To quantify the curcuminoids amount encapsulated in the M-EPL micelle, lyophilized curcuminoids in M-EPL micelles were dissolved in dH2O at the concentration of 1 mg/mL. Two volumes of HPLC-grade acetonitrile was then added in and mixed before quantification using HPLC.

In all the following assays, M-EPL encapsulated curcuminoids were obtained using the dialysis method.

Quantification of curcuminoids using High-Performance Liquid Chromatography (HPLC) An UltiMate 3000 HPLC system with 25D UV-VIS absorption detector (Dionex) and a Nova-Pak C18 3.9×150mm column (Waters) were used. Mobile phase solvents were: (A) 2% acetic acid in HPLC-grade water, purged with helium, and (B) HPLC-grade acetonitrile. All aqueous samples were mixed with two volumes of acetonitrile and filtered through 0.22μm filter. Fifty microliter samples were injected into the column. Gradient elution was applied to separate the three curcuminoids: -2 to 0 minutes, 65% A and 35% B; 0 to 15 minutes, linear gradient from 35% B to 55% B; 15 to 20 minutes, held at 55% B; and from 20 to 21 minutes, B went back to 35%. Flow rate was set at 1 mL/min. Detection wavelength was fixed at 420 nm.

Dynamic light scattering M-EPL and freeze dried curcuminoids in M-EPL micelle were dissolved in dH2O at the concentration of 5 mg/mL and filtered through 0.45 μm filter. The particle size (hydrodynamic diameter) of the samples were then determined using dynamic light scattering method (BIC 90plus particle size analyzer, Brookhaven Instrument) at room temperature. The results were presented as mean ± standard error (n=3).

Differential scanning calorimetry (DSC) Curcuminoids powder, curcuminoids and M-EPL mixture, and curcuminoids encapsulated in M-EPL micelle were analyzed using differentiation scanning calorimetry with a DSC823e thermal analyzer (Mettler Toledo, Columbus, OH) to detect the possible curcuminoids crystals. About 10 mg of each sample were put in the aluminum pan and the lid of the pan was penetrated to form a small hole. Samples were heated from 25 to 200 ^{o}C, at the rate of 10 ^{o}C per minute. Curcuminoids M-EPL mixture contained 5% curcuminoid powder and 95% M-EPL (w/w), and was grinded for better mixing.

Hydrolysis stability of curcuminoids in M-EPL micelles Freeze dried curcuminoids in M-EPL micelle sample were dissolved in dH_2O at concentration of 1 mg/mL (with about 50 μg/mL curcuminoids). Curcuminoids in DMSO was added to dH_2O to make a 50 μg/mL curcuminoids aqueous dispersion. Both solutions were diluted 10 times into PBS (pH7.4). At different time intervals (15, 30, 45 and 60 minutes), the solutions were sampled, acidified with HCl and analyzed with HPLC to quantify the curcuminoids contents.

Cellular antioxidant activity (CAA) assay for free curcuminoids and m-EPL encapsulated curcuminoids HepG2 cells (Passage 8-18) were regularly maintained in MEM with 10% FBS, 100 units/mL Penicillin and 100 μg/mL Streptomycin. CAA assays were performed according to the literature (*173*). Briefly, sixty thousand cells/well were plated in a 96-well microplate in the CAA growth medium (William Medium E supplemented with 5% FBS, 10 mM Hepes, 2mM L-glutamine, 100 units/mL penicillin 100 μg/mL streptomycin). On the next day, cells were treated with curcuminoids, M-EPL encapsulated curcuminoids, or M-EPL alone in the treatment medium (WME + 2 mM L-

glutamine + 10 mM Hepes) with DCFH-FA for 1 hour. Then, cells were washed with PBS and treated with 600 μM ABAP in HBSS. Emission fluorescence intensity at 528 nm (slits 20nm) with excitation at 485nm (slits 20nm) was recorded every 5 minutes for 1 hour at 37 ^{o}C using a Synergy HT multi-mode microplate reader (BioTek). Cells treated with DCFH-FA and then HBSS+ABAP were used as the positive control (P.C.). Cells with DCFH-FA then only HSBB without ABAP were used as the negative control (N.C.).

To calculate the CAA value of each treatment, the area-under-the-curve (AUC) for the plot of fluorescent intensity against time was calculated with trapezoidal method. Then the CAA value was calculated as

$$CAA = 100 * (1 - \frac{AUC\ (treatment) - AUC\ (N.C)}{AUC\ (P.C.) - AUC\ (N.C.)}) \quad (1)$$

Subsequently, F_a/F_u was plotted against the concentration of curcuminoids on double logarithmic scale, where F_a =CAA and F_u=100-CAA. EC_{50} was determined as the concentration where F_a/F_u=1. By linear regression of the data on the plot, this value was able to be obtained mathematically. The molecular weight of curcumin was used to calculate the molar concentration of curcuminoids.

Statistical analysis.

One way-ANOVA analysis with Holm-Sidak method was performed using the SigmaStat software.

Results and Discussion

Characterization of M-EPL micelles using synchrotron small angle X-ray scattering (SAXS)

In our previous studies, M-EPLs (or called OSA-*g*-EPLs) were shown to be able to form micelles and the critical aggregation concentrations (CAC) of M-EPLs with different degree substitution were determined (*158*). In the current work, the micelle structures of M-EPLs were further investigated using synchrotron small-angle X-ray scattering (SAXS). Figure 28 displays the SAXS scattering profiles of 5 mg/ml OSA-*g*-EPLs solutions with different degrees of substitution (8.5%, 12.4%, and 20.5%, respectively). The fitting curves of those SAXS scattering profiles were simultaneously obtained from the inversed Fourier transform of pair distribution function by Irena package in Igor Pro software. The critical aggregation concentrations (CACs) for OSA-*g*-EPL8.5, OSA-*g*-EPL12.4, and OSA-*g*-EPL20.5 were 0.64 mg/ml, 0.32 mg/ml, and 0.18 mg/ml respectively (*158*). Therefore, 5 mg/ml was well above the CACs of the micelles and under that condition OSA-*g*-EPLs formed micelle aggregates. It was found that at the low Q region ($Q < 0.2$ Å^{-1}), OSA-*g*-EPLs formed large aggregates due to the hydrophobic interaction from octenyl succinic anhydride (OSA) groups. In the medium Q region (0.02~0.1 Å^{-1}), all of the SAXS profiles showed a broad peak at $Q \sim 0.04$ Å^{-1}, which corresponded to the spacing between micelles. The intensities and the peak positions of the above peaks depended on the micelle dimensions and the surface charge density of the micelle. In order to obtain the shape and size information of M-EPLs, pair distribution function (PDF) curves were obtained from both Irena Package, a tool imbedded in Igor

Pro software provided by BIOCAT beamline of Advanced Photon Sources (APS) (*174*) and GNOM (*175*).

Figure 29 shows the two PDF curves of OSA-*g*-EPL12.4 solution generated from GNOM and Irena package. It is clear that the data obtained from GNOM and Irena package have negligible difference. Therefore, only one set of dimensional parameters from Irena package were selected herein for display. As shown in Figure 30, the bell shape of all three PDF curves indicated the spherical shape of the large micelle aggregates. However, the dimension parameters of these three OSA-*g*-EPLs were not identical.

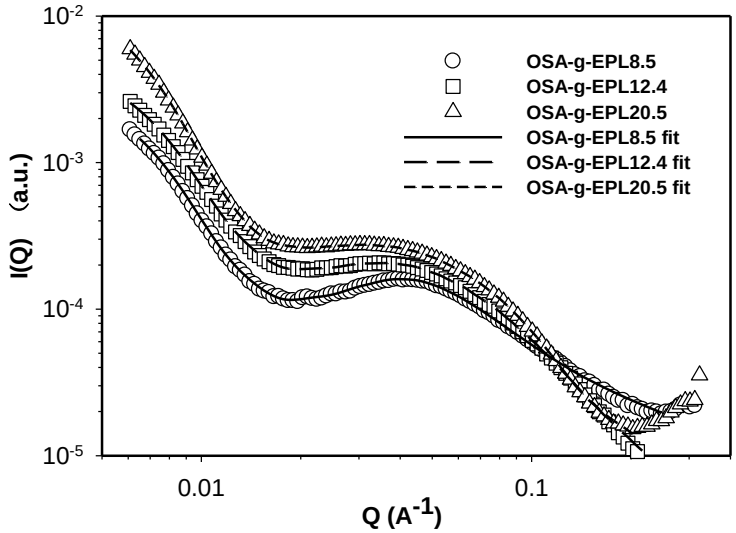

Figure 28 Small-angle x-ray scattering profiles of modified ε-polylysine with different degrees of substitution. The solid line was obtained from the inversed Fourier transform of pair distribution function (PDF) by Irena package in Igor Pro software. PDF curves were normalized for better comparison

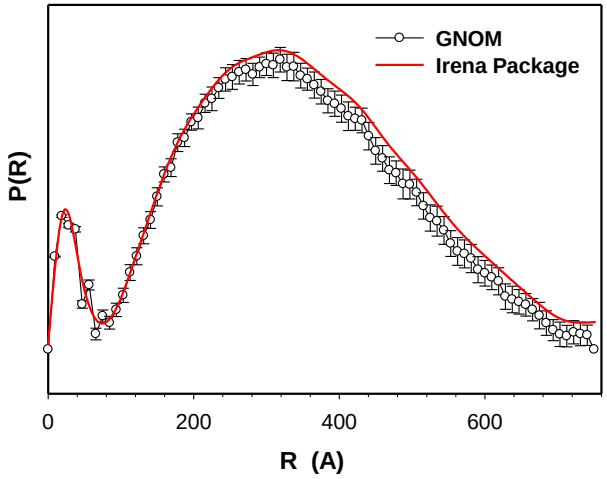

Figure 29 Comparison of pair distribution functions of OSA-g-EPL with 12.4% degree of substitution (DS) generated from either GNOM (empty circles) or Irena package (solid line).

lists the dimension parameters of the micelle aggregates, including maximum dimension (D_{max}), radius of gyration (R_g), peak 1&2 positions and micelle number within a single aggregate. It was found that D_{max}, the largest dimension within size distribution, and R_g, radius of gyration, reached the lowest value for OSA-*g*-EPL12.4 are 752 Å and 268 Å, respectively. The dimensions of those three OSA-g-EPLs were similar with each other although their PDF curves were not exactly overlapping. There appeared two peaks in all three PDF curves of OSA-*g*-EPLs. From, the first peak located at ~24 Å, was reasonably relevant to the size of individual micelle. The second peak, located at ~330 Å with a 15~40 Å shift for large aggregates, corresponded to the average size of OSA-*g*-EPLs micelle aggregate. Therefore, it was thought that the large aggregation was composed of small global micelles tightly connected with each other within the large global micelle aggregate. The aggregation number $n_{aggregation}$ of micelles in one aggregate can be calculated through the forward scattering I (Q=0), which was reasonably used in other amphiphilic structures as well (*176*). The forward scattering I (Q=0) was obtained through a Guinier fit of the scattering profile in the low Q range. It was shown that the aggregation number within one micelle aggregate at 5mg/ml increased from 366 for OSA-*g*-EPL8.5 to 1242 for OSA-*g*-EPL20.5. It suggested that the increase of substitution degrees caused more micelles to aggregate and form larger particles, which can also be verified by the PDF curves' peak shift towards a large value when the degree of substitution was increased. This result was also consistent with the relatively large particle sizes determined by dynamic light scattering (*158*).

Encapsulation of curcuminoids using M-EPL micelles

The hydrophobic cores of M-EPLs micelles may serve as a microenvironment to solubilize water-insoluble bioactive compounds and thus increase their water solubility. In the following section, curcuminoids were used as examples to illustrate the capability of M-EPL micelles to encapsulate and solubilize water-insoluble bioactive compounds.

Table 4. Dimension parameters of modified ε-polylysine of different degrees of substitution

	D_{max} (Å)	R_g (Å)	Peak 1 (Å)	Peak 2 (Å)	$n_{aggregation}$
OSA-*g*-EPL8.5	778	276	24	326	366
OSA-*g*-EPL12.4	752	268	24	311	529
OSA-*g*-EPL20.5	800	308	26	357	1242

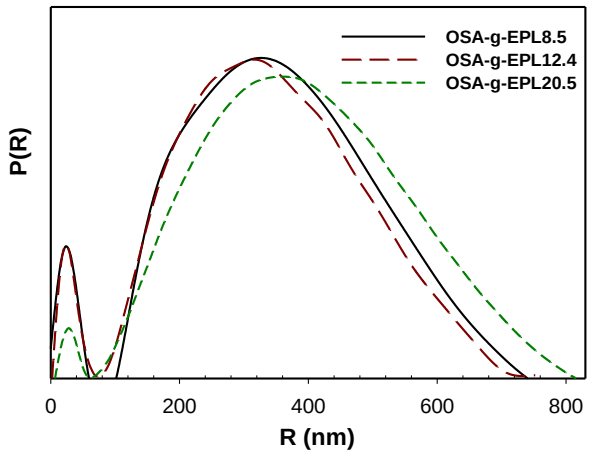

Figure 30. Pair distribution function (PDF) curves of modified ε-polylysine with different degrees of substitution (DS): 8.5% (solid line); 12.4% (long dash line); and 20.5% (short dash line).

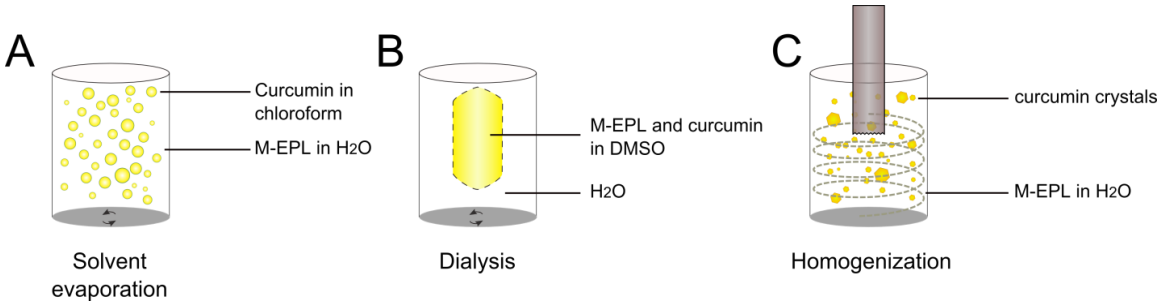

Figure 31 Scheme of three loading methods used to encapsulate curcuminoids into M-EPL micelles: (A) Solvent evaporation - curcuminoids were dissolved in chloroform and M-EPL was dissolved in distilled water (dH_2O). Coarse emulsion was generated by high-speed homogenization. Subsequently, chloroform was removed by evaporation; (B) dialysis - curcuminoids and M-EPL were co-dissolved in DMSO and dialyzed again dH2O to remove DMSO; and (C) high-speed homogenization (HSH) - HSH was used to break down the curcuminoids crystals, and the high shear force facilitated curcuminoids dissolution and encapsulation.

Loading water-insoluble compounds into the hydrophobic core of polymer micelles is usually controlled by kinetics. Different loading methods usually have different efficiencies (*177*). In this study, three loading methods (solvent evaporation, dialysis and homogenization) were compared to find the best way to achieve the highest loading capacity (and thus the water solubility) of curcuminoids in M-EPL micelles (Figure 31). In the solvent evaporation method (Figure 31**A**), chloroform with dissolved curcuminoids was homogenized to form a coarse emulsion in the M-EPL solution. As chloroform evaporated, a fraction of curcuminoids was trapped in the M-EPL micelles. In the dialysis method (Figure 31**B**), M-EPL and curcuminoids were both dissolved in DMSO and dialyzed against dH_2O. As the DMSO inside the dialysis bag was replaced by dH_2O, curcuminoids were gradually encapsulated in M-EPL micelles. In the homogenization method (Figure 31**C**), a simple high-speed homogenization was used. Under high shear, curcuminoids crystals were expected to be broken into smaller size, which according to Ostwald-Freundlich equation, would have greater water solubility and thus be easier to be encapsulated into micelles. In our previous study, similar method was used to encapsulate curcumin into micelles formed by hydrophobically modified starch (*172*)

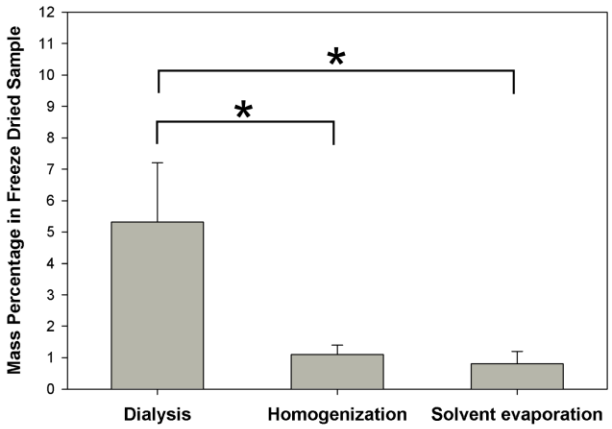

Figure 32 Mass percentages of curcuminoids in freeze-dried M-EPL samples prepared by three loading methods. Data are presented as mean ± standard deviation (n=3). * denotes statistically significant difference (P<0.05).

The encapsulated curcuminoids in the three methods were then quantified by HPLC. As clearly showed in Figure 32, the dialysis method resulted in the highest loading capacity: in dried samples, curcuminoids accounted for 5.3 ± 1.9 % (w/w), which was significantly higher than that in homogenization (1.1 ± 0.3 %) and solvent evaporation methods (0.8 ± 0.4 %). Accordingly, in 1 mg/mL M-EPL micelle solution, the maximal solubilized curcuminoids concentration was 53 ± 19 μg/mL. Compared with the water solubility of curcuminoids (11 ng/mL) (*62*), this represented almost 5,000-fold increase.

The percentages of the three curcuminoid compounds encapsulated in the micelles were also compared with that of curcuminoids raw materials (Table 5). It was found that the composition of curcuminoids prepared by dialysis was similar to that of original curcuminoids powder, while the composition of curcuminoids prepared by either solvent evaporation or high-speed homogenization had a slightly lower content of curcumin, suggesting that different loading methods may have weak preference toward selected curcuminoid components.

Table 5 Composition of curcuminoids encapsulated from the three loading methods: dialysis, high-speed homogenization, and solvent evaporation

Curcuminoids compound	Raw materials	Dialysis	High-speed homogenization	Solvent evaporation
Cur (%)	82.1 ± 1.0	82.4 ± 1.3	77.7 ± 1.0	78.3 ± 5.4
D-Cur (%)	14.8 ± 0.5	14.8 ± 0.9	15.8 ± 0.4	13.9 ± 1.1
BD-Cur (%)	3.1 ± 0.5	2.8 ± 0.3	6.5 ± 0.6	7.8 ± 6.5

Data are presented as mean ± standard deviation (n=3, except for raw materials, n=12).

Additionally, dynamic light scattering was used to examine the particle size of the M-EPL micelles before and after encapsulation of curcuminoids: the hydrodynamic diameter of pure M-EPL micelle was 74.7 ± 1.0 nm with polydispersity of 0.424, while that of M-EPL micelle with curcuminoids was 135.5 ± 1.5 nm with polydispersity as 0.273. The results suggested that the encapsulation of curcuminoids can cause M-EPL micelles to associate and form larger micellar aggregates.

Differential scanning calorimetry (DSC) analysis

After micelle encapsulation, curcuminoids were thought to be solubilized in the core of the M-EPL micelles instead of existing as large crystals. To confirm the encapsulation and solubilization, DSC analyses were performed to detect curcuminoids crystals in the samples of curcuminoids powder, curcuminoids/M-EPL mixture, and curcuminoids in M-EPL micelles. As shown in Figure 33, curcuminoids powder was in crystal form and had a melting peak at 178 ^{o}C. Our HPLC analysis indicated that the curcuminoids powder contained about 82% curcumin, 15% DCur and 3% BDCur (w/w, Table 5). The melting points for curcumin, DCur and BDCur were reported as 184, 172 and 222 ^{o}C, respectively (*178*). Therefore, the melting peak of the curcuminoids powder at 178 ^{o}C may mainly arise from the compounded effect of curcumin and DCur. In the curcumin M-EPL mixture sample, much smaller melting peaks were also noticeable, as indicated by the arrow in Figure 33A and more apparently in Figure 33B, which showed two small peaks locating at 178 ^{o}C and 182 ^{o}C respectively. In contrast, there was no melting peak detected in the curcuminoids/M-EPL micelle sample, suggesting that curcuminoids were indeed encapsulated and solubilized in the M-EPL polymer micelle.

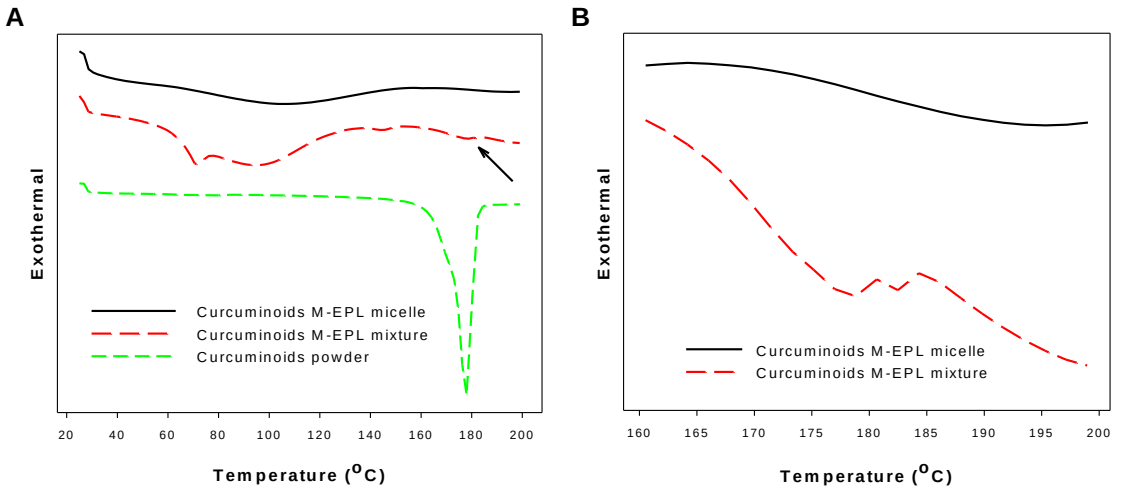

Figure 33 (A) Differential scanning calorimetry (DSC) results of curcuminoids, curcuminoids/M-EPL simple mixture, and curcuminoids encapsulated in M-EPL micelle prepared by dialysis method. Arrow indicates the melting peaks of curcuminoids in the mixture; and (B) Zoom-in DSC curves of simple mixture of curcuminoids and M-EPL as well as curcuminoids encapsulated in M-EPL micelle through dialysis in the temperature from 160 to 200 °C.

The DSC results also suggest that compared with other types of formulations, such as solid lipid nanoparticle and liposome, this micelle encapsulation system is ready to be lyophilized and reconstituted.

M-EPL micelle encapsulation stabilized curcuminoids at pH 7.4

It is well known that although curcumin has higher water solubility in basic aqueous solutions, it undergoes rapid hydrolysis (*88*, *179-181*). In this study, we examined the effect of M-EPL encapsulation on preventing curcuminoids hydrolysis at pH 7.4. As shown in Figure 34**A**, the result suggested that free curcuminoids underwent rapid hydrolysis, while encapsulation in M-EPL micelles was able to stabilize curcuminoids as other micelle systems formed by small-molecular-weight surfactants (*179, 180*).

Since the curcuminoids used in this study contained curcumin, DCur and BDCur, the stability of each individual curcuminoid compound with and without encapsulation was examined simultaneously. As shown in Figure 34**B**, different curcuminoid compounds had different hydrolysis rate at pH 7.4. Namely, curcumin underwent fastest hydrolysis, followed by DCur, while BDCur was relatively resistant to the hydrolysis. To our best knowledge, this was the first time to discover that different curcuminoids showed different stability against hydrolysis at weak alkaline condition. Since BDCur was relatively stable and soluble at pH 7.4, its bioactivity and bioavailability compared with that of curcumin may need further examination.

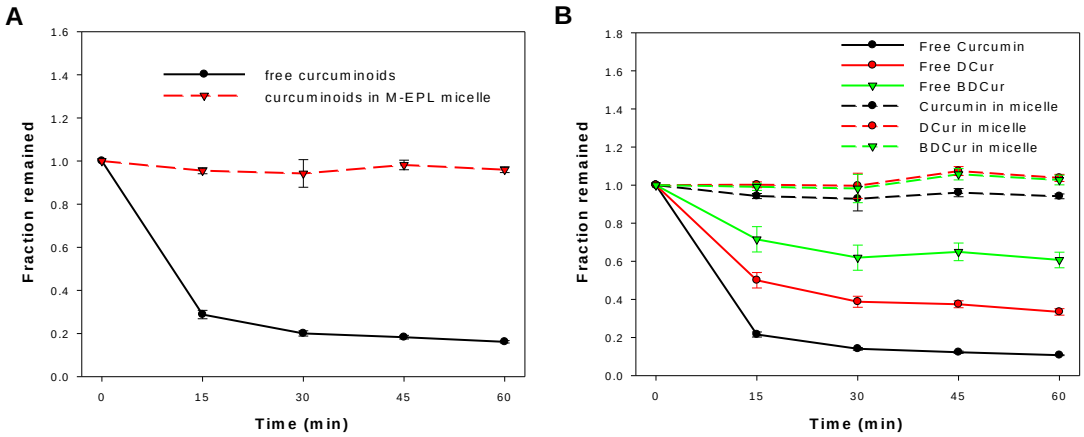

Figure 34 Stability of curcuminoids at pH 7.4: (A) The stability of total curcuminoids for the free curcuminoids versus curcuminoids encapsulated in M-EPL micelle through dialysis; and (B) The stability of curcumin, demethoxycurcumin (DCur), and bisdemethoxycurcumin (BDCur) for their free forms versus each component encapsulated in M-EPL micelle through dialysis. Data are shown as mean ± standard deviation (n=3).

Encapsulated curcuminoids showed elevated cellular antioxidant activity

Curcuminoids, especially curcumin, with their phenolic groups, beta-diketone and double bonds structure, are well-known antioxidant compounds. Using a recently-developed cell-based method (*182*), the cellular antioxidant activity (CAA) of curcuminoids was measured. As shown in Figure 35, the EC_{50} value of curcuminoids was determined as 4.4 μM, which was among the most potent natural antioxidants (*182*). Furthermore, the CAA values of encapsulated curcuminoids were compared with that of free curcuminoids at the concentration of 2 μM, at which, the CAA value of M-EPL used for encapsulation was close to zero (Figure 36). It was clearly shown that encapsulated curcuminoids had greater CAA value than free curcuminoids, suggesting M-EPL micelle encapsulation may serve as a good delivery system for curcumin(oids) and other water-insoluble bioactives. Although it would be ideal to determine the EC_{50} of encapsulated curcuminoids, M-EPL at higher concentrations exhibited various antioxidant activities (not shown) and may interfere with the interpretation of the CAA results for the encapsulated curcuminoids. Therefore, only the situation where modified EPL has negligible CAA value was shown and the CAA values of free curcuminoids and encapsulated curcuminoids were compared.

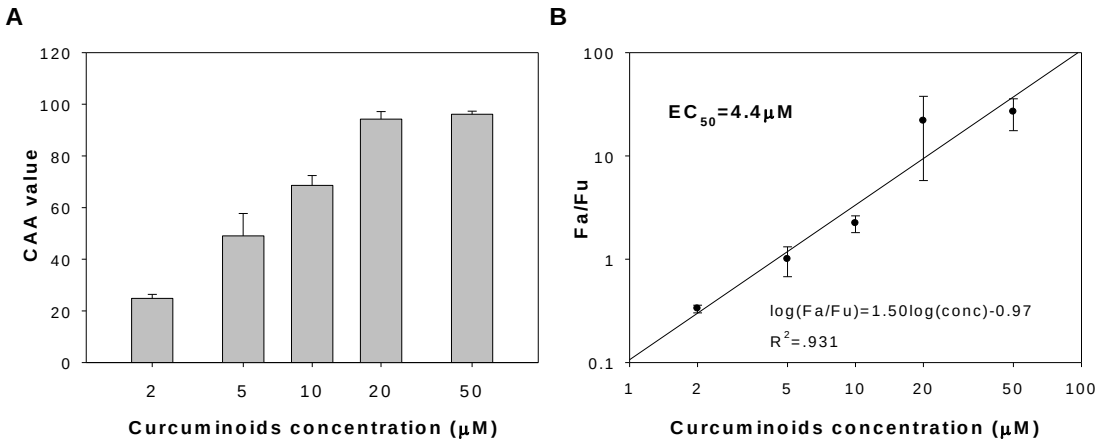

Figure 35 Measurement of the cellular antioxidant activity of curcuminoids: (A) Cellular antioxidant activity (CAA) of curcuminoids at different concentrations; and (B) Determination of the EC_{50} of curcuminoids. Data are shown as mean ± standard deviation (n=3).

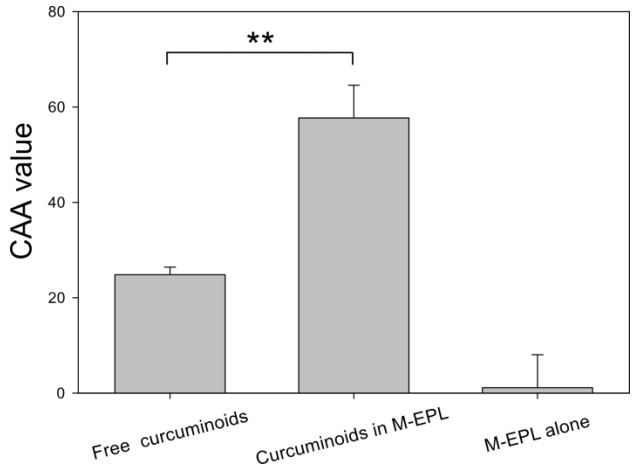

Figure 36 Comparison of the CAA values of free curcuminoids and encapsulated curcuminoids. CAA values were determined at the curcuminoids concentration of 2 μM. Data are presented as mean ± standard deviation (n=4). ** denoted for very significant difference ($p<0.001$, t-test).

Two mechanisms may be used to explain the enhanced cellular antioxidant activity upon encapsulation. First, free curcuminoids were technically dispersed from DMSO solution into the cell media, which may form sub-micron sized particles and have limited solubility. Encapsulated curcuminoids, on the other hand, were originally in the dissolved form in the micelle core and may still largely remain soluble form upon dilution in the treatment media. Therefore, the concentration of *dissolved* curcuminoids was expected to be greater in curcuminoids micelle solution than in curcuminoids dispersion. The second possible mechanism may be the rapid hydrolysis of curcuminoids at weak basic condition. Treatment media were at pH 7.4, which may cause rapid degradation of curcuminoids, as shown in Figure 34. On the other hand, encapsulation may stabilize curcuminoids against hydrolysis. Thus, the curcuminoids amount and the cellular antioxidant activity from the micelle encapsulation were expected to be greater. On the other hand, these interpretations did not exclude the possibility that M-EPL had specific interaction with the HepG2 cells which might facilitate the movement of curcuminoids into/onto the cells.

Conclusion

In summary, modified epsilon polylysine was able to form polymer micelles. From the SAXS analysis, the M-EPL micelles were spherical and able to further form micelle aggregates. This micelle system was used to encapsulate curcuminoids. It was demonstrated that dialysis method generated a higher loading capacity than either the solvent evaporation or high-speed homogenization method. The micelle encapsulation was confirmed as no crystals of curcuminoids were detected after encapsulation. Meanwhile, it was shown that upon encapsulation, curcuminoids were stabilized against hydrolysis at pH 7.4, and had enhanced cellular antioxidant activity compared with free

curcumin. This work suggested that M-EPL may serve as a delivery system for curcuminoids and other water-insoluble nutraceuticals.

CHAPTER 5. HIGH PERMEATION RATE OF CURCUMIN THROUGH CACO-2 MONOLAYER BY PASSIVE DIFFUSION

Curcumin is a polyphenolic bioactive compound found in the spice turmeric, and possesses many health-promoting benefits, such as anti-cancer, anti-inflammatory, anti-oxidation and anti-microbial activities (*1-5*). These benefits of curcumin, however, are curtailed by its low oral bioavailability (*6*). Therefore, improvement of curcumin's oral bioavailability should be focused in the functional food research.

Solubilization, absorption and metabolism are three important steps that modulate the oral bioavailability. It is known that low water solubility and rapid metabolism limit the bioavailability of curcumin. Curcumin is water insoluble. The water solubility is estimated as no more than 11ng/mL (*7*). Most of the orally administered curcumin was found in feces (*8, 9*). Meanwhile, absorbed curcumin undergoes rapid metabolism. The major metabolites from oral administration are curcumin glucuronide and sulfate (*10, 11*).

On the other hand, our understanding about the absorption/permeation mechanism of solubilized curcumin is still very limited. Two research groups used everted rat intestinal sac assay to examine the absorption of curcumin (*12, 13*). The results on the percentage of intestinal absorption, however, were conflicting. Moreover, the authors neither examined the absorption mechanism nor provided quantitative results on the curcumin absorption/permeation rate.

Caco-2 cell monolayers, in comparison, have been widely used to determine the permeation rate and to examine the permeation mechanisms of bioactive compounds (*14*). Moreover, different studies demonstrated that *in vivo* absorption could be well predicted from the apparent permeation rate (P_{app}) across the Caco-2 cell monolayers (*15-17*). Although the P_{app} obtained from different laboratories are different, there is a general trend that a high P_{app} implies high absorption. Generally speaking, $P_{app} > 1 \times 10^{-6}$ cm/s means high permeation, while $P_{app} < 1 \times 10^{-7}$ cm/s implies low permeation (*15, 16*). At the same time, the absorption mechanisms can also be examined. By performing two-way (apical to basolateral and basolateral to apical) permeation experiments and calculating the rate ratio, the existence of potential active efflux/uptake can be identified. In general, if P_{app}(B-A)/P_{app}(A-B) is greater than 2 or less than 0.5, the active uptake or efflux mechanisms are suggested respectively. Otherwise, the absorption mechanism may simply be passive diffusion (*18*).

Since curcumin is water insoluble and solubilization is the prerequisite of absorption, many formulations such as protein complexation (*19-22*) and various lipid-based formulations (*23-27*) have been developed to increase the solubilization of curcumin. Proteins have hydrophobic cores, thus are able to solubilize curcumin. The binding between proteins and curcumin is strong. For example, the equilibrium constants of curcumin and different proteins are between 10^4 and 10^6 M^{-1} (*19, 21, 22*). In comparison, lipid-based formulations do not solubilize curcumin directly in aqueous solution. Instead, after lipid digestion, triglycerides in the formulation are hydrolyzed into fatty acids, which contribute to the intrinsic bile-phospholipids mixed micelles. Consequently, curcumin that is originally dissolved in the lipid-based formulation is now solubilized in

the micelle aqueous solution (*28*). The binding between curcumin and small molecular weight micelles is much weaker than the protein complexation, with the binding constant in the magnitude of only 10^2-10^3 M^{-1} (*29*, *30*).

In this study, the permeation rate measurements using Caco-2 cell monolayers have been carried out to investigate the absorption of solubilized curcumin. The absorption mechanism was examined by comparing the permeation rates of curcumin in two opposite directions (apical to basolateral versus basolateral to apical) across the Caco-2 monolayers. Meanwhile, the effect of different solubilization agents, such as dimethyl sulfoxide (DMSO), bile-fatty acid mixed micelles, and bovine serum albumin (BSA) on the permeation rates of curcumin was also examined. This research may illustrate the limiting factors as well as the effect of different formulations on curcumin absorption.

Materials and Methods

Materials. Curcumin, which contains about 85% curcumin, 11% demethoxycurcumin and 4% bisdemethoxycurcumin (26), was obtained from Sabinsa Corporation, USA. Lucifer yellow and dimethyl sulfoxide (DMSO) were purchased from Sigma-Aldrich. Glacial acetic acid, HPLC-grade water and acetonitrile were from J.T. Baker.

Caco-2 cell line was generously provided by Dr. Judith Storch, Department of Nutrition, Rutgers, the State University of New Jersey, USA. Dulbecco's Modified Eagle Medium (DMEM), Hank's Buffered Salt Solution (HBSS), fetal bovine serum (FBS), 100X non-essential amino acids, 100X penicillin and Streptomycin, 0.25% trypsin with ethylenediaminetetraacetic acid (EDTA), 1M 4-(2-hydroxyethyl)-1-piperazineethane-

sulfonic acid (HEPES) and bovine serum albumin (BSA) were all purchased from Fisher Scientific. Transwell permeable polycarbonate inserts (0.4μm) and 12-well cell culture plates were obtained from Corning.

Maintenance of Caco-2 cell culture. Cells were maintained in DMEM with 10% FBS, 1X non-essential amino acids and 1X penicillin and streptomycin, at 37^{o}C with 5% CO2. Cells of passage 35-45 to keep relatively constant cellular phenotypes were used in this study.

Permeation experiments across Caco-2 monolayers. Procedures for the determination of apparent permeation rate of curcumin across Caco-2 generally followed the detailed protocol described previously (*18*). To generate Caco-2 cell monolayers in the insert filters of 12-well plates, 0.5 mL Caco-2 cells were plated onto the insert (in the apical compartment) at the density of 6×10^5 cell/mL. 1.5 mL culture media were subsequently added in the lower (basolateral) compartment of each well. Media were changed every two days. Permeation experiments were performed after 21- 29 days of plating.

In the permeation experiments, 20 μg/mL curcumin in the donor media were obtained by diluting curcumin DMSO solution, or BSA/mixed micelle solubilized curcumin into donor media. Two donor media were used as noted in the text: *a.* HBSS + 25 mM HEPES, pH 7.4; *b.* HBSS + 10 mM methanesulfonic acid, pH 6.5. HBSS + 25mM HEPES + 4% BSA, pH7.4 was used as receiving medium throughout the study. BSA was added to solubilize permeated curcumin, while the addition of BSA to the receiving media could mimic the *in vivo* condition (*18*). In the permeation direction of apical to

basolateral (A-B) compartment, 0.4 mL donor media with 20 μg/mL curcumin was added to the apical compartment and 1.2 mL receiving media were added to the basolateral compartment. In the direction of B-A, 1.2mL donor media with 20 μg/mL curcumin was added to the basolateral compartment and 0.4mL receiving media were added in the apical chamber. Plates were then put in a shaker at 100 rpm and 37 ^{o}C. After 15, 30, 45, 60 minutes of permeation, half volumes of the receiving media were removed and the same volumes of fresh media were replenished.

The removed receiving media were mixed with two volumes of acetonitrile by vortexing briefly and centrifuged at 16,000g in a bench-top microcentrifuge for 15 minutes. The supernatants were filtered through 0.45 μm filter and analyzed with HPLC for curcumin quantification.

Cumulative quantity of curcumin permeated at each time interval was calculated and plotted against time. The initial slope was then used to calculate the apparent permeation rate (P_{app}) using the following equation:

$$P_{app} = \left(\frac{dQ}{dt}\right)\left(\frac{1}{AC_0}\right) \quad (1)$$

where dQ/dt is the rate of curcumin permeation. *A* is the surface area of the insert (1.1cm^2), C_0 is the initial curcumin concentration.

Quality control of Caco-2 cell monolayers. To ensure the integrity of Caco-2 monolayers, transepithelial electrical resistance (TEER) value and the apparent permeation rate of lucifer yellow were determined.

TEER value was measured before each experiment using Evohm2 epithelial voltmeter (World Precision Instruments), and calculated as

$$TEER\ (\Omega \cdot cm^2) = (TEER(\Omega) - TEER_{background}(\Omega)\ ) \times Area(cm^2) \qquad (2)$$

where TEER(Ω) is the electrical resistance across Caco-2 monolayers directly read from the Evohm2 epithelial voltmeter, $TEER_{background}(\Omega)$ is that across the insert only (without cells). Area(cm^2) is the area of the insert, 1.1cm^2.

Meanwhile, the permeation rate of lucifer yellow, a paracellular permeation marker was determined in the direction of A-B (*14*). Lucifer yellow at 1 mg/mL in donor media *b* was added to the apical chamber. Permeated lucifer yellow in the receiving compartment (with no BSA added, since lucifer yellow is water soluble) was quantified as arbitrary fluorescence emission intensity at 540nm (with 20nm slits) excited at 430nm (with 10nm slits). P_{app} of lucifer yellow was determined using the same equation as curcumin.

Solubilization of curcumin in BSA and in bile-fatty acid mixed micelles. Solubilization of curcumin in BSA (formation of curcumin-BSA complex) was achieved by pipetting curcumin DMSO solution into 4% BSA in donor solution *b* (*31*) .

Curcumin solubilized in bile-fatty acid mixed micelles were obtained by *in vitro* lipid digestion of curcumin organogel (*27*). Briefly, curcumin organogel was made by dissolving curcumin in monostearin-medium chain triglyceride organogel, which was then digested by pancreatic lipase and ultracentrifuged at 50,000 rpm to remove undigested organogel and precipitated curcumin. The resultant aqueous solution was bile-fatty acid mixed micelles with solubilized curcumin, which was further diluted to 20 μg/mL curcumin in donor solution *b* for permeation experiments.

High performance liquid chromatography (HPLC). Curcumin was quantified by HPLC, using a UltiMate 3000 HPLC system with 25D UV-VIS absorption detector (Dionex). Nova-Pak C18 3.9×150mm column (Waters) was used. Mobile phase solvents were: (A). 2% acetic acid in water, purged with helium, and (B). acetonitrile. Fifty microliters samples were injected into the column. Gradient elution was applied to separate the three curcuminoids: 0 to 2 min, 65% A and 35% B; 2 to 17 min, linear gradient from 35% B to 55% B; 17 to 22 min, held at 55% B; 22 to 23 min, B went back to 35% linearly. Flow rate was set at 1 mL/min. Detection wavelength was 420 nm.

Statistical analysis. One-way ANOVA analysis was performed using SigmaStat with SigmaStat integration. All the data shown are mean ± standard deviation, n=3.

Results

Development of HPLC method to quantify curcumin

Curcumin, demethoxycurcumin (D-Cur) and bisdemethoxycurumin (BD-Cur) were three major curcuminoids that co-exist in most curcumin products . The amount of D-Cur and BD-Cur could account for about 15% or more. Therefore, a sensitive HPLC method to separate and quantify the three curcuminoids was established first before the investigation of the permeation mechanism of curcumin.

Figure 37 showed a typical HPLC chromatogram separating the three compounds in the curcumin samples used in this study. The retention times for BD-Cur, D-Cur and curcumin were approximately 9.80, 10.32 and 10.95 minutes, respectively. Meanwhile, since the three compounds had similar mass absorption coefficient (*32*), the mass percentages of the three compounds were calculated directly from the peak areas of the

three peaks: 82.1 ± 1.0 % for curcumin, 14.8 ± 0.5 % for D-Cur, and 3.1 ± 0.5% for BD-Cur, which is consistent with the previous report (*26*)

Different standard concentrations (10, 20, 50, 100, 200, 500 ng/mL, 1, 2, 5, 10, 20, 50, 100 μg/mL) of total curcuminoids were analyzed by HPLC to generate calibration curves for the three curcuminoid compounds. Since the concentration range was broad, four calibration curves of different concentration ranges were generated for each of the three compounds and the total curcuminoids (Table 6).

.

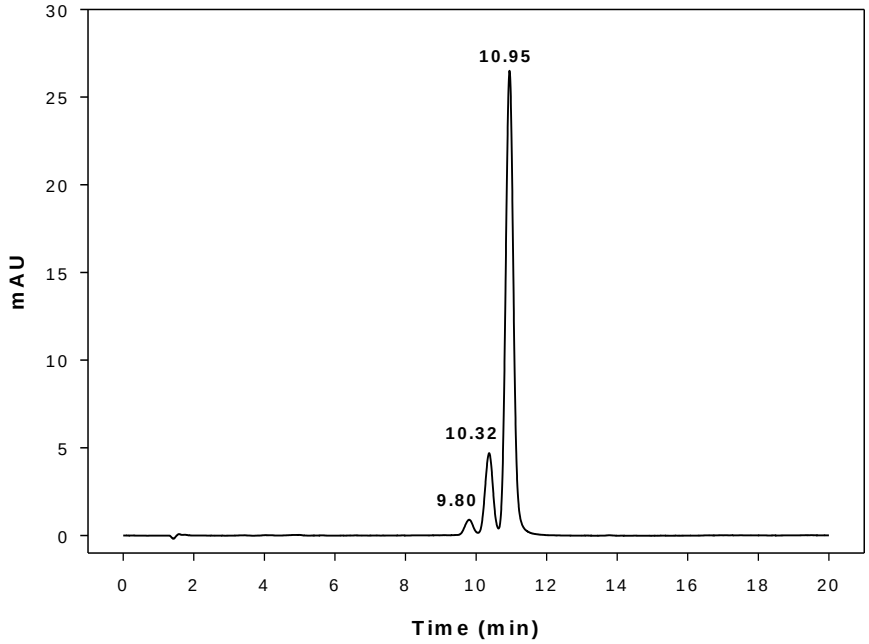

Figure 37 A typical chromatogram of three curcuminoids analyzed by HPLC. Fifty microliter injection of 0.2 µg/mL total curcuminoids were shown here.

Table 6 Summary of the equations of the calibration curves for curcumin, D-Cur , BD-Cur and total curcuminoids from HPLC.

	X range (concentration, μg/mL)	Y range (peak area, mAU)	Equation	r^2
Curcumin	0.0082 - 0.082	0.0073 - 0.68	Y=8.142X + 0.0027	0.9975
	0.082 - 0.82	0.68 - 6.95	Y=8.494X - 0.0725	0.9993
	0.82 - 8.2	6.95 - 69	Y=8.412X - 0.2793	0.9997
	8.2 - 82	69 - 600	Y=7.143X + 16.7867	0.9993
D-Cur	0.00148 - 0.0148	0.012 - 0.12	Y=8X - 0.0002	0.9954
	0.0148 - 0.148	0.12 - 1.24	Y= 8.441X - 0.0176	0.9986
	0.148 - 1.48	1.24 - 12.4	Y=8.414X - 0.0891	0.9996
	1.48 - 14.8	12.4 - 122	Y=8.22X - 0.3027	0.9992
BD-Cur	0.00062 - 0.0031	0.005 - 0.0213	Y=6.594X - 0.009	0.9999
	0.0031 - 0.031	0.0213 - 0.2417	Y=7.904X - 0.0069	0.9968
	0.031 - 0.31	0.2417 - 2.6387	Y=8.674X - 0.0682	0.9989
	0.31 - 3.1	2.6387 - 31.668	Y=10.435X - 0.5751	0.9998
Total curcuminoids	0.01 - 0.1	0.0847 - 0.8203	Y=8.094X - 0.0017	0.9974
	0.1 - 1	0.8203 - 8.4343	Y=8.468X - 0.0971	0.9991
	1 - 10	8.4343 - 84.158	Y=8.421X - 0.4366	0.9997
	10 - 100	84.158 - 753.418	Y=7.404X + 15.9089	0.9997

Examination of the permeation mechanism of curcumin

Two quality control procedures were performed to confirm that the Caco-2 cell monolayers were confluent and suitable for the permeation study: **A.** Only the wells with the TEER values greater than 300 $\Omega \cdot cm^2$ were used (*18*); **B.** the permeation rate of lucifer yellow, a paracellular transport marker, is expected to be less than 1×10^{-6} cm/s (*33*), which was determined as $0.10 \pm 0.01 \times 10^{-6}$ cm/s in this study. Therefore, the Caco-2 cell monolayers were appropriate to be used in the permeation study.

Subsequently, the permeation rate of solubilized curcumin (by DMSO dispersion) was determined in the direction of A-B, with donor media pH set at 6.5, to mimic the acidic microenvironment in the small intestine (*34*). As shown in Figure 38**A**, over 2% of curcumin was transported through the Caco-2 cell monolayers in 60 minutes. The corresponding P_{app}(A-B) was determined as $7.1 \pm 0.6 \times 10^{-6}$ cm/s , which was thought as a fast permeation rate and implied a fast absorption rate *in vivo* (*15, 16*).

The absorption mechanism of curcumin was then investigated by performing permeation experiments in both A-B and B-A directions with the pH of both donor and receiving compartments set at 7.4. As shown in Figure 38**B**, P_{app}(A-B) and P_{app}(B-A) were 8.6 ± 0.8 and $11.5 \pm 1.4 \times 10^{-6}$ cm/s, respectively and the efflux ratio P_{app}(B-A)/P_{app}(A-B) was calculated as 1.4, which was less than 2, a common cut-off to suggest an active efflux. Therefore, the mechanism of permeation was suggested as passive diffusion with no active efflux/uptake involved.

Based on the investigation above, it is suggested that solubilized curcumin was able to permeate through Caco-2 cell monolayers fairly rapidly and the permeation

mechanism was passive diffusion. Therefore, the permeation/absorption after solubilization was not thought as a limiting factor for the oral bioavailability of curcumin, while solubilization may be the major hurdle for proper absorption. As long as curcumin is solubilized, it is expected to be able to permeate/get absorbed rapidly.

Effect of different solubilization agents on the permeation of curcumin

Complexation with proteins and encapsulation in micelles are two direct approaches to solubilize hydrophobic compounds. Since solubilization limited the permeation of curcumin, the effect of protein complexation and micelle encapsulation on the permeation rate was examined subsequently.

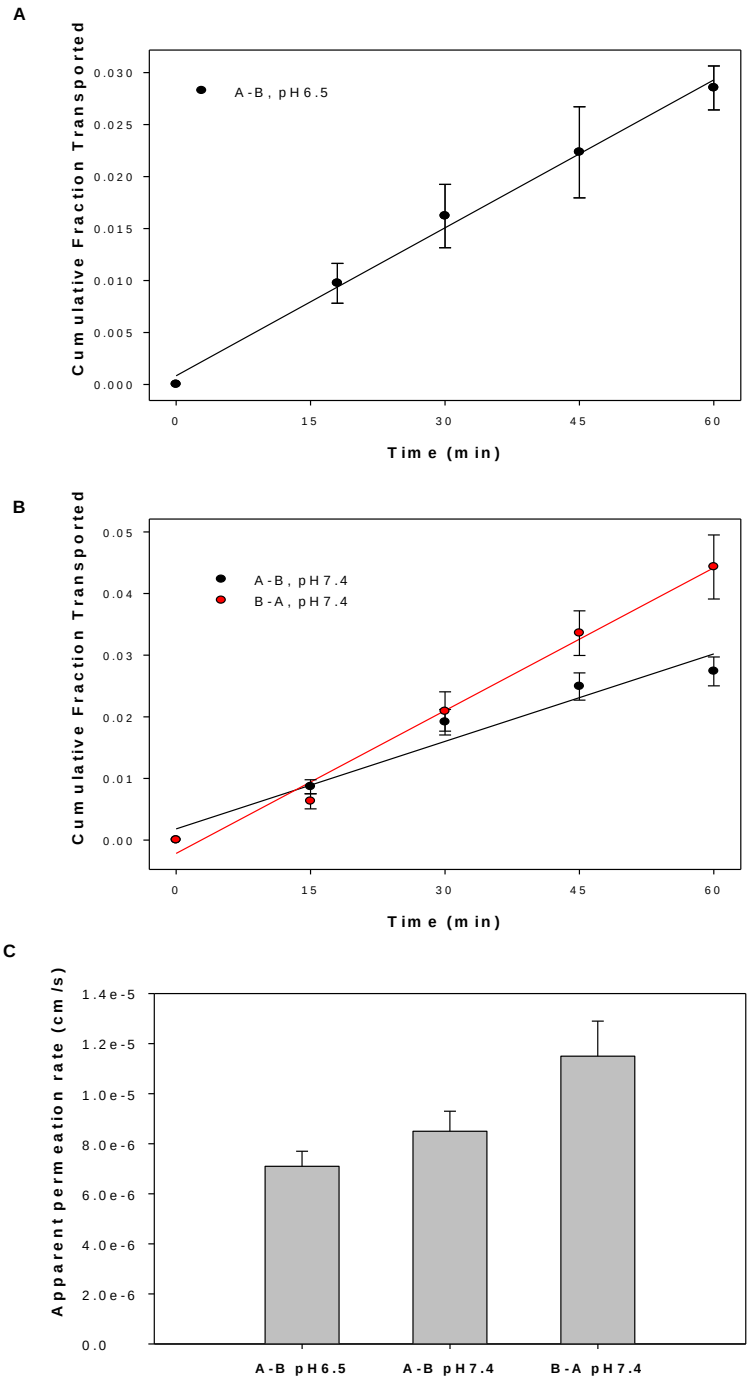

Figure 38 Transport of curcumin over time: (A) in the direction of A-B with donor compartment pH set at pH 6.5; and (B) in the direction of A-B and B-A with donor compartment pH set at pH 7.4. (C) Apparent permeation rates of dimethyl sulfoxide (DMSO)-solubilized curcumin in different conditions.

As an example of protein complexation, BSA was used to form complex with and solubilize curcumin. As shown in **Error! Reference source not found.A** and **4B**, adding SA to the donor media, while solubilizing curcumin, slowed down its permeation. The permeation rate of BSA solubilized curcumin was only $3.5 \pm 0.3 \times 10^{-6}$ cm/s, significantly lower ($p<0.001$) than that for DMSO-solubilized curcumin ($7.1 \pm 0.6 \times 10^{-6}$ cm/s). Meanwhile, the permeation rate of micelle-solubilized curcumin was also determined. Curcumin organogel was digested by lipase *in vitro* and the curcumin solubilized in the bile-fatty acid mixed micelles were used in the permeation assay. The rate for this mixed micelle - encapsulated curcumin was $10.9 \pm 0.5 \times 10^{-6}$ cm/s, which was significantly higher ($p<0.001$) than that for BSA-solubilized and DMSO-solubilized curcumin. The observation that different solubilization agents affected the permeated rate may be due to the different binding constants between curcumin with the solubilization agents. It was found in the literature that the equilibrium constant of curcumin binding with serum albumin was in the magnitude of 10^5 M^{-1} (*19, 31*), while the constant of curcumin binding with micelles were reported to be only in the magnitude of 10^2-10^3 M^{-1} (*29, 30*). Therefore, it was suggested that solubilization agents may affect the permeation rate of curcumin and that strong binding between the solubilization agents with curcumin may decrease the permeation rate.

Discussion

In the present study, the permeation mechanism of curcumin was investigated using Caco-2 cell monolayers. First, a HPLC method to quantify curcumin separately from other curcuminoids was developed. Subsequently, the mechanism of passive diffusion for

the rapid permeation of solubilized curcumin was demonstrated. Finally, the effects of different solubilization agents on the permeation rates of curcumin were investigated.

In the literature, two groups used everted rat intestine model to examine the absorption of curcumin and showed conflicting results (*12, 13*). In Ravindranath and Chandrasekhara's work, only about 2.5% curcumin was found in the intestinal tissues after 3-hour incubation, while Suresh and Srinivasan found that about 40-80% curcumin was absorbed and argued that the deviated observation with the previous research may be due to the improved sensitivity of the analytical methods, from thin layer chromatography to HPLC. In our study, a rapid permeation rate of curcumin across Caco-2 monolayers was observed, which is consistent with the latter work and suggests that absorption of solubilized curcumin may not be the limiting factor for curcumin's oral bioavailability.

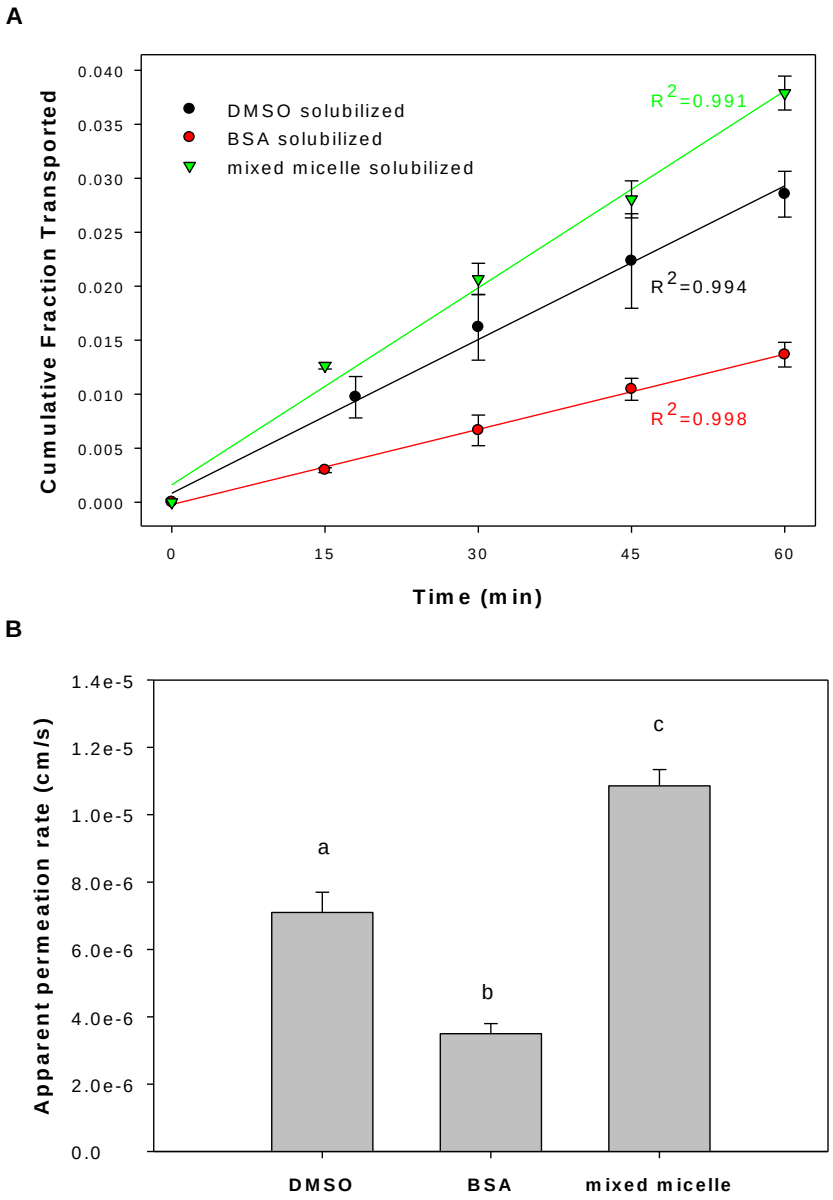

Figure 39 Effect of solubilization agents on the permeation of curcumin across Caco-2 cell monolayers: (A) Transport of curcumin solubilized by dimethyl sulfoxide (DMSO), BSA and mixed micelles. (B) Comparison of the permeation rates of curcumin solubilized by DMSO, BSA and mixed micelles. Different letters (i.e., a, b, c) indicates significant difference.

Recently, Wahlang *et al.* also used Caco-2 cell monolayers to investigate the permeation of curcumin (*35*). In their research, the permeation mechanism was found as passive diffusion, which is consistent with what we found here. Different from our finding, however, P_{app}(A-B) was determined as 2.9 ± 0.9 $\times 10^{-6}$cm/s, and thus the absorption rate was considered as low. To compare the detailed experiment methods, we found that the presence of BSA or not in the receiving solution may represent the biggest difference between the two studies. In our research, 4% BSA was added to the receiving solution, which mimicked the *in vivo* environment better, where the transport of hydrophobic drug in the circulatory system after absorption is through binding with plasma proteins (*34*). Meanwhile, since curcumin is water insoluble, in the absent of BSA, the partition of curcumin from the Caco-2 cells into the receiving compartments may significantly decrease the apparent permeation rate, resulting in a higher curcumin concentration inside the Caco-2 cells, where it is much better solubilized. Actually, in the paper from Wahlang *et al*, it was indeed found that curcumin was accumulated inside the Caco-2 cells over time. Based on these analyses, it is arguable that our conclusion that curcumin permeated fairly rapidly may reflect better the *in vivo* situation. On the other hand, we also admit that compared with some highly permeable compounds, the permeation rate of curcumin can only be regarded as moderately rapid. However, the key issue is that we do not think the absorption is the limiting factor and more effort should be put into improving the solubilization of curcumin.

Technically, it is also noticed that curcumin undergoes degradation under neutral-basic conditions, which may affect its concentration in the donor compartment over time. Nevertheless, the absorption rate was measured under pH 6.5, and thus the degradation

may not affect the curcumin concentration significantly. When the absorption mechanism was investigated, pH 7.4 was used in the donor compartment and degradation was expected. However, since only the ratio of permeation rates in two opposite directions were used to draw our conclusion, the impact of degradation should be minimal. On the other hand, the plots of accumulated curcumin transport over time in Figure 38 revealed a good linearity and seemed not affected by the concentration change of curcumin.

Metabolism of curcumin may occur during the absorption in the small intestine or across the Caco-2 monolayers. In our present studies, unfortunately, we were unable to identify the possible metabolites of curcumin, limited by the lack of proper instrumentation. If the biotransformation is substantial, the actual permeation rate should be even higher than the apparent rate reported here, which may further support our conclusion that solubilized curcumin is able to be absorbed rapidly.

The last part of this research investigated the effect of solubilization agents on the permeation of curcumin. The results obtained were P_{app}(mixed micelle) > P_{app} (DMSO) > P_{app}(BSA complex). Since only free solubilized curcumin is expected to be able to permeate across Caco-2 cell monolayers (*28*), the partition of curcumin from within the solubilization agents to freely soluble in the donor solution may affect the apparent permeation rate. Therefore, mixed micelle solubilized curcumin permeated more rapidly than solubilized BSA, as the binding between micelle and curcumin is much weaker that BSA. On the other hand, although DMSO, as a versatile solubilization agent, is widely used in Caco-2 monolayers experiments, after dispersion of curcumin DMSO solution into the donor medium, the curcumin aqueous solution was in supersaturated state and some of curcumin may crystallize in the media. Therefore, the concentration of the

actually solubilized curcumin may be less than 20 μg/mL and thus showed a lower permeation rate than micelle solubilized curcumin. Based on these analyses, a diagram in Figure 40 summarizes our understanding of the solubilization and permeation of curcumin. The apparent permeation rate is directly determined by the free solubilized curcumin in the media, while solubilization agents, such as mixed micelles, protein complexes and DMSO dispersion all provide the free solubilized curcumin. After dispersion of curcumin DMSO solution into aqueous solution, part of supersaturated curcumin crystallizes, while others remains solubilized. In the case of protein complexation and mixed micelle encapsulation, free solubilized curcumin is obtained by partition. Subsequently, free solubilized curcumin permeates across Caco-2 cell monolayers (or small intestine epithelium *in vivo*) by passive diffusion into the basolateral compartment (or into the circulatory system *in vivo*).

It is possible that the excipients used to solubilize curcumin, such as DMSO, BSA protein and bile salt-fatty acid mixed micelles might affect the integrity of Caco-2 cell monolayers. To monitor the confluence of the monolayers, TEER values before and after the permeation experiments were monitored and no significant decrease was observed for all of the three excipients, which was consistent with the literature (*34*). Moreover, since curcumin was water insoluble, it was thus thought to permeate transcellularly, but not paracellularly. Therefore, even changes in the TEER values may not affect the permeation of curcumin.

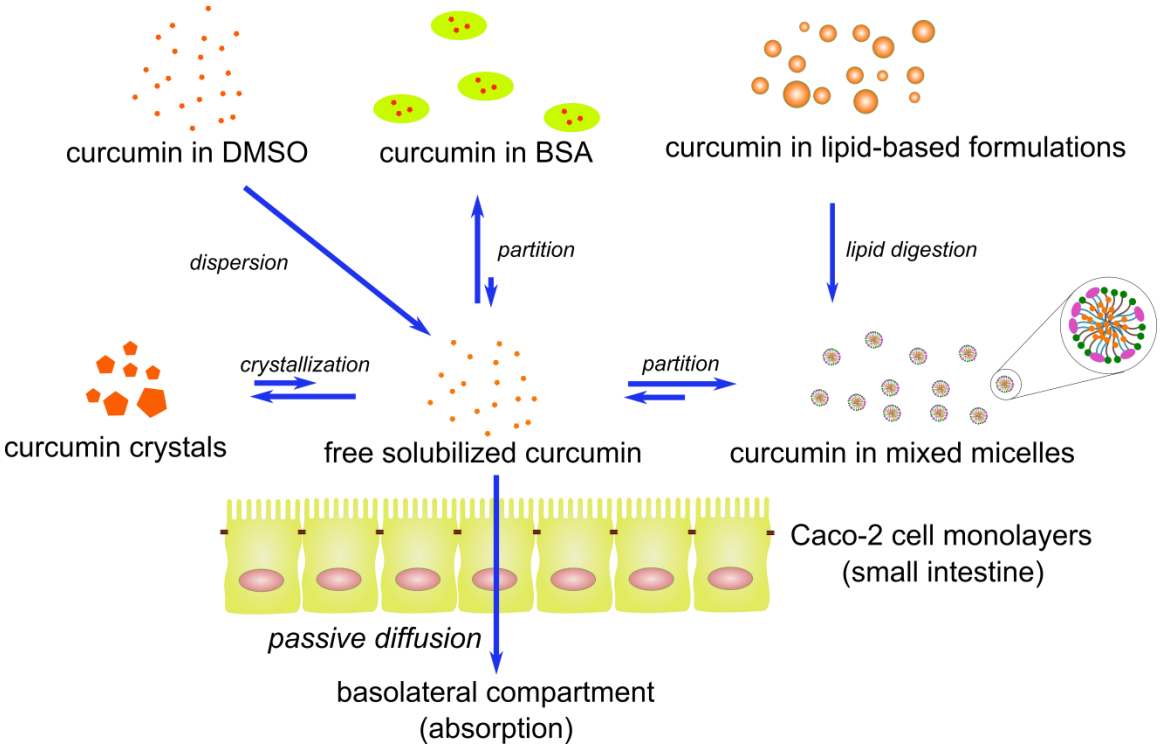

Figure 40 Diagram summarizing the solubilization and permeation of curcumin. Solubilization of curcumin is achieved by dimethyl sulfoxide (DMSO) dispersion, BSA complexation and mixed micelle encapsulation (generated by lipid digestion of lipid-based formulations). After dispersion of curcumin DMSO solution into aqueous solution, part of supersaturated curcumin crystallizes, while others remains solubilized. In the case of protein complexation and mixed micelle encapsulation, free solubilized curcumin is obtained by partition. Subsequently, free solubilized curcumin permeates across Caco-2 cell monolayers (or small intestine epithelium *in vivo*) by passive diffusion into the basolateral compartment (or into the circulatory system *in vivo*).

In the aspect of formulation design, based on the results of this work, we suggest that solubilization should be the primary target for the formulation design and that micelle encapsulation, with weaker binding with curcumin, may be preferred. Furthermore, it is also implied that lipid-based formulations are promising in improving the solubilization of curcumin. In the lipid-based formulations, curcumin is initially solubilized in lipid phase, and after oral consumption, lipid is digested and turned into mixed micelles which solubilize curcumin in aqueous solutions and improve the absorption and the oral bioavailability of curcumin. For instance, in our previous study, it was shown that curcumin nanoemulsion is able to improve the *in vivo* anti-inflammatory activity of curcumin (*26*).

Conclusion

In summary, a HPLC quantification method was developed to quantify curcumin separately from other co-existing curcuminoids. Using Caco-2 cell monolayers model, it was revealed that solubilized curcumin permeated rapidly via the mechanism of passive diffusion, suggesting solubilization is the main limiting factor for curcumin absorption. Moreover, it was also suggested that different solubilization agents may affect the permeation rate: protein complexation slowed down the permeation while micelle encapsulation accelerated the permeation. This study further implied that lipid-based formulations are promising in improving the oral bioavailability of curcumin, as they are able to solubilize curcumin after digestion and also increase the permeation of solubilized curcumin.

CHAPTER 6. DEVELOPMENT OF A FOOD-GRADE ORGANOGEL WITH HIGH BIOACCESSIBILITY AND LOADING OF CURCUMINOIDS

The objective of this study was to develop an organogel system for high-loading (> 1%) delivery of curcumin with high bioaccessibility, examined by *in vitro* lipolysis experiments. In order to achieve high loading and bioaccessibility, we compared different oils and the effect of different types of additives. In the end, the organogel was formulated as medium chain triacylglycerols (MCT) with added Span 20 and monostearin. The curcuminoids loading was about 2.6%, and the percent bioaccessibility was about 80% in the fasted state.

Organogel-based delivery systems are relatively new in food science. Organogels were formed by liquid oils trapped by the extensive crystalline networks of organogelators, such as monoglycerides, fatty acids and fatty alcohols (*183*). Although there are already some applications of organogels in dermal and transdermal delivery, the oral delivery of nutraceuticals using organogel is still very limited.

Materials and methods

Materials Curcuminoids were obtained from Sabinsa Corporation, which contains about 82% curcumin, 15% D-Cur and 3% BD-Cur. Medium chain triacylglycerols (MCT) was provided by Stepan Company (Neobee 1053). Coconut oil, Canola oil, and corn oil were all purchased from a local supermarket. Span 20 (sorbitan monolaurate), Span 40 (sorbitan monopalmitate), Span 60 (sorbitan monostearate) and Span 80 (sorbitan monooleate) were obtained from Sigma-Aldrich (St. Louis, MO). 1-Monoolein and 1-

monomyristin was purchased from Spectrum Chemical (New Brunswick, NJ). 1-monolaurin, 1-monopalmitin and 1-monostearin (60% min) was acquired from TCI America (Portland, OR). HPLC-grade water was from Alfa Aesar (Lawrence, KS). Glacial acetic acid and HPLC-grade acetonitrile were purchased from J.T. Baker (Phillipsburg, NJ). Lecithin (Phospholipon 85G) was a gift provided by American Lecithin Company (Oxford, CT). Pancreatin with 8X USP specification and Tris maleate were obtained from Sigma Aldrich. Sodium taurodeoxycholate (Na TDC) was purchased from CalBiochem (La Jolla, CA).

Determination of metastable solubility of curcuminoids In 10g oils (MCT, Canola, coconut or corn oils), 0.5g curcuminoids were added and heated to ~140 ℃ under stirring to ensure complete dissolution in oils. After 5 days (120 hr) of storage at room temperature, oils were centrifuged at 14,000g for 5 min, and then filtered through 0.22 μm filter. One hundred microliters of filtrates were diluted 1000 times in 1:2 (v/v) distilled water (dH_2O)-acetonitrile and analyzed using HPLC.

To determine the metastable solubility of curcuminoids in MCT with other additives, one gram additives (Span 20, Span 40, Span 60, Span 80 or monoolein) was firstly dissolved in 10g MCT (under heating if necessary), followed by the addition of 0.5g curcuminoids as described above.

***In vitro* lipolysis of curcuminoids in lipids** In response to food consumption, the concentrations of bile salts and endogenous phospholipids in the small intestine lumen are higher in the fed state than in the fasted state. Accordingly, two lipolysis buffers were prepared to mimic the different chemical environments in the fasted and fed states (Table

7). The procedure of *in vitro* lipolysis experiments was described in the published literature (*184*). Briefly, pancreatin preparation was made by mixing 1g pancreatin with 5mL fasted/fed-state buffer, centrifuged and kept on ice. In 9 mL fasted/fed-state buffer, 0.25g lipids with curcuminoids and 1mL pancreatin preparation were added to start the lipolysis. During the 30-min lipolysis, pH was maintained at 7.50 ± 0.02 by adding 0.25N NaOH and temperature was kept at 37 ± 1 ^{o}C. The volume of consumed NaOH over time was recorded throughout the lipolysis experiments.

After 30 min, the whole end products of digestion were ultracentrifuged at 50,000 rpm (Type 60 Ti rotor, about 180,000 g, Beckman Coulter) for 40 min. Subsequently, the aqueous phase was filtered through 0.22 μm filters. The filtrate was directly used to measure the particle size of the mixed micelles. After acidified with HCl, the filtrate was mixed with 2 volume of acetonitrile for HPLC analysis.

Determination of the percent bioaccessibility The percent bioaccessibility was calculated as:

$$\%\ \text{Bioaccessibility} = \frac{\text{mass of solubilized curcuminoids}}{\text{mass of curcuminoids in lipid}} \times 100\% \qquad (1)$$

The mass of solubilized curcuminoids was the product of the concentration of solubilized curcuminoids in the aqueous phase after lipolysis and the volume of the aqueous phase. The mass of curcuminoids in lipid was calculated from the concentration of the curcuminoids in oil, mass of the oil (0.25g) and the density of the oils. For all the four oils, 0.92 g/mL was used. The density of 35 mg/mL curcuminoids in MCT + Span 20 was determined as 0.98 ± 0.01 mg/mL. The density of organogel with curcuminoids was estimated as 1 g/mL.

Table 7 Recipes of lipolysis buffers in the fasted and fed states

	Fasted state	Fed state
Tris maleate (mM)	50	50
NaCl (mM)	150	150
$CaCl_2 \cdot 2H_2O$ (mM)	5	5
NaTDC (mM)	5	20
Phosphatidylcholine (mM)	1.25	5

Determination of the extent of lipolysis The extent of lipolysis was defined as the percentage of triglycerides digested in the *in vitro* lipolysis experiments. It was assumed that there were exclusively triglycerides in the basic oils, and that digestion of one molecule of triglycerides released exactly two molecules of fatty acids and consumed two molecules of NaOH. Consequently,

$$\text{Extent}_{\text{lipolysis}} = \frac{\text{Vol}_{\text{NaOH}} \times \text{Conc}_{\text{NaOH}}}{2 \times \text{Mole}_{\text{triglyceride}}} \times 100\% \quad (2)$$

Where Vol_{NaOH} is the volume of NaOH consumed in the lipolysis. The amount of NaOH used for mock lipolysis (with no lipid added) was subtracted. $\text{Conc}_{\text{NaOH}}$ is the concentration of NaOH (i.e., 0.25N). $\text{Mole}_{\text{triglyceride}}$ of 250 mg lipid was calculated from the average molecular weight of the triglycerides, which was estimated using the saponification value of the oil:

$$\text{Mw}_{\text{triglyceride}} = \frac{3 \times 1000 \times \text{Mw}_{\text{KOH}}}{\text{SV}} \quad (3)$$

Where Mw_{KOH} is the molecular weight of KOH, the mass of which is used to express the saponification value (SV). SVs used for MCT, Canola, coconut and corn oils were 334, 187, 252 and 190, respectively.

High-performance liquid chromatography (HPLC) An UltiMate 3000 HPLC system equipped with a 25D UV-VIS absorption detector (Dionex) and a Nova-Pak C18 3.9×150mm column (Waters) was used. Mobile phase solvents were: (A) water with 2% acetic acid, and (B) acetonitrile. Fifty microliters of samples were injected. Elution condition was: 0 to 2 min, 65% A and 35% B; 2 to 17 min, linear gradient from 35% B to

55% B; 17 to 22 min, held at 55% B; 22 to 23 min, B went back to 35% linearly. Flow rate was 1 mL/min. Detection wavelength was set at 420 nm.

Preparation of curcuminoids organogel Five percent curcuminoids and 10% Span 20 (w/w) were first dissolved in MCT under heating. After 120 h, MCT was filtered to remove curcuminoids precipitation. Twenty percent (w/w) monostearin was added and dissolved under heating. The solution was set at room temperature and organogel formed within a few hours.

Polarized light microscopy.Nikon TE-2000-U inverted microscope equipped with a CCD camera (Retiga EXi, QImaging) was used to record the images from polarized light microscope.

Particle size measurement The aqueous phase after ultracentrifugation was filtered through 0.22 μm filter. Subsequently, the particle sizes (hydrodynamic diameters) of the samples were determined with dynamic light scattering method using a BIC 90Plus particle size analyzer (Brookhaven Instrument, NY) at room temperature. The results were presented as mean ± standard deviation (n=3).

Statistical analysis SigmaPlot 10.0 software with SigmaStat integration (Systat Software) was used to perform all the statistical analysis. One-Way and Two-Way Analysis of Variance (ANOVA) tests were followed by Holm-Sidak method, with overall significance level set at 0.05. Non-normal raw data were first transformed to meet the requirement of ANOVA analysis.

Results and discussion

Selection of the basic oils for organogel

To develop a food-grade organogel system for delivery of curcuminoids, the first step is to choose the proper oil. In this study, four oils, MCT, Canola, Coconut, and corn oils, were chosen as the candidates. MCT and coconut oils are rich in saturated fatty acids: MCT exclusively consists of caprylic (C8:0) and capric (C10:0) triglycerides, while in coconut oil, there are more than 60% of lauric (C12:0) and myristic (C14:0) acids. On the other hand, Canola and corn oils are highly unsaturated: oleic acid (a monounsaturated fatty acid, C18:1) is enriched in Canola oil, while there is a high percentage of linoleic acid (a polyunsaturated fatty acid, C18:2) in the corn oil.

In the literature, the solubility of curcumin(oids) in various oils is very low (*4*, *76*). However, it is also known that much larger amount of curcuminoids was able to be dissolved in heated oils and remained soluble in the oil for a relatively long period of time. Therefore, in this study, the metastable (120 hour) solubility of curcuminoids in four oils was first determined. As shown in Figure 41, the metastable solubility was all in the mg/mL magnitude. The highest metastable solubility was in corn oil, which was 16.6 ± 3.1 mg/mL and significantly higher than that in the other three oils (One-Way ANOVA).

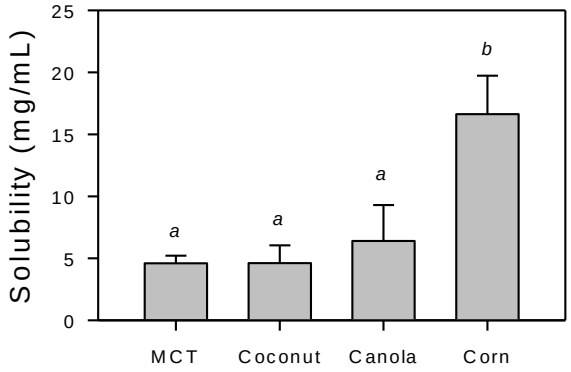

Figure 41 Metastable solubility of curcuminoids in four basic oils. Error bars show the standard deviation, n=3. Different letters (a or b) indicate significant difference from One-Way ANOVA.

In addition to the metastable solubility, the percent bioaccessibility of curcuminoids after lipolysis was thought to be a more important factor determining the choice of the basic oil. Therefore, about 1 mg/mL curcumin was dissolved in the four oils and the percent bioaccessibility of curcuminoids was determined after *in vitro* lipolysis in both fasted and fed states (Figure 42A). Different from the results in the metastable solubility, lipolysis of MCT generated the highest percent bioaccessibility (72.1 ± 6.4% and 72.2 ± 10.1%, in the fasted and fed states, respectively), followed by coconut oil, and then Canola and corn oils. Meanwhile, the results in Figure 42A also revealed that no significant difference was detected in the percent bioaccessibility between the fasted state and fed state (Two-Way ANOVA). These results suggested that oil type played a more important role than the effect of food consumption.

Furthermore, the composition of the solubilized curcuminoids after lipolysis was also determined by HPLC (Table 8). It was found that in both fasted and fed states, the percentage of curcumin, the major curcuminoid, was significantly lower in Canola and corn oils than that in the original curcuminoids powder (82.1 ± 1.0 %, n=12). Since it was previously shown that among the three curcuminoids, curcumin was most susceptible to hydrolysis (*185*), this result suggested that during the process of *in vitro* lipolysis, some of the curcuminoids were not fully solubilized and thus not stabilized in the mixed micelle system, but instead were exposed to the weak alkaline environment and subsequently hydrolyzed.

In the *in vitro* lipolysis experiments, the extent of lipolysis of the oils was also estimated (Figure 42B). It was revealed from Two-Way ANOVA that after 30-min lipolysis, MCT was digested most completely (i.e., in the fasted state, 78.9 ± 10.5 %; and

in the fed state, 91.3 ± 7.0 %), followed by coconut oil, then Canola oil and corn oil. In addition, the extent of lipolysis was higher in the fed state than in the fasted state, which was consistent with previous results (*186*).

To investigate the correlation between the extent of lipolysis and the percent bioaccessibility, Pearson's Product Moment Correlation test was performed. With the correlation coefficient of 0.874 and p value of 2.43×10^{-8}, the extent of lipolysis and the percent bioaccessibility was positively correlated (Figure 42C), suggesting that the increase of the extent of lipolysis, by emulsification for instance, could improve the percent bioaccessibility.

The results shown above suggested that, although the metastable solubility of curcuminoids in MCT was not the highest, the *in vitro* lipolysis of MCT generated the highest bioaccessibility. Therefore, MCT was chosen as the basic oil for the preparation of organogel.

Increase of the curcuminoids loading in MCT

In many scenarios, formulations with high nutraceuticals loading are desired. Meanwhile, high nutraceuticals loading usually provides great flexibility to downstream applications. Specifically for curcuminoids, since they are polar compounds and do not have high solubility in oil intrinsically, it was thought that by incorporating other more polar additives in the oil, the (metastable) solubility of curcuminoids may be increased.

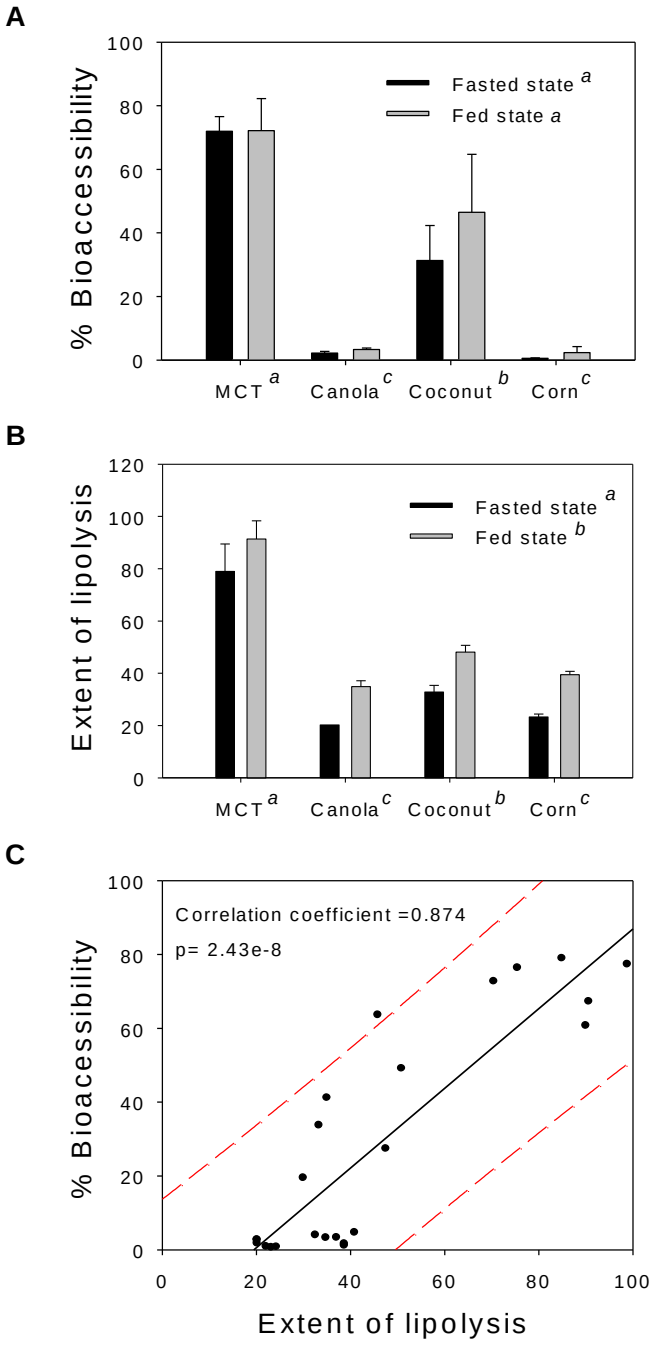

Figure 42 Comparison of the lipolysis of curcuminoids in four basic oils. (A) The percent bioaccessibility of curcuminoids after lipolysis of four basic oils; (B) the extent of lipolysis of four basic oils; and (C) the correlation of the percent bioaccessibility and the extent of lipolysis. Data from fasted- and fed-state lipolysis are combined. The solid line shows the linear regression. Two broken curves indicate 95% prediction intervals. Error bars in (A) and (B) show the standard deviation (n=3). Different letters (a or b) indicate significant difference from Two-Way ANOVA.

Table 8 Percentage of each curcuminoid solubilized after lipolysis in the fasted and fed states

Oil	Curcumin (%)	D-Cur (%)	BD-Cur (%)
MCT (fasted-state)	78.1 ± 0.4	17.8 ± 0.3	4.1 ± 0.1
Canola (fasted-state)	26.5 ± 8.8 *	30.0 ± 0.6	43.4 ± 8.4
Coconut (fasted-state)	74.1 ± 5.7	20.6 ± 3.8	5.4 ± 1.9
Corn (fasted-state)	14.3 ± 2.6 *	17.1 ± 4.9	72.9 ± 7.3
MCT (fed-state)	81.1 ± 0.5	18.1 ± 0.6	4.3 ± 0.4
Canola (fed-state)	19.4 ± 4.4 *	26.7 ± 1.1	52.4 ± 4.6
Coconut (fed-state)	77.2 ± 4.8	21.3 ± 4.2	6.0 ± 2.6
Corn (fed-state)	55.5 ± 31.1 *	16.9 ± 10.8	28.3 ± 19.5

Data are presented as mean ± standard deviation (n=3). * denotes for significant difference from the original curcuminoids powder

In the scale of food science, five food-grade high-HLB-value additives (Span 20, Span 40, Span 60, Span 80 and monoolein) were added to MCT and the metastable solubility of curcuminoids were determined. As shown in Figure 43, the metastable solubility of curcuminoids in MCT + 10% Span 20 was 37.5 ± 2.7 mg/mL, significantly higher than that with the other additives (One-Way ANOVA). Compared with the metastable solubility in MCT alone, it increased by about 8.2 folds. Therefore, Span 20 was chosen as the additive in MCT to improve the loading of curcuminoids.

Development of the curcuminoids organogel

In the previous section, it was shown that the incorporation of Span 20 greatly increased the loading of curcuminoids in MCT. However, since it was only metastable, after over one-month storage, the precipitation of curcuminoids was significant. To overcome this problem, an organogel was developed, in which the precipitation of curcumin was expected to be decelerated substantially.

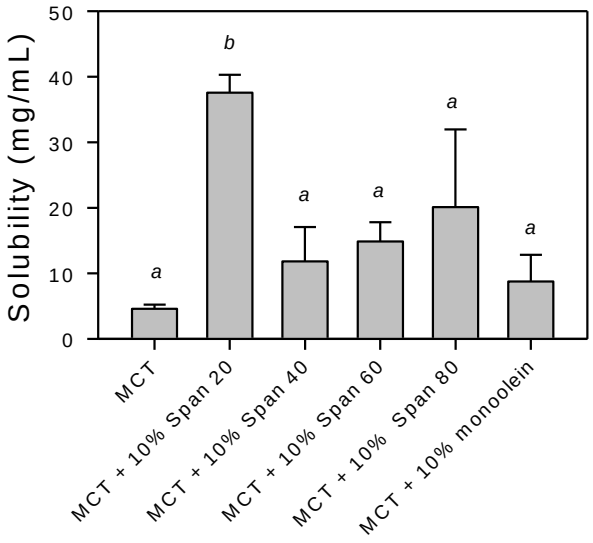

Figure 43 Metastable solubility of curcuminoids after adding different additives. Error bars show the standard deviation (n=3). Different letters (a or b) indicate significant difference from One-Way ANOVA.

In the literature, it was already known that the incorporation of monoglycerides, fatty alcohols and phytosterols in the lipid was able to form organogels (*183*). Considering the potential food application of the organogel in this study, monoglycerides, a group of molecules with GRAS-status, were selected to prepare the organogel. Twenty percent (w/w) of monolaurin, monomyristin, monopalmitin or monostearin was added to the curcuminoids MCT-Span 20 oil. Although MCT with 10% of every monoglyceride formed organogel, surprisingly, only the addition of 20% monostearin in the curcuminoids oil formed the organogel (Figure 44A). Monolaurin and monomyristin seemed not to affect at all and incorporation of monopalmitin increased the viscosity significantly but did not solidify the MCT. These results suggested that the curcuminoids and Span 20 affected the formation of the crystalline networks of monoglycerides. In the prepared organogel, there was about 2.6% (w/w) curcuminoids.

As shown in Figure 44A, the organogel formed was not transparent, mainly due to the extensive crystal formation of monostearin. This statement was supported by the polarized light microscopy results. Curcuminoids crystals precipitated in MCT were needle-shaped, as shown in Figure 44C. Under the polarized light microscope, twenty percent monostearin in MCT revealed extensive birefringence (Figure 44D) and was similar to that of organogel with curcuminoids (Figure 44B). More important, there were no apparent needle-like crystals detected in curcuminoids organogel, suggesting that in the organogel, only monostearin crystallized and solidified MCT.

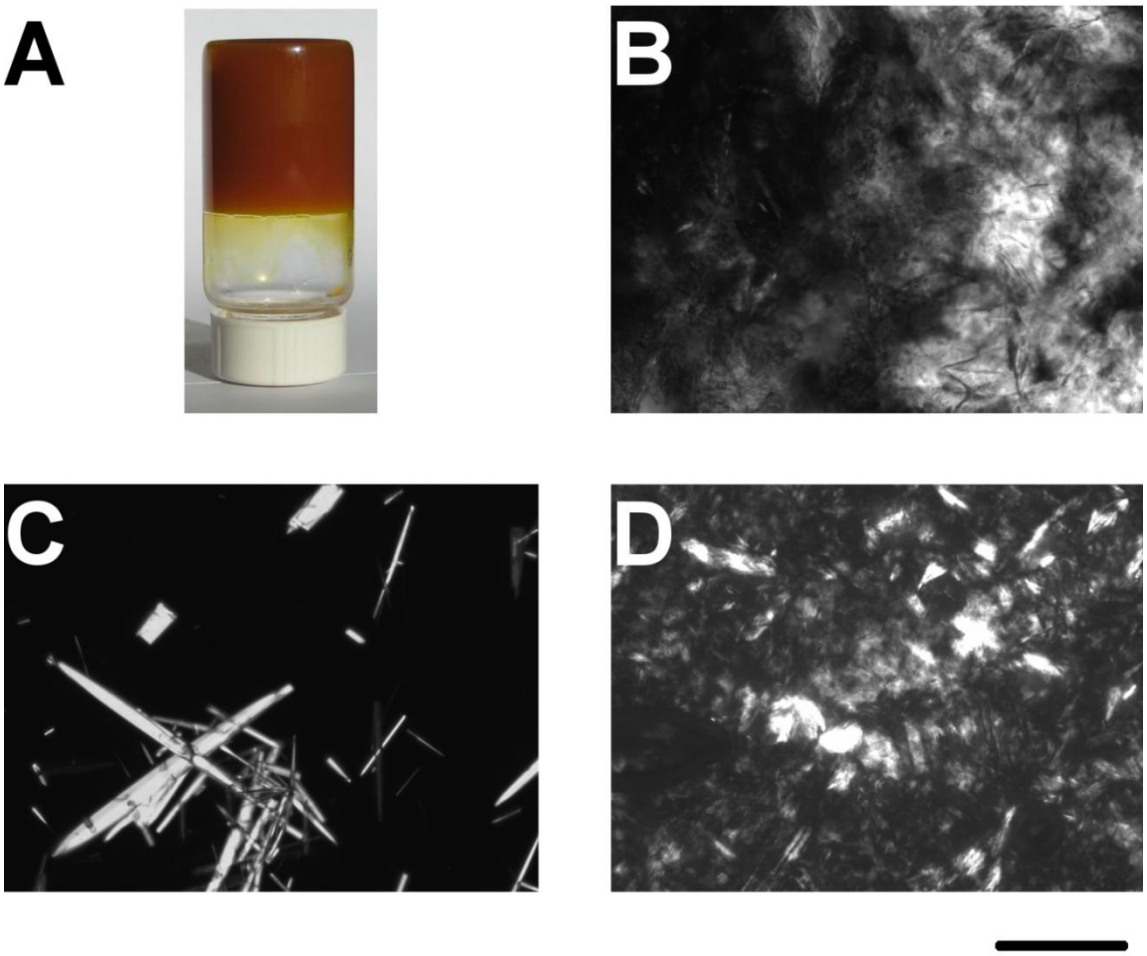

Figure 44 (A) The photograph of the developed curcuminoids organogel, as well as the polarized light microscope images of (B) MCT-monostearin organogel, (C) curcuminoids precipitates in MCT, and (D) curcuminoids organogel. Scale bar indicates 100 μm.

To evaluate the efficacy of curcuminoids in the organogel formulation, the percent bioaccessibility of curcuminoids were determined on three formulations: curcuminoids in MCT-Span 20 oil (~ 36 mg/g curcuminoid), curcuminoids in organogel (~ 26mg/g), and unformulated curcuminoids (~ 35 mg/g curcuminoids powder dispersed in water). As revealed in Figure 45A, compared with unformulated curcuminoids, MCT-Span 20 oil and organogel were able to provide much higher bioaccessibility: in the fasted state, it increased by 107-fold and 100-fold, respectively for MCT-Span 20 oil and organogel; and in the fed state, it increased by 25-fold and 21-fold respectively. From Two-Way ANOVA, it was further suggested that there was no significant difference detected in the percent bioaccessibility between MCT-Span 20 and organogel. Meanwhile, the fasted-state lipolysis provided significantly higher bioaccessibility than fed state, suggesting that organogel may be consumed before other foods, to ensure a better bioaccessibility. On the other hand, for unformulated curcuminoids, the fed state may make curcuminoids more bioaccessible than the fasted state (0.79 ± 0.06 % *versus* 2.65 ± 0.11, t-test, $p < 0.001$), which was consistent with the general knowledge that oil-soluble compounds are better "absorbed" when taken with food.

The extent of lipolysis of organogel was also compared with that of MCT-Span 20 oil (Figure 45B). Two-Way ANOVA analysis revealed that the extent of lipolysis in fasted state was higher than that in fed state, which was consistent with the results reported above. On the other hand, there was no significant difference detected between MCT-Span20 and organogel, which was different from the previous finding (*187*). This may be due to the observation that at 37 °C, the gel started to become viscous liquid.

Additionally, the structure of orgenogels may be further interrupted under mechanical stress (stirring *in vitro* and mechanical grinding in the stomach).

To further investigate the structures of the mixed micelles with solubilized curcuminoids inside after lipolysis, particle sizes of the mixed micelles were determined by dynamic light scattering (

Table 9). The sizes of the mixed micelles in the fed state were below 10 nm, suggesting that there was no aggregation of micelles, while the size in the fasted state was about 100 nm, suggesting the formation of micelle aggregates or more complex structures. Since the only difference between the fasted and fed states was the concentrations of Na TDC and phosphatidylcholine, these results suggested that the component concentrations in the mixed micelle system had an impact on the micelle structure. Also from the Two-Way ANOVA, the micelle size for organogel was significantly different from that of MCT-Span 20 oil, which revealed that Span-20 and monostearin (or their digestion products) also affected the micelle structure. On the other hand, since the bioaccessibility from either MCT-Span 20 oil or organogel was similar, the micelle structures had negligible effect on the solubilization process of curcuminoids.

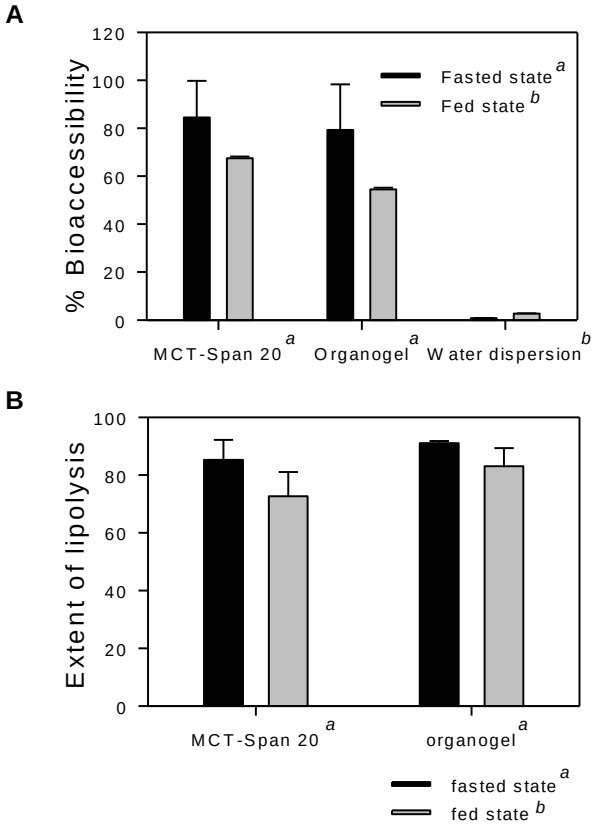

Figure 45 Comparison of lipolysis of high-dose curcuminoids in MCT-Span 20, organogel and water dispersion, in the fed and fasted states. (A) The percent bioaccessibility of curcuminoids after lipolysis, and (B) the extent of lipolysis of MCT-Span 20 and organogel. Error bars show the standard deviation (n=3). Different letters (a or b) indicate significant difference from Two-Way ANOVA.

Table 9 Particle sizes of curcuminoids micelles after lipolysis

	Micelle size (diameter, nm)	Polydispersity
MCT-Span20[a] (Fed state [a])	7.6 ± 0.2	0.205 ± 0.027
MCT-Span20[a] (Fasted state [b])	100.6 ± 4.4	0.251 ± 0.024
Organogel [b] (Fed state [a])	7.4 ± 0.4	0.196 ± 0.028
Organogel [b] (Fasted state [b])	88.4 ± 6.7	0.210 ± 0.002

Data are presented as mean ± standard deviation (n=3). Different letters indicate significant difference within the same factor

Conclusion

In this study, a new curcuminoids organogel with high loading and bioaccessibility has been developed. MCT was chosen as the basic oil due to its rapid digestibility and the high bioaccessibility of curcuminoids. Incorporation of Span 20 greatly increased the loading. Additionally, monostearin functioned as an organogelator to form organogel and stabilize the metastable curcuminoids. From statistical analysis, it was revealed that the bioaccessibility of curcuminoids was not affected by the formation of organogel, and the fasted state generated a higher bioaccessibility than the fed state. This organogel has the potential to stand alone for curcuminoids delivery as well as to be used as the oil phase of emulsions for downstream functional foods application.

CHAPTER 7. IMPROVING THE ORAL BIOAVAILABILITY OF CURCUMINOIDS USING ORGANOGEL BASED NANOEMULSIONS

In previous section, I have demonstrated the development of a food-grade organogel for curcumin encapsulation and oral delivery. *In vitro* digestion of the organogel leads to high percent of curcumin bioaccessibility. Meanwhile, the loading of curcumin in the organogel is high, achieved by using Span 20 to increase the solubility of curcumin in the oil and monostearin as the organogelator to stabilize curcumin from crystallization.

Direct oral administration of the organogel may be inconvenient and the *in vivo* oral bioavailability of curcumin in the organogel is yet to be examined. Therefore, to continue our study, this work focuses on development of organogel-based o/w nanoemulsion. Its *in vivo* fate after oral administration is examined using *in vitro* lipolysis assay and Caco-2 cell monolayers model. The oral bioavailability is also investigated using experimental animals. The present work may provide more convenient solution for oral delivery of curcumin organogel and also shed light on the absorption mechanism of nanoemulsions

Materials and methods

Materials Curcumin (82% purity, with 15% DCur and 3% BDCur) was provided by Sabinsa Corporation. Medium chain triacylglycerols (MCT, Neobee 1053) were obtained from Stepan Company. Modified starch (HiCap 100) was obtained from National Starch. Whey protein isolate (WPI) was from Davisco Foods International. And 1-monostearin (about 60% purity) was from TCI America. Lecithin (Phospholipon 85G) was provided by Lipoid. Pancreatin with 8X USP specification (P7545), sulfatase (S9626) and

glucuronidase (G7017) were obtained from Sigma Aldrich. Additionally, analytical grade β-17-estradiol acetate, Tween 20 (Polyoxyethylene (20) sorbitan monolaurate), Span20 (sorbitan monolaurate), and Tris maleate, sodium taurodeoxycholate (Na TDC) and glacial acetic acid and HPLC-grade acetonitrile and H_2O were used in this study.

All the cell culture media and reagents were purchased from Fisher Scientific. Transwell permeable polycarbonate inserts (0.4μm) and 12-well cell culture plates were obtained from Corning.

Preparation of curcumin organogel and organogel-based nanoemulsions Curcumin organogel was prepared as previously described (*188*), with increased curcumin loading. Briefly, Span 20 saturated MCT, monostearin and curcumin was mixed at the ratio of 10:2:1.2 (w/w, about 9% curcumin in organogel), followed by heating to dissolve curcumin completely and then setting at room temperature.

To prepare curcumin organogel-based nanoemulsions, water, organogel and emulsifier (modified starch, WPI and Tween 20) were mixed at the ratio of 3:2:1 (w/w) using mechanical stirrer and then ultrasonicated at about 175W for accumulatively 5 mins.

Particle size measurement Nanoemulsions were diluted 200 times into dH_2O and mixed well. The particle sizes (hydrodynamic diameters) of the lipid droplets were determined with dynamic light scattering method using a BIC 90plus particle size analyzer (Brookhaven Instrument) at ambient temperature.

***In vitro* lipolysis of formulations** *In vitro* lipolysis was performed according to our previous work (*188*). Briefly, 0.25g organogels or 0.75g nanoemulsions were digested using pancreatin under fast state for 30 mins at 37^{o}C. The pH of the solution was

maintained at 7.5 by adding NaOH manually. Amount of NaOH added over time was recorded throughout the digestion. After digestion, the solution was ultracentrifuged and the amount of curcumin in the aqueous phase was determined using HPLC.

The extent of lipolysis in this pH-stat titration was determined using the consumed NaOH amount.

$$\text{Extent}_{\text{lipolysis}} = \frac{\text{NaOH amount consumed}}{\text{theoretical NaOH amount for complete lipolysis}} \times 100\% \text{.....(1)}$$

To calculate the amount of NaOH required for complete lipolysis, it was assumed that one molecule of MCT, monostrearin and Tween 20 consumed two, one and one molecules of NaOH, respectively.

From the HPLC quantification, the percent bioaccessibility of curcumin was calculated as

$$\%\ \text{Bioaccessibility} = \frac{\text{amount of solubilized curcuminoids in aqueous phase}}{\text{amount of curcuminoids in the formulations}} \times 100\% \text{ .....(2)}$$

Determination of the permeation rate across Caco-2 cell monolayers The procedures for Caco-2 cell monolayers permeation assay followed our previous study (*189*). Briefly, Caco-2 cell (passage number 35-45) monolayers were used after 21-29 days of culture. Free curcumin (by DMSO dispersion) and formulated curcumin with the concentration of 20 μg/mL were added into the apical compartment (HBSS + 10 mM methanesulfonic acid, pH 6.5). After different time (15, 30, 45, 60 mins), media in basolateral compartment (HBSS + 25mM HEPES + 4% BSA, pH7.4) were removed and two volumes of acetonitrile were added before the HPLC analysis of curcumin. The apparent permeation rate was calculated as

$$P_{app} = \left(\frac{dQ}{dt}\right)\left(\frac{1}{AC_0}\right) \quad \text{.....(3)}$$

Where P_{app} is the apparent permeation rate, dQ/dt is the mass transport rate, A is the surface area of the insert; and C_0 is the initial curcumin concentration in the apical compartment (20 μg/mL).

For digested curcumin nanoemulsion, the solution was firstly heated at 95^{o}C for 5min to inactivate enzymes in the pancreatin.

High-performance liquid chromatography (HPLC) analysis HPLC quantification of curcumin was performed using an UltiMate 3000 HPLC system with a 25D UV-VIS absorption detector (Dionex) and a Nova-Pak C18 3.9×150mm column (Waters). Mobile phase solvents were: (A) water with 2% acetic acid, and (B) acetonitrile. Elution condition was: 0 to 2 min, 65% A and 35% B; 2 to 17 min, linear gradient from 65% A and 35% B to 45% A and 55% B; 17 to 22 min, held at 45% A and 55% B; 22 to 23 min, mobile phase went back to 65% A and 35% B. Flow rate was 1 mL/min. Fifty microliters of samples were injected. Detection wavelength was set at 420 nm for curcumin and 280 nm for β-17-estradiol *acetate in the pharmacokinetics studies.*

Pharmacokinetics analysis on mice Female CD-1 mice (22-26g) were used for the pharmacokinetics analysis of curcumin. After fast overnight, mice were administrated with curcumin nanoemulsion or curcumin water suspension at the dose of 240mg/kg by oral gavage. At different time intervals (0.5, 1, 2, 4, 8, 12, 24 hours), blood samples were withdrawn by cardiac puncture. After centrifugation at 5000g for 15mins, plasma was removed and stored at -80^{o}C till HPLC analysis.

Before HPLC quantification, 150 μL plasma samples were mixed with equal volume of enzyme solutions (10mg/mL sulfatase and 10 μL/mL of glucuronidase in 0.1M sodium acetate buffer, pH5.0) at 37 ^{o}C for 1 hour to convert curcumin sulfate and glucuronide to free curcumin. Subsequently, 10 ul 1mg/ml β-17-estradiol acetate in ethyl acetate was added as the internal control (*190*). After extracted with ethyl acetate for three times and re-dissolved in 1:2 (v/v) dH_2O: acetonitrile, the samples were ready for HPLC analysis.

The areas-under-the curve (AUC) for the plot of the plasma concentration over time were calculated using trapezoidal method. C_{max} and T_{max} were directly obtained from the curves.

Statistics analysis Student t-test, Pearson Product Moment Correlation and One-way Analysis of Variance (ANOVA) were performed using SigmaPlot 10.0 software with SigmaStat integration (Systat Software).

Results

In my previous section, food-grade organogel was developed for curcumin oral delivery with high *in vitro* bioaccessibility and curcumin loading. In this work, nanoemulsions based on the organogel were generated; its absorption mechanism was examined and the oral bioavailability of curcumin in the nanoemulsion was investigated.

Tween 20 was chosen as the emulsifier

To develop curcumin organogel-based nanoemulsions, three common food-grade emulsifiers, modified starch, WPI and Tween 20, were compared in terms of the *in vitro* bioaccessibility of curcumin after lipolysis. As shown in Figure 46A, the *in vitro* bioaccessibility of curcumin for organogel and organogel-based emulsions ranged from

13% to 47 %. From One-way ANOVA, Tween 20 emulsion was able to generate similar *in vitro* bioaccessibility as the organogel, while modified starch- and WPI-emulsified emulsions showed significantly lower bioaccessibility. Therefore, Tween 20 was selected as the emulsifier to generate organogel-based emulsions.

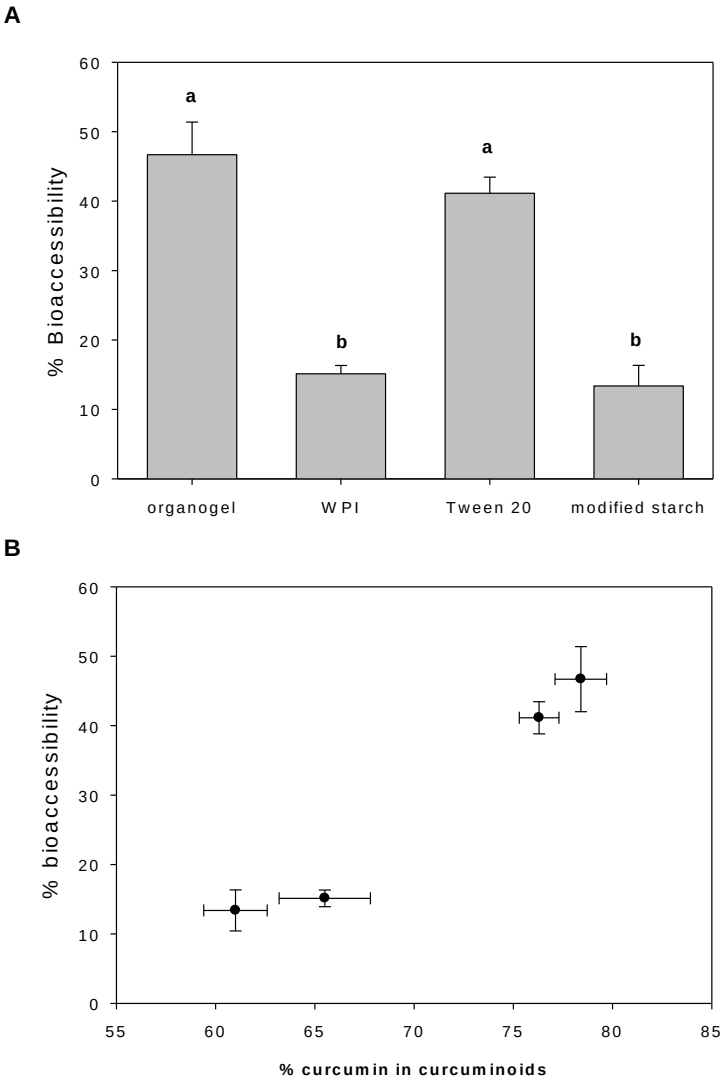

Figure 46 Selection of the emulsifier based on the percent bioaccessibility after *in vitro* lipolysis. (A) Comparison of the percent bioaccessibility of curcumin from different organogel-based nanoemulsions and the organogel. Different letters indicate significant difference. (B) Correlation of the percent bioaccessibility with the percentage of curcumin in the total solubilized curcuminoids. Data are presented as mean ± standard deviation (n=3).

Table 10 Percentage of each curcuminoid in the raw material and solubilized after lipolysis of formulations

	Curcumin (%)	D-Cur (%)	BD-Cur (%)
raw material [a]	82.1 ± 1.0	14.8 ± 0.5	3.1 ± 0.5
Organogel [b]	78.4 ± 1.3	16.4 ± 1.0	5.1 ± 0.4
WPI emulsion [c]	65.5 ± 2.3	24.3 ± 1.1	10.2 ± 1.2
Tween 20 emulsion [b]	76.3 ± 1.0	18.0 ± 0.7	5.7 ± 0.3
modified starch emulsion [c]	61.0 ± 1.6	27.0 ± 1.1	12.0 ± 0.5

Different letters indicate significant difference in the percentage of curcumin. Data are presented as mean ± standard deviation (n=3, except for raw material, n=12).

Since the curcumin raw material used in this study contained D-cur and BD-cur, the percentage of each of these three curcuminoids was also determined (Table 10). In the raw material, curcumin accounted for 82% of total curcuminoids, which was higher than that in all the digested formulations. Following the same trend as the *in vitro* bioaccessibility, the percentage of curcumin for organogel was similar to that for the Tween 20 emulsions, but higher than WPI and modified starch emulsions (One-way ANOVA). It was also noticeable that *in vitro* bioaccessibility correlated positively with the percentage of curcumin among the three curcuminoids (Figure 46B, Pearson Product Moment Correlation, correlation coefficient 0.984, P Value 0.0164). High percentage of curcumin corresponded to high *in vitro* bioaccessibility. Previously, it was demonstrated that at weak alkaline conditions, D-cur and BD-cur degraded more slowly than curcumin, leading to decreased curcumin percentage over time (*191*). Considering the *in vitro* lipolysis was performed at pH7.5, it was suggested that different emulsifiers had different protection effect on curcumin during lipolysis, which resulted in different *in vitro* bioaccessibility and curcumin percentage. It was also noticed that the *in vitro* bioaccessibility of curcuminoids in organogel was lower than what was reported previously. The reason may lie in that the curcumin loading in the organogel was increased significantly from about 3% to 9%.

Since Tween 20 was selected as the emulsifier for organogel-based nanoemulsions, the diameter of the organogel particle after emulsification was determined using dynamic light scattering (Figure 47). It was shown that the average particle size (diameter) was 218 nm. The polydispersity was 0.280, suggesting a narrow distribution.

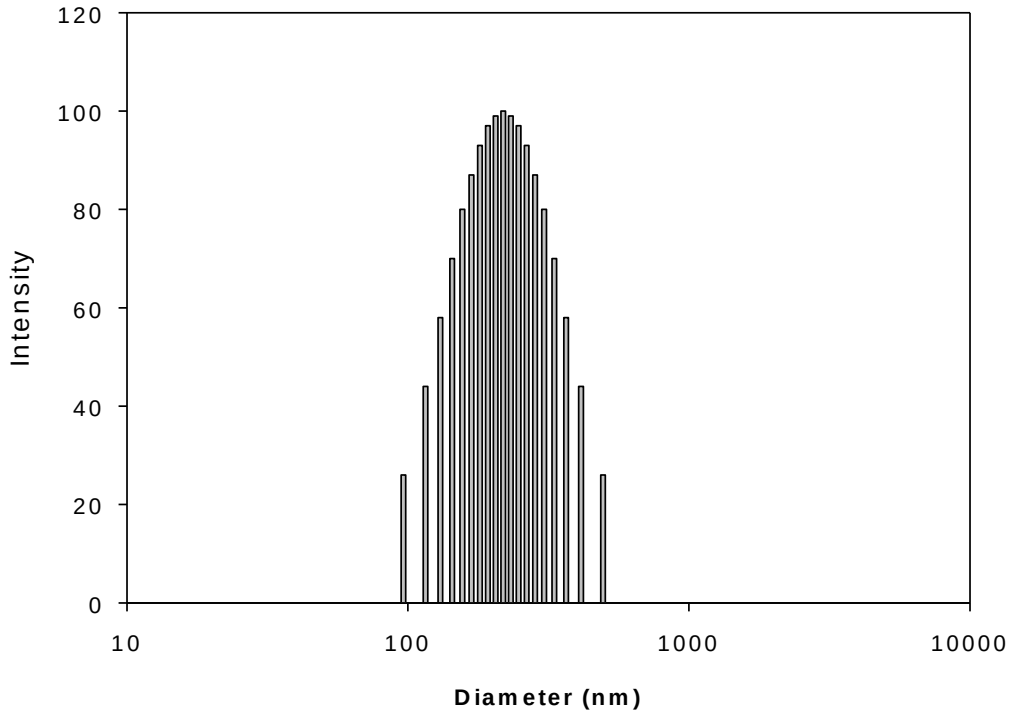

Figure 47 . Particle size distribution of Tween-20 nanoemulsion.

Lipolysis of nanoemulsions was faster and more complete than that of the organogel

In the process to determine the *in vitro* bioaccessibility, the lipolysis titration profile and the extent of lipolysis over time was also recorded. Although Tween 20 nanoemulsion and organogel were able to generate similar *in vitro* bioaccessibility, their lipolysis titration profiles were distinct. As shown in Figure 48A, the initial digestion rate for nanoemulsion was much higher than the organogel. The reason may lie in the difference in surface area of the lipid particles. With smaller droplet size, nanoemulsions have much larger surface area for lipase catalyzed hydrolysis (*192*). Meanwhile, after 30 minutes digestion, the extent of lipolysis for organogel-based nanoemulsion was also significantly greater than the organogel (Figure 48B), suggesting that digestion of nanoemulsions was more complete.

Lipolysis preceded absorption of curcumin in the nanoemulsion

The absorption mechanism for curcumin in the organogel-based nanoemulsion was investigated using Caco-2 cell monolayers to mimic the small intestine epithelium. There are two possible mechanisms for curcumin nanoemulsion absorption: (1) Nanoemulsions are digested by lipase and simultaneously curcumin is solubilized by bile salts-fatty acids mixed micelles. Subsequently, solubilized curcumin permeates across the epithelium layer. This represents the classic digestion-absorption route applicable for all the lipid-based formulations; (2) intact nanoemulsions, because of their small size, are able to directly permeate across the small intestine layer without digestion.

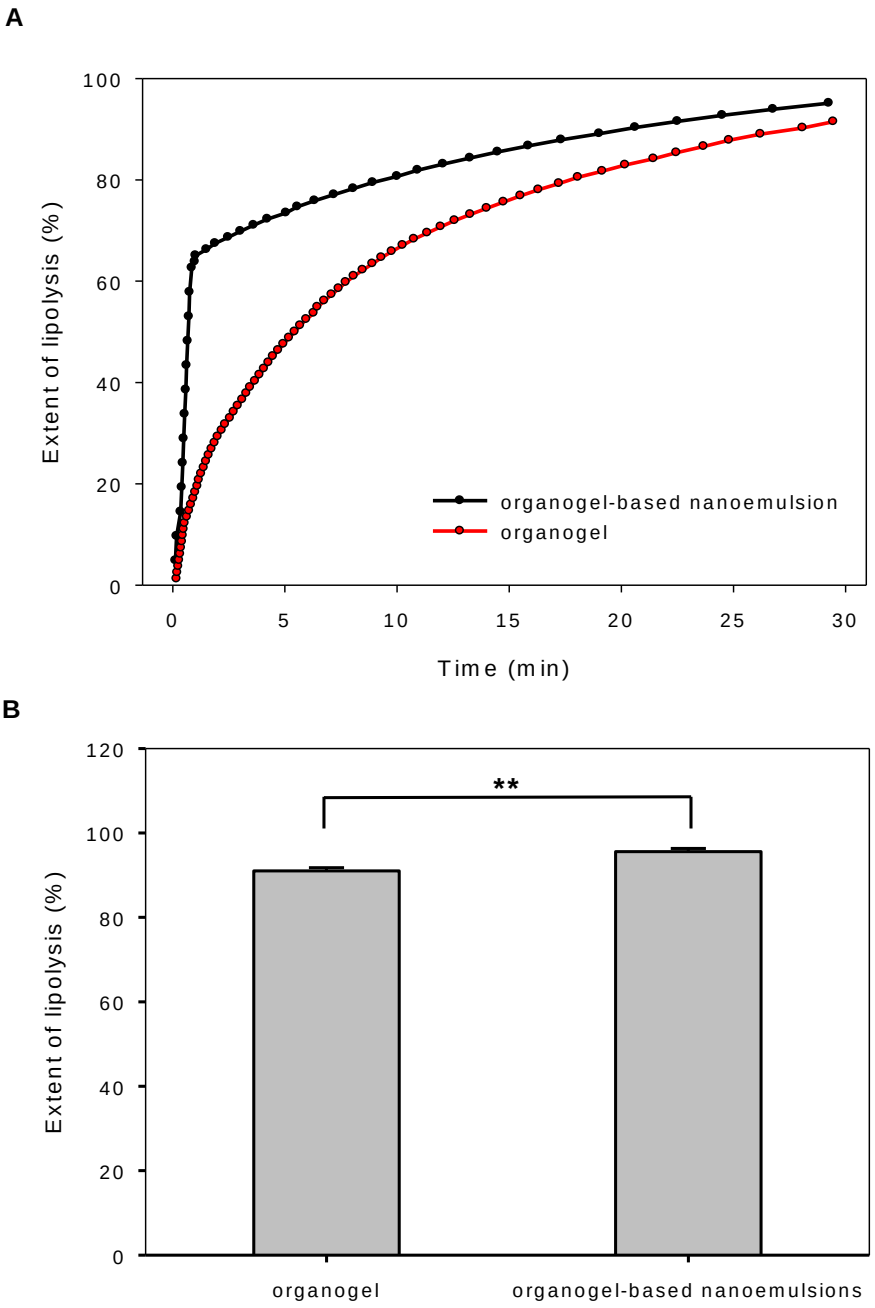

Figure 48 Comparison of the *in vitro* lipolysis of the organogel and organogel-based Tween 20 nanoemulsion, in the aspect of (A) the lipolysis profile and (B) the extent of lipolysis

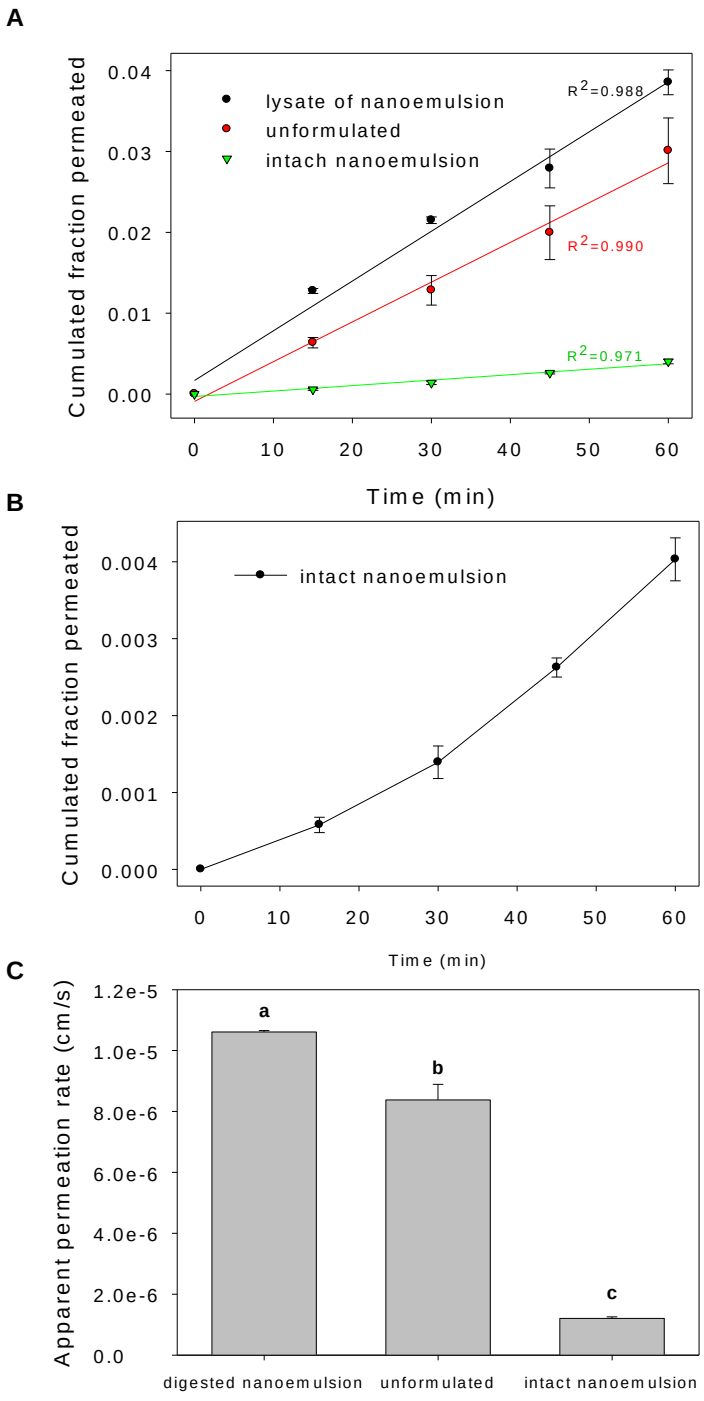

Figure 49 Determination of the curcumin permeation rate in unformulated form, intact nanoemulsion and digested nanoemulsion. (A) The cumulative fractions of curcumin transported from the three formulations. (B) The cumulative fraction of curcumin transported from the intact nanoemulsion only, showing the increasing permeation rate. (C) Comparison of the permeation rate of curcumin from the three formulations

To illustrate the absorption mechanism of curcumin in the organogel-based nanoemulsion, permeation experiments across Caco-2 cell monolayers were performed. The curcumin permeation rates for unformulated curcumin (by DMSO dispersion), intact nanoemulsion and digested nanoemulsion were compared (Figure 49A). It was shown from One-way ANOVA that curcumin from the digested nanoemulsion had the highest permeation rate, followed by unformulated curcumin. In contrast, curcumin in the intact nanoemulsions permeated most slowly. Although these results alone could not exclude the possibility that intact nanoemulsions were able to permeate directly across the Caco-2 cell monolayers, it still suggested that the major absorption mechanism for curcumin nanoemulsion was the digestion-absorption route. Furthermore, to closely look at the permeation curve for curcumin from the intact nanoemulsion, the slope of the curve increased as a function of time (Figure 49B) and the TEER value did not change significantly (not shown), suggesting that the available curcumin in the donor compartment increased over time, which may result from the release of curcumin from the lipid phase of the nanoemulsion to the aqueous phase. This result further confirmed that digestion-absorption was the major mechanism for curcumin absorption from nanoemulsions. Before its absorption, curcumin may need to be solubilized in the aqueous phase, either by digestion of the lipid phase or diffusion from the nanoemulsion.

The permeation rate for unformulated curcumin was determined as $8.4 \pm 0.5 \times 10^{-6}$ cm/s in this study, which was similar to what we reported previously ($7.1 \pm 0.7 \times 10^{-6}$ cm/s (*189*), Student's t-test, $p>0.05$).

Improved oral bioavailability of curcumin in nanoemulsions

To directly investigate the oral bioavailability of curcumin in organogel-based nanoemulsion, pharmacokinetics analysis was performed on mice after oral administration with curcumin water suspension or curcumin nanoemulsions. Since no curcumin was detected in the plasma for unformulated curcumin, all the plasma samples were treated with glucuronidase and sulfatase to convert curcumin glucuronide and sulfate back to curcumin before the HPLC quantification. As shown in Figure 50A, the curcumin plasma concentration for the nanoemulsion was apparently higher than that for unformulated curcumin. From the plot of concentrations over time, the C_{max} for unformulated curcumin was only 2.0 ± 1.1 μg/mL, and in contrast the C_{max} for nanoemulsion was 36.7 ± 6.5 μg/mL and was 18-fold higher than that of unformulated curcumin. The $AUC_{0-\infty}$ for unformulated curcumin was 25.8 μg/mL·h, while the $AUC_{0-\infty}$ for curcumin nanoemulsion was 242.3 μg/mL·h, which represented more than 9-fold increase in the oral bioavailability (**Error! Reference source not found.**).

Table 11 Pharmacokinetic parameters of curcumin formulations after oral administration

Formulation	dose (mg/kg)	C_{max}(μg/mL)	T_{max} (h)	$AUC_{0-\infty}$ (μg/mL·h)
free curcumin	240	2.0 ± 1.1	1	25.8
curcumin nanoemulsion	240	36.7 ± 6.5	1	242.3

Data for C_{max} are presented as mean ± SEM (n=4).

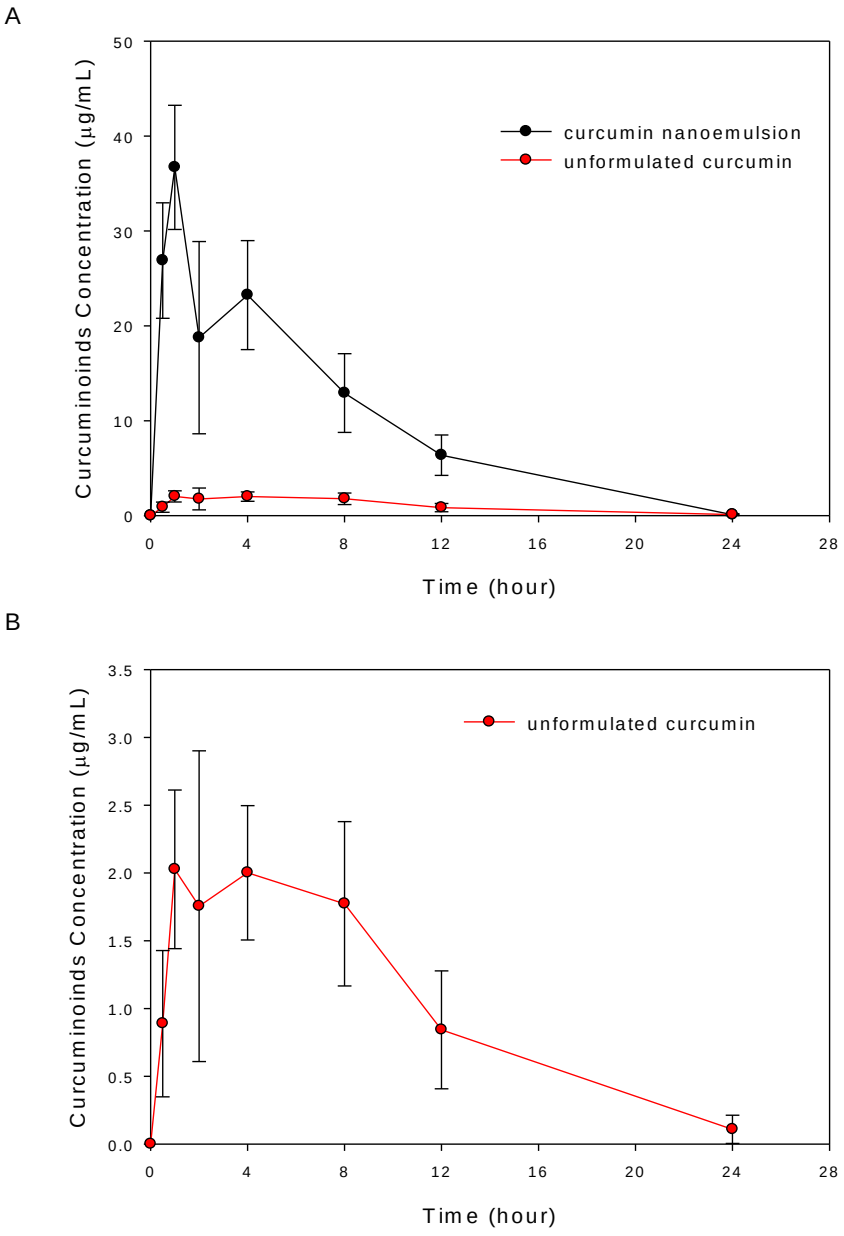

Figure 50 Plasma concentrations of curcumin, after enzyme treatment, from unformulated curcumin and curcumin nanoemulsion. (A) compares the curcumin plasma concentrations from both formulations. (B) shows only the concentration from unformulated curcumin

Discussion

In this work, organogel-based nanoemulsions were developed for encapsulation and oral delivery of curcumin. Tween 20 was selected as the emulsifier based on the *in vitro* bioaccessibility from lipolysis experiments. Using Caco-2 cell monolayers model, it was suggested that digestion-absorption may be the major absorption mechanism for curcumin. Meanwhile, *in vivo* pharmacokinetic analysis confirmed that the oral bioavailability of curcumin in the nanoemulsion increased significantly compared with unformulated curcumin.

Solubilization and metabolism are two main hurdles for the oral bioavailability of curcumin. The organogel-based formulation developed here targeted the solubilization, as the selection of formulation composition was based on *in vitro* bioaccessibility of curcumin after mimicked digestion (*in vitro* lipolysis assay). The effect of formulations on curcumin metabolism needs to be addressed by comparing the ratio of curcumin to its metabolites between oral administration of formulated and unformulated curcumin. However, the plasma concentration of curcumin from unformulated treatment was too low to be detected and we had to enzymatically convert the major curcumin metabolites back to curcumin for bioavailability comparison. Therefore, No conclusions were drawn on the effect of formulation on the curcumin metabolism.

On the other hand, it is not expected that the formulation would affect the curcumin metabolism, especially the first-pass hepatic metabolism. In some scenarios, lipid-based formulation would enable the encapsulated highly lipophilic (clogP > 5) compounds to escape the first-pass metabolism (*139*). Since the clogP value of curcumin is only 3.2 (PubChem, CID969516) and the lipid phase does not consist of long-chain triglyceride, it

is not expected that curcumin delivered using the nanoemulsion will be incorporated in chylomicrons and escape the first-pass metabolism (*139*). Therefore, the increased oral bioavailability from formulation may largely be attributed to the increase in the solubilization.

The absorption mechanism of the nanoemulsion was examined using *in vitro* Caco-2 cell monolayer model. It was demonstrated that the permeation rate of curcumin was significantly higher for the digested nanoemulsion than the intact nanoemulsion, suggesting that the classic digestion-absorption route was still the primary absorption mechanism for curcumin in the nanoemulsion. However, more detailed *in vivo* experiments are needed to examine whether intact nanoemulsions are able to permeate across the gut wall, since only in the *in vivo* experiments the interaction of the nanoemulsion with the mucus layer and the M cells can be examined (*193*).

Meanwhile, this work only examined the permeation rate of Tween 20 stabilized nanoemulsions. Since the coating of the lipid droplet may affect the interaction with Caco2 cells and/or the epithelium lining the digestive tract, the effect of the surface properties of the nanoemulsions on the permeation rate and mechenism still remains elusive.

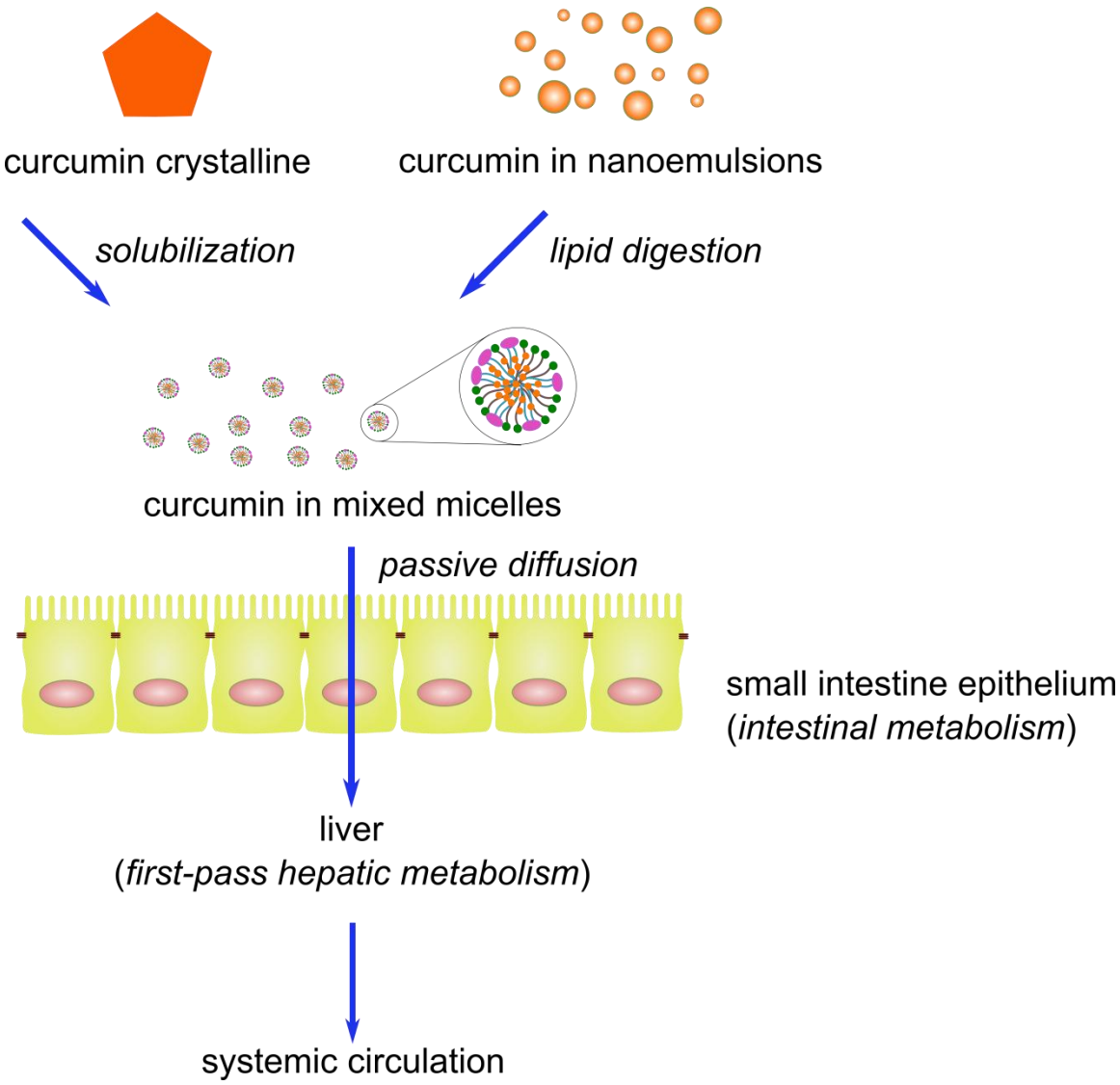

Figure 51 Scheme of the absorption and metabolism of unformulated (crystalline) curcumin and curcumin nanoemulsion. After orally administered, curcumin crystallines are solubilized in the mixed micelle solutions, which may be time and energy consuming. On the other hand, in curcumin nanoemulsion, lipolysis of the lipid phase of the nanoemulsion contributes to the mixed micelles and simultaneously, curcumin is solubilized inside the micelles. By passive diffusion, solubilized curcumin permeates across the small intestine and is carried to the liver before entry into the systemic circulation. Metabolism of curcumin may occur during the absorption in the small intestine (intestinal metabolism) and in the liver (hepatic metabolism).

Based on the results in this work, the *in vivo* destiny of orally administered curcumin nanoemulsion and unformulated curcumin was compared in Figure 51. Inside the digestive tract, nanoemulsions undergo rapid digestion (lipolysis) and turn into free fatty acids and monoacylglycerols, both of which contribute to the mixed micelles in the small intestine lumen. Along with the lipolysis, curcumin that originally solubilized in the lipid phase is gradually partitions in the mixed micelles. Subsequently, curcumin permeates across the small intestine epithelium by passive diffusion. After bypassing the liver, curcumin enters the systemic circulation and become bioavailable. Metabolism of curcumin may involve the intestinal metabolism and hepatic metabolism. In comparison, the absorption and metabolism of unformulated curcumin may be the same as the curcumin nanoemulsion. The key difference is that unformulated curcumin (crystalline) needs to be solubilized in the mixed micelle solution, which may be time and energy consuming. As we previously demonstrated, the extent of solubilization is very limited (*188*). Moreover, the pH of the major portion of the small intestine is neutral and weak alkaline, under which, curcumin undergoes rapid degradation (*191*). Therefore, the difference in the curcumin solubilization results in the difference in the oral bioavailability.

Conclusion

In this work, organogel-based nanoemulsions were developed for encapsulation and oral delivery of curcumin. The nanoemulsions revealed fast rate and high extent of digestion. The major absorption mechanism of curcumin in the nanoemulsion may be the classic digestion-absorption. Furthermore, the oral bioavailability of curcumin in the nanoemulsion showed 9-fold improvement from the unformulated crystalline. This study

demonstrated the application of organogel-based nanoemulsions in the oral delivery system for lipophilic compounds, and provided a practical food-grade formulation for curcumin delivery in functional foods.

CHAPTER 8. INVESTIGATION OF THE CYTOTOXICITY OF FOOD-GRADE NANOEMULSIONS ON CACO-2 CELL MONOLAYERS AND HEPG2 CELLS

Generally speaking, food-grade nanoemulsions are oil-in-water emulsions with oil droplet size (diameter) less than 200 nm. Because of this feature, they have better stability, optical transparency and larger surface area. As an emerging delivery system, nanoemulsions have shown to improve the oral bioavailability of hydrophobic bioactives (*77, 194*). As an important application of nanotechnology in food science, nanoemulsions draw many attentions and are expected to have broader application in food science.

On the other hand, the toxicity associated with nanoparticles represents one of the major concerns for nanotechnology. Many nanoparticles, such as carbon nanotubes and metal oxide nanoparticles, have been found toxic *in vivo* (*195-197*). However, to our best knowledge, there are so far no studies addressing the toxicity of food-grade nanoemulsions.

Compared with other types of nanoparticles, food-grade nanoemulsions have many unique features, such as safety of the components, digestibility, and exclusively oral administration. All the components in the nanoemulsions are either generally considered as safe (GRAS) or food additives. The common oil phase, triacylglycerols, and many emulsifiers, such as lecithin, modified starch, and proteins undergo digestion in the gastrointestinal tract. The exposure organs for food-grade nanoemulsions may be limited to the digestive system. Meanwhile, micron-sized emulsions are widely used in food industry and regarded safe.

The small intestine and the liver are two very important organs in the digestive system. During digestion and absorption, nanoemulsions could directly interact with the small intestine epithelium. After absorption in the small intestine, it is possible that intact nanoemulsions could be transported to the liver via portal vein. Therefore, the possible toxicity of nanoemulsions needs to be examined on these two organs.

Human cancer derived cells lines can be used to examine the *in vitro* toxicity (cytotoxicity). Caco-2 cells are derived from human colon cancers. After about 3-weeks' culture, they differentiate to polarize, generate microvilli on the apical side of the cell membrane and form tight junctions between adjacent cells (*198*). Because of these characteristics, Caco-2 cell monolayers are usually used to mimic the small intestine epithelium, and the permeability of bioactives across Caco-2 cell monolayers is used to predict the absorption *in vivo* (*16*). Meanwhile, HepG2 cells are derived from human liver cancer and are commonly used for *in vitro* assessment of the hepatic toxicity (*199, 200*).

In the present study, the possible cytotoxicity of food-grade nanoemulsions were investigated by using two *in vitro* cell culture systems and comparing with micron-sized emulsions with the same composition. To mimic the exposure of the small intestine to the nanoemulsions, Caco-2 cell monolayers were treated with nanoemulsions and the cell membrane leakage and tight junction integrity were examined. To investigate the toxicity on the liver, HepG2 cells were treated with nanoemulsions and micron-sized emulsions and the cell proliferation/viability rate were compared. These studies may provide the first set of evidence for the possible toxicity of food-grade nanoemulsions.

Materials and methods

Materials Medium chain triglyceride (MCT) was provided by Stepan Company (NEOBEE 1053). Modified starch was obtained from National Starch (HiCap 100). Tween 20 was purchased from Fisher Scientific. Whey protein isolate (WPI) was from Davisco Foods Internationals (BiPro).

Dulbecco's Modified Eagle Medium (DMEM), Minimum Essential Medium Eagle (MEM), Hank's Buffered Salt Solution (HBSS), fetal bovine serum (FBS), 100X non-essential amino acids, 100X penicillin and streptomycin and bovine serum albumin (BSA) were all purchased from Fisher Scientific. Transwell permeable polycarbonate inserts (0.4μm) were obtained from Corning.

Preparation of micron-sized and nanoemulsions. Ten gram emulsions consisted of 8.5g dH_2O, 1.0g MCT and 0.5g emulsifiers (modified starch, Tween 20 or WPI) were briefly mixed by magnetic stirring. To prepare micron-sized emulsions, the mixture was homogenized at 6500 rpm for 5 mins with a high speed homogenizer (ULTRA–TURRAX T-25 basic, IKA Works). Nanoemulsions with the same compositions were generated by ultrasonication at about 175W for accumulatively 5 mins.

Measurement of the oil droplet size of emulsions Photographs of diluted micron-sized emulsions and nanoemulsion were taken with Nikon TE-2000U inverted microscope. The surface-averaged diameters of micron-sized emulsions were determined by using ImageJ software to analyze nine photographs. Particle size of nanoemulsions was measured with DLS-based BIC90 plus particle size analyzer equipped with a

Brookhaven BI-9000AT digital correlator (Brookhaven Instrument) at a fixed scattering angle of 90^{o} at ambient temperature.

Maintenance of Caco-2 and HepG2 cell culture Caco-2 cells (passage 35-45) were maintained in DMEM with 10% FBS, 1X non-essential amino acids and 1X penicillin and streptomycin. HepG2 cells (passage 7-17) were cultured in MEM with 10% FBS, 1X penicillin and streptomycin. Cells were incubated at 37^{o}C with 5% CO_2.

Generation and treatment of Caco-2 cell monolayers To generate Caco-2 cell monolayers, 0.5 mL 6×10^{5} cell/mL Caco-2 cells were plated onto the inserts (apical compartment) of 12-well plates. Subsequently, 1.5 mL culture media were added in the lower compartment of each well. Media were changed every two days. Cytotoxicity experiments were performed after 21- 29 days of plating.

Before the experiments, Caco-2 cell monolayers were washed with and kept in HBSS (0.5ml in apical compartment and 1.5ml in basolateral compartment) for 20-30 mins at 37^{o}C before the treatment.

Five microliters micron-sized emulsions or nanoemulsions were directly added in the apical compartment to make 1-100 dilution. Then the Caco-2 cell monolayers were kept in a platform shaker set at 100rpm at 37^{o}C for 2 hours.

Lactate dehydrogenase leakage assay After treatment of Caco-2 cell monolayers with nano- and micron-sized emulsions, 50 uL media from the apical chamber was removed and the lactate dehydrogenase (LDH) leakage was determined using the fluorescence intensity at excitation 560nm and emission 590 nmusing CytoTox-ONE™ Homogeneous Membrane Integrity Assay kit (Promega). One-hundred-time diluted

emulsions in HBSS were used as the negative control. Cell lysates of the Caco-2 cell monolayers were used as the positive control. Percentage of relative LDH leakage was calculated as:

$$\%\, relative\ LDH\ leakage = \frac{FI\ (treatment) - FI(negative\ control)}{FI(positive\ control) - FI(negative\ control)} \times 100\% \quad \text{.....(1)}$$

Where FI stands for fluorescence intensity with excitation 560nm and emission 590 nm, described in the commercial kit.

Measurement of transepithelial electrical resistance (TEER) Right before the emulsion treatment, the TEER across Caco-2 cell monolayers was measured using the Evom2 epithelial voltmeter (World Precision Instrument). After treatment, Caco-2 cell monolayers were washed with and incubated in HBSS for 20-30 mins, before the post-treatment TEER measurement.

Changes in TEER were expressed as % relative TEER.

$$\%\, relative\ TEER = \frac{post-treatment\ TEER}{pre-treatment\ TEER} \times 100\% \quad \text{.....(2)}$$

MTT assay on HepG2 cells The MTT assay on HepG2 cells were performed as previously published (*172*). Briefly, cells were plated at the density of 1000 cell/well and treated with different dilutions of nanoemulsion or micron-sized emulsions (from 1:100 to 1:1600) for about 24 hours, followed by incubation with MTT and UV-Vis absorption measurement.

Statistics Analysis One-Way and Two-Way analysis of variance (ANOVA) was performed using SigmaPlot 10.0 with SigmaStat integration (Systat software).

Results

In this work, the possible cytotoxicity of nanoemulsions was examined by comparing the cellular response to the treatment of nanoemulsions and micron-sized emulsions, assuming micron-sized emulsions are not toxic.

Generation of micron-sized emulsions and nanoemulsions

To investigate the size effect of food-grade emulsions on the cytotoxicity, three micron-sized emulsions and nanoemulsions with the same compositions were prepared by high speed homogenization and ultrasonication, respectively. Modified starch, Tween 20 and whey protein isolates (WPI) were chosen to represent different types of emulsifiers. As shown in Figure 52 and Table 12, for all the micron-sized emulsions, the particle size (diameter) of the oil droplets was between 5-10 μm. In comparison, the average oil droplet size in the nanoemulsions was less than 200 nm, representing about 50-fold reduction. In Figure 52, the photographs for the nanoemulsions only showed the oil droplets in the "tail" region of the particle size distribution, and the majority of nano-sized oil droplets were not able to be visualized with optical microscopy.

Table 12 Summary of the particle size of prepared nanoemulsions and micron-sized emulsions

	micron-sized emulsion	nanoemulsion	
	$D_{2,0}$ (μm)	diameter (nm)	polydispersity
modified starch	10.3 ± 1.0	155 ± 1.4	0.272 ± 0.002
tween 20	5.7 ± 0.8	168.2 ± 0.7	0.303 ± 0.014
WPI	8.7 ± 0.9	172.7 ± 1.8	0.271 ± 0.009

Data for micron-sized emulsion are presented as mean ± standard deviation, n=9. Data for nanoemulsion are shown as mean ± standard error, n=3.

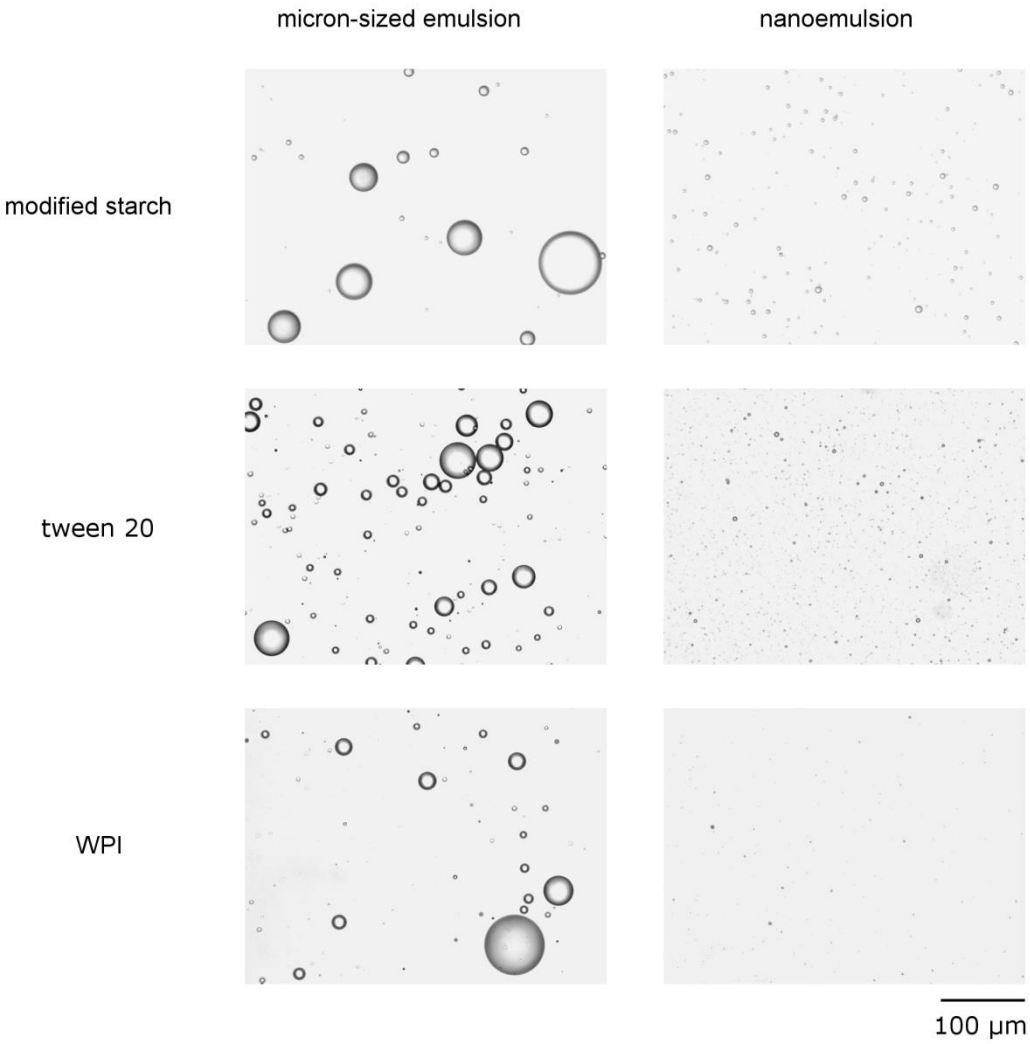

Figure 52 Micrographs of micron-sized emulsions and nanoemulsions made with modified starch, Tween 20 and WPI, respectively

Examination of the cell membrane integrity on Caco-2 cell monolayers

Caco-2 cell monolayers were treated with micron-sized emulsions and nanoemulsions to mimic the exposure of the small intestine epithelium to the emulsions. After treatment, the cell membrane integrity was examined by detecting LDH leakage (Figure 53). For untreated Caco-2 cell monolayers, less than 3% of cells had cell membrane rapture throughout the experiment procedures. For the monolayers treated with nanoemulsions and micron-sized emulsions, there were about 3 – 6 % cells with LDH leakage. From One-Way ANOVA, it was revealed that there was no significant difference in the LDH leakage between untreated cells and most of the emulsion treatment, except for the nanoemulsion made with modified starch. More importantly, no significant difference was detected between all the three pairs of micron-sized emulsions and nanoemulsions, suggesting that nanoemulsions did not possess more cytotoxicity on the Caco-2 cell monolayers than regular micron-sized emulsions.

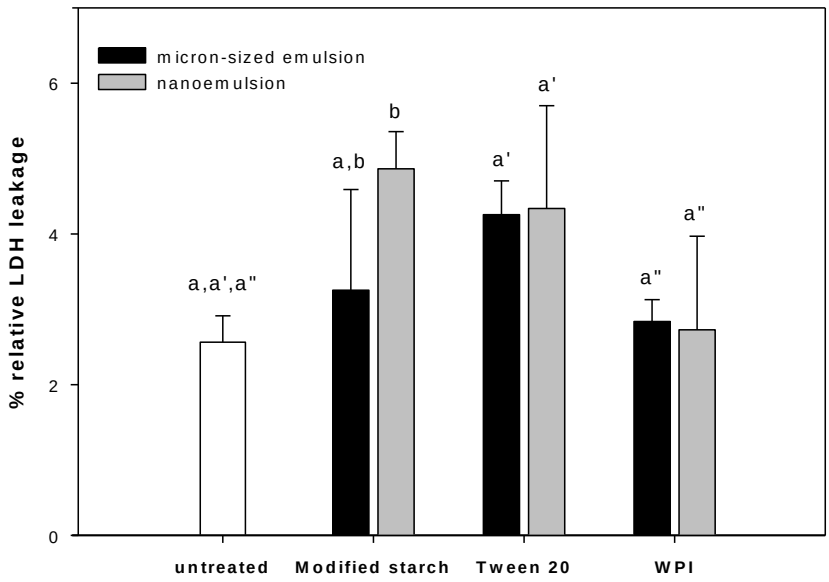

Figure 53 LHD leakage of untreated Caco-2 cell monolayers, or treated with different micron-sized emulsions or nanoemulsions. Data are presented as mean ± standard deviation (n=3). Different letters indicates significant difference ($p<0.05$).

Investigation of the tight junction integrity in the Caco-2 cell monolayers

After well differentiation, tight junctions form between adjacent Caco-2 cells, similar to that in the small intestine epithelium. Disruption of the tight junction may make the cell monolayer more permeable for water-soluble (toxic) compounds, which should be avoided in normal physiological condition. In this study, the TEER values of Caco-2 cell monolayers treated with nanoemulsions were compared to that with micron-emulsions and untreated. As shown in Figure 54, One-Way ANOVA revealed that compared with no treatment, modified starch and WPI emulsions caused TEER decrease, and that Tween 20 emulsion had no apparent effect on the tight junction integrity. These observations are consistent with other groups' finding that some types of emulsifiers and surfactants may interrupt the tight junctions (*201, 202*). More importantly, comparing the three nanoemulsions with the corresponding micron-sized emulsions respectively, there was no significant difference in terms of the TEER change. With the assumption that regular micron-emulsions are considered safe, nanoemulsions did not display additional disruption on the tight junctions.

Together with the results on the LDH leakage in the previous section, it was illustrated that compared with micron-sized emulsions, no elevated toxicity was detected for nanoemulsions on Caco-2 cell monolayers, suggesting that nanoemulsions may not be toxic to the small intestine epithelium.

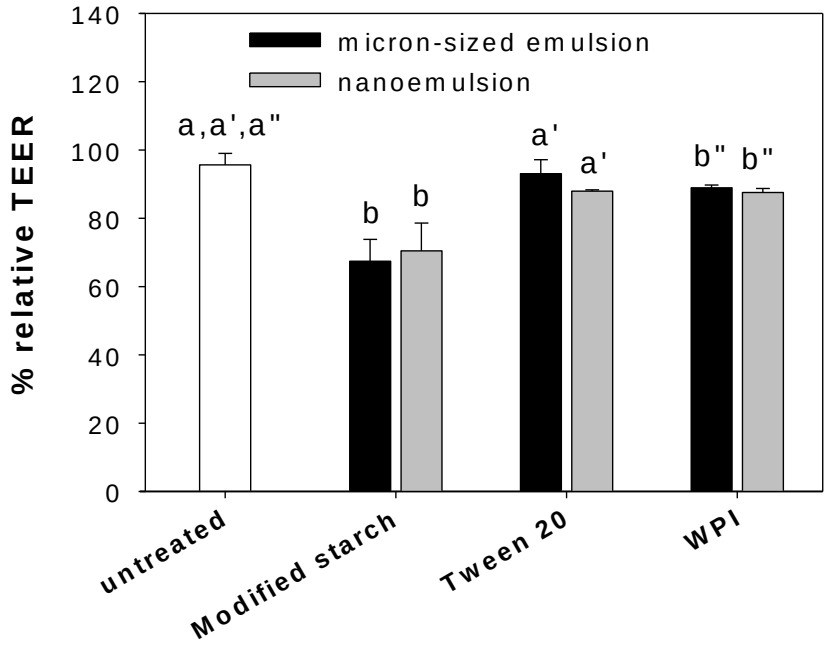

Figure 54 Relative TEER of untreated Caco-2 cell monolayers, or treated with different micron-sized emulsions or nanoemulsions. Data are presented as mean ± standard deviation (n=3). Different letters indicates significant difference ($p<0.05$).

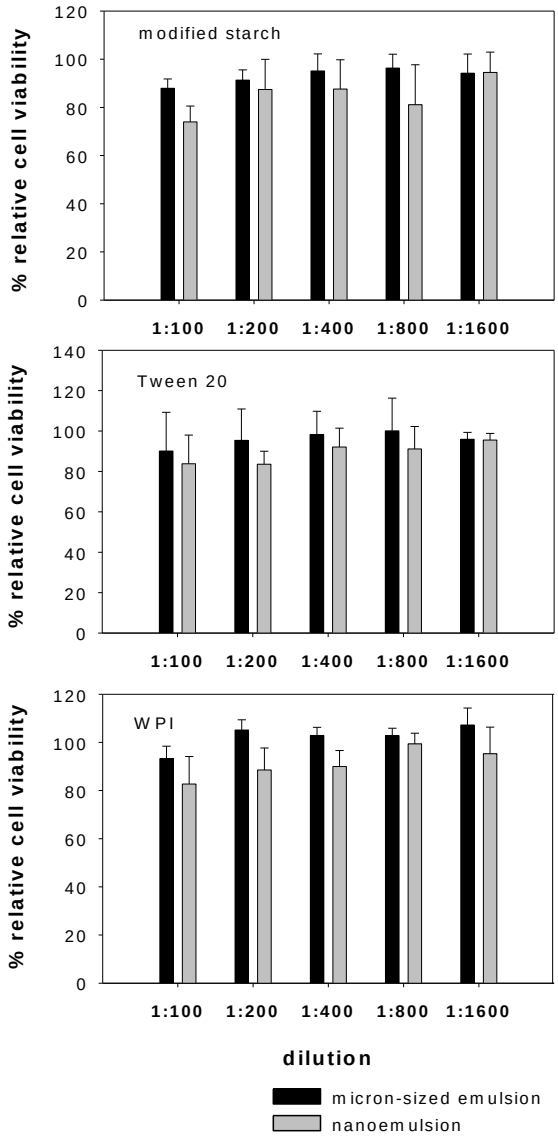

Figure 55 Cytotoxicity of nanoemulsions on HepG2 cells. Data are presented as mean ± standard deviation (n=4).

Examination of the cytotoxicity on HepG2 cells

To examine the possible toxicity of the nanoemulsions on the liver, HepG2 cells were used as a model and treated with micron-sized emulsions and nanoemulsions of different dilutions (Figure 55). From Two-Way ANOVA, it was revealed that nanoemulsions made with modified starch and WPI caused less cell proliferation/viability than the corresponding micron-sized emulsions ($p=0.0105$ and $p=3.21\times10^{-5}$, respectively). On the other hand, Tween 20 nanoemulsion did not affect the cell proliferation/viability more than its micron-sized counterpart ($p=0.231$). These results suggested that different emulsifiers may affect the toxicity of nanoemulsions, and more in vivo studies are required to examine the hepatotoxicity of nanoemulsions.

Discussion

In this work, three nanoemulsions were manufactured and their possible toxicity was examined *in vitro*. It was found that compared with micron-sized emulsions, nanoemulsions did not affect the cell membrane and tight junction integrity of Caco-2 cell monolayers. However, nanoemulsions formed by modified starch and WPI were found to affect the proliferation/viability of HepG2 cells.

The aim of this work was focused on food-grade nanoemulsions. The exposure routes of the nanoemulsions were thus limited to the digestive tract, especially the small intestine considering its large surface area, and possibly the liver, where the digested and absorbed food was carried to for possible metabolism and storage. Based on these considerations, Caco-2 cell monolayers and HepG2 cells were chosen to mimic the small intestine epithelium and the liver hepatocytes, respectively. Meanwhile, micron-sized

emulsions were prepared in parallel and served as the control, since it was generally accepted that regular (micron-sized) emulsions did not bear toxicity to the human body.

In the two experiments on Caco-2 cell monolayers, nanoemulsions did not reveal apparent toxicity on Caco-2 cell monolayers, suggesting that nanoemulsions may not bear significant toxicity to the small intestine. Actually, it was expected that food-grade nanoemulsions undergoes digestion once ingested along other foods and since its very large surface area, it is digested much faster than regular micron-sized emulsions (*192*). In the *in vivo* scenario, only a small portion of intact nanoemulsions may have the chance to interact with the small intestine epithelium directly. This interaction, in the mimicked *in vitro* environment as shown in this study, did not reveal apparent toxicity.

In terms of the hepatic toxicity, it was shown here that modified starch- and WPI-stabilized nanoemulsions affected the proliferation/viability of HepG2 cells, while Tween 20 stabilized nanoemulsions did not reveal significant difference compared with micron-sized emulsions. The reason for this difference in the emulsifiers was still unknown. One hypothesis is that modified starch and WPI are both (modified) biological molecules and may interact with cell membrane through specific receptors while Tween 20 is synthetic and contains multiply polyethylene glycol (PEG) moieties which may prevent/decrease the interaction with cells, as shown in the case of PEGylated proteins and PEGylated quantum dots nanoparticles (*203, 204*). On the other hand, although nanoemulsions formed with modified starch and WPI showed increased cytotoxicity on HepG2 cells, the *in vivo* implication is still unclear, since there is so far no evidence showing that intact food-grade nanoemulsions are able to permeate through the epithelium layers lining the digestive tract and be transported to the liver.

Although in real practice, nanoemulsions are usually used as delivery vehicles for lipophilic compounds, only empty nanoemulsions were used here, considering the possibility that bioactives may act on cells and thus make it hard to interpret the results. To really address the toxicity issue of the nanoemulsion-encapsulated bioactives, *in vivo* experiments are required and the adverse effect caused by increased oral bioavailability of the bioactives should be carefully examined (*205, 206*).

Conclusions

The possible toxicity of food-grade nanoemulsions was examined *in vitro*, using Caco-2 cell monolayers and HepG2 cells to mimic the response of the small intestine epithelium and the liver, respectively. It was found that, compared with micron-sized emulsions with the same compositions, nanoemulsions did not reveal significantly more toxicity on Caco-2 cell monolayers and that nanoemulsions made with modified starch and whey protein isolate affected the proliferation/viability of HepG2 cells. These results suggested that nanoemulsions may not affect the small intestine epithelium and that the hepatic toxicity of nanoemulsions may need further investigation *in vivo*.

SUMMARY AND FUTURE WORK

Nutraceuticals are natural bioactive compounds that have many health-promoting properties. Functional foods with incorporated nutraceuticals provide extra health benefit beyond basic nutrition and represent an emerging trend in food science and industry. However, the oral bioavailability of many nutraceuticals is unfortunately low, leading to insufficient concentrations *in vivo* to perform the bioactivities that usually shown *in vitro*.

My Ph.D. research focuses on the improvement of the oral bioavailability of polyphenols, using curcumin as an example. Curcumin enriched in turmeric has antioxidant, anti-cancer and anti-inflammatory activities. However, its oral bioavailability is low due to water insolubility and rapid metabolism. Using *in vitro* Caco-2 cell monolayers model, I demonstrated that permeation of solubilized curcumin is fast and via passive diffusion, suggesting that solubilization limits its absorption. Subsequently, my effort was put onto solubilization of curcumin through food-grade formulations using nanotechnology. On one hand, biopolymer-based micelles were generated from modified starch and self-synthesized modified epsilon polylysine. Upon encapsulation, the water solubility of curcumin was greatly increased and curcumin was stabilized against alkaline degradation. Moreover, the *in vitro* anti-cancer and cellular antioxidant activities of curcumin were also enhanced. On the other hand, I developed food-grade curcumin organogel with high loading and *in vitro* bioaccessibility. Furthermore, based on the organogel, nanoemulsions were generated and revealed increased digestion rate , extent of digestion, and improved oral bioavailability on mice. Additionally, to illuminate the mechanism of the nanoemulsion absorption, my *in vitro* results suggested that the major mechanism may still be the classic digestion, solubilization and permeation, not direct

uptake/permeation of intact nanoemulsions. Moreover, the toxicity of nanoemulsions was examined *in vitro*. Three tested nanoemulsions did not show significant toxicity on Caco-2 cell monolayers, which suggested that nanoemulsions may not affect the integrity of the small intestine epithelium.

The exploration of science is endless. Many aspects of this study still need to be further investigated. For the newly synthesized MEPL, its toxicity is still elusive. The application in emulsification is not yet fully investigated. M-EPL with high degree of substitution may need to be examined further since it may have much lower CAC.

The organogel system may need to be further optimized in terms of organogelator and the process of making emulsions. After the emulsion is prepared, the nanoscale structure of the organogel needs to be investigated more.

Probably, the toxicity caused by the nanoemulsion formulation is the most important question that remains to be addressed. The increased concentration, altered metabolism of phytochemicals in the body and the nanoscale formulations themselves may all likely cause toxicity to human body, and need to be carefully examined.

REFERENCE

1. He, J.; Liu, J.; Zhang, G., Slowly Digestible Waxy Maize Starch Prepared by Octenyl Succinic Anhydride Esterification and Heat-Moisture Treatment: Glycemic Response and Mechanism. *Biomacromolecules* **2008,** 9, (1), 175-184.
2. *Functional Foods: Opportunities and Challenges*; Institute of Food Technologiests: 2005.
3. *Report on Functional Foods*; Food Quality and Standards Services, Food and Agriculture Organization of the United Nations: 2007.
4. Cui, J.; Yu, B.; Zhao, Y.; Zhu, W. W.; Li, H. L.; Lou, H. X.; Zhai, G. X., Enhancement of oral absorption of curcumin by self-microemulsifying drug delivery systems. *International Journal of Pharmaceutics* **2009,** 371, (1-2), 148-155.
5. Corson, T. W.; Crews, C. M., Molecular Understanding and Modern Application of Traditional Medicines: Triumphs and Trials. **2007,** 130, (5), 769-774.
6. Halliwell, B.; Rafter, J.; Jenner, A., Health promotion by flavonoids, tocopherols, tocotrienols, and other phenols: direct or indirect effects? Antioxidant or not? *Am J Clin Nutr* **2005,** 81, (1), 268S-276.
7. Howitz, K. T.; Sinclair, D. A., Xenohormesis: Sensing the chemical cues of other species. *Cell* **2008,** 133, (3), 387-391.
8. Jambhekar, S. S.; Breen, P. J., *Basic Pharmacokinetics*. Pharmaceutical Press: 2009.
9. The Merck Manual Online. http://www.merck.com/mmpe/sec20/ch303/ch303c.html (April 5),
10. Widmainer, E.; Raff, H.; Strang, K., *Vander's Human Physiology: The Mechanism of Body Function*. 11 ed.; McGraw-Hill: 2007.
11. Porter, C. J. H.; Charman, W. N., Intestinal lymphatic drug transport: an update. *Advanced Drug Delivery Reviews* **2001,** 50, (1-2), 61-80.
12. Atal, C. K.; Dubey, R. K.; Singh, J., Biochemical basis of enhanced drug bioavailability by piperine: evidence that piperine is a potent inhibitor of drug metabolism. *Journal of Pharmacology and Experimental Therapeutics* **1985,** 232, (1), 258-262.
13. Bhardwaj, R. K.; Glaeser, H.; Becquemont, L.; Klotz, U.; Gupta, S. K.; Fromm, M. F., Piperine, a Major Constituent of Black Pepper, Inhibits Human P-glycoprotein and CYP3A4. *Journal of Pharmacology and Experimental Therapeutics* **2002,** 302, (2), 645-650.
14. Wacher, V. J.; Salphati, L.; Benet, L. Z., Active secretion and enterocytic drug metabolism barriers to drug absorption. *Advanced Drug Delivery Reviews* **2001,** 46, (1-3), 89-102.
15. Artursson, P.; Palm, K.; Luthman, K., Caco-2 monolayers in experimental and theoretical predictions of drug transport. *Advanced Drug Delivery Reviews* **2001,** 46, (1-3), 27-43.
16. Hubatsch, I.; Ragnarsson, E. G. E.; Artursson, P., Determination of drug permeability and prediction of drug absorption in Caco-2 monolayers. *Nat. Protocols* **2007,** 2, (9), 2111-2119.

17. Stenberg, P.; Norinder, U.; Luthman, K.; Artursson, P., Experimental and Computational Screening Models for the Prediction of Intestinal Drug Absorption. *J. Med. Chem.* **2001,** 44, (12), 1927-1937.
18. Artursson, P.; Karlsson, J., Correlation between oral drug absorption in humans and apparent drug permeability coefficients in human intestinal epithelial (Caco-2) cells. *Biochemical and Biophysical Research Communications* **1991,** 175, (3), 880-885.
19. Aggarwal, B. B.; Sundaram, C.; Malani, N.; Ichikawa, H., CURCUMIN: THE INDIAN SOLID GOLD. In *The Molecular Targets and Therapeutic Uses of Curcumin in Health and Disease*, 2007; pp 1-75.
20. Damodaran, S.; Parkin, K. L.; Fennema, O. R., *Fennema's Food Chemistry*. 4 ed.; CRC Press: 2007.
21. Aggarwal, B. B.; Kumar, A.; Bharti, A. C., Anticancer potential of curcumin: Preclinical and clinical studies. *Anticancer Research* **2003,** 23, (1A), 363-398.
22. Joe, B.; Vijaykumar, M.; Lokesh, B. R., Biological properties of curcumin-cellular and molecular mechanisms of action. *Crit. Rev. Food Sci. Nutr.* **2004,** 44, (2), 97-111.
23. Duvoix, A.; Blasius, R.; Delhalle, S.; Schnekenburger, M.; Morceau, F.; Henry, E.; Dicato, M.; Diederich, M., Chemopreventive and therapeutic effects of curcumin. *Cancer Lett.* **2005,** 223, (2), 181-190.
24. Sharma, R. A.; Gescher, A. J.; Steward, W. P., Curcumin: The story so far. *Eur. J. Cancer* **2005,** 41, (13), 1955-1968.
25. Dahl, T. A.; McGowan, W. M.; Shand, M. A.; Srinivasan, V. S., PHOTOKILLING OF BACTERIA BY THE NATURAL DYE CURCUMIN. *Arch. Microbiol.* **1989,** 151, (2), 183-185.
26. Dempe, J. S.; Scheerle, R. K.; Pfeiffer, E.; Metzler, M., Absorption and metabolism of curcumin In the Caco-2 Millicell (R) system. *Naunyn-Schmiedebergs Arch. Pharmacol.* **2009,** 379, 346.
27. Han, S.; Yang, Y., Antimicrobial activity of wool fabric treated with curcumin. *Dyes and Pigments* **2005,** 64, (2), 157-161.
28. Liang, G.; Yang, S.; Jiang, L.; Zhao, Y.; Shao, L.; Xiao, J.; Ye, F.; Li, Y.; Li, X., Synthesis and Anti-bacterial Properties of Mono-carbonyl Analogues of Curcumin. *Chemical & Pharmaceutical Bulletin* **2008,** 56, (2), 162-167.
29. Lutomski, J.; Kedzia, B.; Debska, W., WIRKUNG DES ATHANOLEXTRAKTES UND AKTIVER SUBSTANZEN AUS CURCUMA LONGA AUF BAKTERIEN UND PILZE. *Effect of an Alcohol Extract an Active Ingredients from Curcuma longa on Bacteria and Fungi* **1974,** 26, (05), 9-19.
30. Mishra, S.; Narain, U.; Mishra, R.; Misra, K., Design, development and synthesis of mixed bioconjugates of piperic acid-glycine, curcumin-glycine/alanine and curcumin-glycine-piperic acid and their antibacterial and antifungal properties. *Bioorganic & Medicinal Chemistry* **2005,** 13, (5), 1477-1486.
31. Rai, D.; Singh, J. K.; Roy, N.; Panda, D., Curcumin inhibits FtsZ assembly: an attractive mechanism for its antibacterial activity. *Biochem J* **2008,** 410, (1), 147-155.
32. Tajbakhsh, S.; Mohammadi, K.; Deilami, I.; Zandi, K.; Fouladvand, M.; Ramedani, E.; Asayesh, G., Antibacterial activity of indium curcumin and indium diacetylcurcumin. *Afr. J. Biotechnol.* **2008,** 7, (21), 3832-3835.

33. Mou-Tuan, H.; Harold, L. N.; Krystyna, F., Inhibitory effects of curcumin on tumorigenesis in mice. *Journal of Cellular Biochemistry* **1997,** 67, (S27), 26-34.
34. Huang, M. T.; Ma, W.; Lu, Y. P.; Chang, R. L.; Fisher, C.; Manchand, P. S.; Newmark, H. L.; Conney, A. H., EFFECTS OF CURCUMIN, DEMETHOXYCURCUMIN, BISDEMETHOXYCURCUMIN AND TETRAHYDROCURCUMIN ON 12-O-TETRADECANOYLPHORBOL-13-ACETATE-INDUCED TUMOR PROMOTION. *Carcinogenesis* **1995,** 16, (10), 2493-2497.
35. Huang, M. T.; Ma, W.; Yen, P.; Xie, J. G.; Han, J.; Frenkel, K.; Grunberger, D.; Conney, A. H., Inhibitory effects of topical application of low doses of curcumin on 12-O-tetradecanoylphorbol-13-acetate-induced tumor promotion and oxidized DNA bases in mouse epidermis. *Carcinogenesis* **1997,** 18, (1), 83-88.
36. Lu, Y.-p.; Chang, R. L.; Lou, Y.-r.; Huang, M.-T.; Newmark, H. L.; Reuhl, K. R.; Conney, A. H., Effect of curcumin on 12-O-tetradecanoylphorbol-13-acetate- and ultraviolet B light-induced expression of c-Jun and c-Fos in JB6 cells and in mouse epidermis. *Carcinogenesis* **1994,** 15, (10), 2363-2370.
37. Huang, M.-T.; Lou, Y.-R.; Ma, W.; Newmark, H. L.; Reuhl, K. R.; Conney, A. H., Inhibitory Effects of Dietary Curcumin on Forestomach, Duodenal, and Colon Carcinogenesis in Mice. *Cancer Res* **1994,** 54, (22), 5841-5847.
38. Mahmoud, N. N.; Carothers, A. M.; Grunberger, D.; Bilinski, R. T.; Churchill, M. R.; Martucci, C.; Newmark, H. L.; Bertagnolli, M. M., Plant phenolics decrease intestinal tumors in an animal model of familial adenomatous polyposis. *Carcinogenesis* **2000,** 21, (5), 921-927.
39. Rao, C. V.; Simi, B.; Reddy, B. S., INHIBITION BY DIETARY CURCUMIN OF AZOXYMETHANE-INDUCED ORNITHINE DECARBOXYLASE, TYROSINE PROTEIN-KINASE, ARACHIDONIC-ACID METABOLISM AND ABERRANT CRYPT FOCI FORMATION IN THE RAT COLON. *Carcinogenesis* **1993,** 14, (11), 2219-2225.
40. Tanaka, T.; Makita, H.; Ohnishi, M.; Hirose, Y.; Wang, A. J.; Mori, H.; Satoh, K.; Hara, A.; Ogawa, H., CHEMOPREVENTION OF 4-NITROQUINOLINE 1-OXIDE-INDUCED ORAL CARCINOGENESIS BY DIETARY CURCUMIN AND HESPERIDIN - COMPARISON WITH THE PROTECTIVE EFFECT OF BETA-CAROTENE. *Cancer Res.* **1994,** 54, (17), 4653-4659.
41. Chuang, S. E.; Kuo, M. L.; Hsu, C. H.; Chen, C. R.; Lin, J. K.; Lai, G. M.; Hsieh, C. Y.; Cheng, A. L., Curcumin-containing diet inhibits diethylnitrosamine-induced murine hepatocarcinogenesis. *Carcinogenesis* **2000,** 21, (2), 331-335.
42. Chan, M. M. Y.; Huang, H. I.; Fenton, M. R.; Fong, D., In vivo inhibition of nitric oxide synthase gene expression by curcumin, a cancer preventive natural product with anti-inflammatory properties. *Biochem. Pharmacol.* **1998,** 55, (12), 1955-1962.
43. Moghaddam, S. J.; Barta, P.; Mirabolfathinejad, S. G.; Ammar-Aouchiche, Z.; Garza, N. T.; Vo, T. T.; Newman, R. A.; Aggarwal, B. B.; Evans, C. M.; Tuvim, M. J.; Lotan, R.; Dickey, B. F., Curcumin inhibits COPD-like airway inflammation and lung cancer progression in mice. *Carcinogenesis* **2009,** 30, (11), 1949-1956.
44. Dance-Barnes, S. T.; Kock, N. D.; Moore, J. E.; Lin, E. Y.; Mosley, L. J.; D'Agostino, R. B.; McCoy, T. P.; Townsend, A. J.; Miller, M. S., Lung tumor promotion by curcumin. *Carcinogenesis* **2009,** 30, (6), 1016-1023.

45. Bachmeier, B. E.; Nerlich, A. G.; Iancu, C. M.; Cilli, M.; Schleicher, E.; Vene, R.; Dell'Eva, R.; Jochum, M.; Albini, A.; Pfeffer, U., The chemopreventive polyphenol Curcumin prevents hematogenous breast cancer metastases in immunodeficient mice. *Cell. Physiol. Biochem.* **2007,** 19, (1-4), 137-152.
46. Huang, M. T.; Lou, Y. R.; Xie, J. G.; Ma, W.; Lu, Y. P.; Yen, P.; Zhu, B. T.; Newmark, H.; Ho, C. T., Effect of dietary curcumin and dibenzoylmethane on formation of 7,12-dimethylbenz[a]anthracene-induced mammary tumors and lymphomas/leukemias in Sencar mice. *Carcinogenesis* **1998,** 19, (9), 1697-1700.
47. Lim, G. P.; Chu, T.; Yang, F. S.; Beech, W.; Frautschy, S. A.; Cole, G. M., The curry spice curcumin reduces oxidative damage and amyloid pathology in an Alzheimer transgenic mouse. *J. Neurosci.* **2001,** 21, (21), 8370-8377.
48. Yang, F. S.; Lim, G. P.; Begum, A. N.; Ubeda, O. J.; Simmons, M. R.; Ambegaokar, S. S.; Chen, P. P.; Kayed, R.; Glabe, C. G.; Frautschy, S. A.; Cole, G. M., Curcumin inhibits formation of amyloid beta oligomers and fibrils, binds plaques, and reduces amyloid in vivo. *J. Biol. Chem.* **2005,** 280, (7), 5892-5901.
49. Cheng, A. L.; Hsu, C. H.; Lin, J. K.; Hsu, M. M.; Ho, Y. F.; Shen, T. S.; Ko, J. Y.; Lin, J. T.; Lin, B. R.; Wu, M. S.; Yu, H. S.; Jee, S. H.; Chen, G. S.; Chen, T. M.; Chen, C. A.; Lai, M. K.; Pu, Y. S.; Pan, M. H.; Wang, Y. J.; Tsai, C. C.; Hsieh, C. Y., Phase I clinical trial of curcumin, a chemopreventive agent, in patients with high-risk or pre-malignant lesions. *Anticancer Res.* **2001,** 21, (4B), 2895-2900.
50. Sharma, R. A.; McLelland, H. R.; Hill, K. A.; Ireson, C. R.; Euden, S. A.; Manson, M. M.; Pirmohamed, M.; Marnett, L. J.; Gescher, A. J.; Steward, W. P., Pharmacodynamic and Pharmacokinetic Study of Oral Curcuma Extract in Patients with Colorectal Cancer. *Clinical Cancer Research* **2001,** 7, (7), 1894-1900.
51. Garcea, G.; Berry, D. P.; Jones, D. J. L.; Singh, R.; Dennison, A. R.; Farmer, P. B.; Sharma, R. A.; Steward, W. P.; Gescher, A. J., Consumption of the Putative Chemopreventive Agent Curcumin by Cancer Patients: Assessment of Curcumin Levels in the Colorectum and their Pharmacodynamic Consequences. *Cancer Epidemiology Biomarkers & Prevention* **2005,** 14, (1), 120-125.
52. Hanai, H.; Iida, T.; Takeuchi, K.; Watanabe, F.; Maruyama, Y.; Andoh, A.; Tsujikawa, T.; Fujiyama, Y.; Mitsuyama, K.; Sata, M.; Yamada, M.; Iwaoka, Y.; Kanke, K.; Hiraishi, H.; Hirayama, K.; Arai, H.; Yoshii, S.; Uchijima, M.; Nagata, T.; Koide, Y., Curcumin Maintenance Therapy for Ulcerative Colitis: Randomized, Multicenter, Double-Blind, Placebo-Controlled Trial. *Clinical Gastroenterology and Hepatology* **2006,** 4, (12), 1502-1506.
53. Dhillon, N.; Wolff, R. A.; Abbruzzese, J. L.; Hong, D. S.; Camacho, L. H.; Li, L.; Braiteh, F. S.; Kurzrock, R., Phase II clinical trial of curcumin in patients with advanced pancreatic cancer. *J Clin Oncol (Meeting Abstracts)* **2006,** 24, (18_suppl), 14151-.
54. Chainani-Wu, N.; Silverman Jr, S.; Reingold, A.; Bostrom, A.; Mc Culloch, C.; Lozada-Nur, F.; Weintraub, J., A randomized, placebo-controlled, double-blind clinical trial of curcuminoids in oral lichen planus. *Phytomedicine* **2007,** 14, (7-8), 437-446.
55. Baum, L. P.; Lam, C. W. K. P.; Cheung, S. K.-K. M.; Kwok, T. M. D.; Lui, V. M.; Tsoh, J. M.; Lam, L. M. D. M.; Leung, V. F.; Hui, E. F.; Ng, C. H.; Woo, J. M. D.; Chiu, H. F. K. F.; Goggins, W. B. S.; Zee, B. C.-Y. P.; Cheng, K. F. M. D.; Fong, C. Y. S. R. N.; Wong, A. B.; Mok, H. B.; Chow, M. S. S. P.; Ho, P. C. P.; Ip, S. P. P.; Ho, C. S. P.; Yu, X. W. P.; Lai, C. Y. L. M.; Chan, M.-H. F.; Szeto, S. F.; Chan, I. H. S. P.; Mok, V.

M. D., Six-Month Randomized, Placebo-Controlled, Double-Blind, Pilot Clinical Trial of Curcumin in Patients With Alzheimer Disease. *Journal of Clinical Psychopharmacology* **2008,** 28, (1), 110-113.
56. Chirio, D.; Gallarate, M.; Trotta, M.; Carlotti, M. E.; Gaudino, E. C.; Cravotto, G., Influence of alpha- and gamma- cyclodextrin lipophilic derivatives on curcumin-loaded SLN. *J. Incl. Phenom. Macrocycl. Chem.* **2009,** 65, (3-4), 391-402.
57. Anand, P.; Kunnumakkara, A. B.; Newman, R. A.; Aggarwal, B. B., Bioavailability of Curcumin: Problems and Promises. *Mol. Pharm.* **2007,** 4, (6), 807-818.
58. Lao, C.; Ruffin, M.; Normolle, D.; Heath, D.; Murray, S.; Bailey, J.; Boggs, M.; Crowell, J.; Rock, C.; Brenner, D., Dose escalation of a curcuminoid formulation. *BMC Complementary and Alternative Medicine* **2006,** 6, (1), 10.
59. Shoba, G.; Joy, D.; Joseph, T.; Majeed, M.; Rajendran, R.; Srinivas, P. S. S. R., Influence of Piperine on the Pharmacokinetics of Curcumin in Animals and Human Volunteers. *Planta Med* **1998,** 64, (04), 353-356.
60. Pan, M.-H.; Huang, T.-M.; Lin, J.-K., Biotransformation of Curcumin Through Reduction and Glucuronidation in Mice. *Drug Metabolism and Disposition* **1999,** 27, (4), 486-494.
61. Aggarwal, B. B.; Sung, B., Pharmacological basis for the role of curcumin in chronic diseases: an age-old spice with modern targets. *Trends in Pharmacological Sciences* **2009,** 30, (2), 85-94.
62. Kaminaga, Y.; Nagatsu, A.; Akiyama, T.; Sugimoto, N.; Yamazaki, T.; Maitani, T.; Mizukami, H., Production of unnatural glucosides of curcumin with drastically enhanced water solubility by cell suspension cultures of Catharanthus roseus. *Febs Letters* **2003,** 555, (2), 311-316.
63. Suresh, D.; Srinivasan, K., Studies on the in vitro absorption of spice principles - Curcumin, capsaicin and piperine in rat intestines. *Food and Chemical Toxicology* **2007,** 45, (8), 1437-1442.
64. Tønnesen, H. H., Solubility, chemical and photochemical stability of curcumin in surfactant solutions. Studies of curcumin and curcuminoids, XXVIII. *Pharmazie* **2002,** 57, (12), 820-4.
65. Iwunze, M. O., Binding and distribution characteristics of curcumin solubilized in CTAB micelle. *J. Mol. Liq.* **2004,** 111, (1-3), 161-165.
66. Pan, C. J.; Tang, J. J.; Weng, Y. J.; Wang, J.; Huang, N., Preparation, characterization and anticoagulation of curcumin-eluting controlled biodegradable coating stents. *Journal of Controlled Release* **2006,** 116, (1), 42-49.
67. Leung, M. H. A.; Colangelo, H.; Kee, T. W., Encapsulation of curcumin in cationic micelles suppresses alkaline hydrolysis. *Langmuir* **2008,** 24, (11), 5672-5675.
68. Lapenna, S.; Bilia, A. R.; Morris, G. A.; Nilsson, M., Novel Artemisinin and Curcumin Micellar Formulations: Drug Solubility Studies by NMR Spectroscopy. *Journal of Pharmaceutical Sciences* **2009,** 98, (10), 3666-3675.
69. Ma, Z. S.; Shayeganpour, A.; Brocks, D. R.; Lavasanifar, A.; Samuel, J., High-performance liquid chromatography analysis of curcumin in rat plasma: application to pharmacokinetics of polymeric micellar formulation of curcumin. *Biomed. Chromatogr.* **2007,** 21, (5), 546-552.
70. Ma, Z. S.; Haddadi, A.; Molavi, O.; Lavasanifar, A.; Lai, R.; Samuel, J., Micelles of poly(ethylene oxide)-b-poly(epsilon-caprolactone) as vehicles for the solubilization,

stabilization, and controlled delivery of curcumin. *J. Biomed. Mater. Res. Part A* **2008,** 86A, (2), 300-310.
71. Sou, K.; Oyajobi, B. O.; Goins, B.; Phillips, W. T.; Tsuchida, E., Characterization and Cytotoxicity of Self-Organized Assemblies of Curcumin and Amphiphatic Poly(ethylene glycol). *J. Biomed. Nanotechnol.* **2009,** 5, (2), 202-208.
72. He, Y.; Huang, Y. B.; Cheng, Y., Structure Evolution of Curcumin Nanoprecipitation from a Micromixer. *Crystal Growth & Design* **2010,** 10, (3), 1021-1024.
73. Onoue, S.; Takahashi, H.; Kawabata, Y.; Seto, Y.; Hatanaka, J.; Timmermann, B.; Yamada, S., Formulation Design and Photochemical Studies on Nanocrystal Solid Dispersion of Curcumin With Improved Oral Bioavailability. *J. Pharm. Sci.* **2010,** 99, (4), 1871-1881.
74. Bisht, S.; Feldmann, G.; Soni, S.; Ravi, R.; Karikar, C.; Maitra, A.; Maitra, A., Polymeric nanoparticle-encapsulated curcumin ("nanocurcumin"): a novel strategy for human cancer therapy. *Journal of Nanobiotechnology* **2007,** 5, (1), 3.
75. Sahu, A.; Bora, U.; Kasoju, N.; Goswami, P., Synthesis of novel biodegradable and self-assembling methoxy poly(ethylene glycol)-palmitate nanocarrier for curcumin delivery to cancer cells. *Acta Biomaterialia* **2008,** 4, (6), 1752-1761.
76. Lin, C. C.; Lin, H. Y.; Chen, H. C.; Yu, M. W.; Lee, M. H., Stability and characterisation of phospholipid-based curcumin-encapsulated microemulsions. *Food Chemistry* **2009,** 116, (4), 923-928.
77. Wang, X. Y.; Jiang, Y.; Wang, Y. W.; Huang, M. T.; Ho, C. T.; Huang, Q. R., Enhancing anti-inflammation activity of curcumin through O/W nanoemulsions. *Food Chemistry* **2008,** 108, (2), 419-424.
78. Ganta, S.; Amiji, M., Coadministration of Paclitaxel and Curcumin in Nanoemulsion Formulations To Overcome Multidrug Resistance in Tumor Cells. *Molecular Pharmaceutics* **2009,** 6, (3), 928-939.
79. Lee, M. H.; Lin, H. Y.; Chen, H. C.; Thomas, J. L., Ultrasound Mediates the Release of Curcumin from Microemulsions. *Langmuir* **2008,** 24, (5), 1707-1713.
80. Sou, K.; Inenaga, S.; Takeoka, S.; Tsuchida, E., Loading of curcumin into macrophages using lipid-based nanoparticles. *International Journal of Pharmaceutics* **2008,** 352, (1-2), 287-293.
81. Tiyaboonchai, W.; Tungpradit, W.; Plianbangchang, P., Formulation and characterization of curcuminoids loaded solid lipid nanoparticles. *International Journal of Pharmaceutics* **2007,** 337, (1-2), 299-306.
82. Yadav, V. R.; Suresh, S.; Devi, K.; Yadav, S., Novel formulation of solid lipid microparticles of curcumin for anti-angiogenic and anti-inflammatory activity for optimization of therapy of inflammatory bowel disease. *J. Pharm. Pharmacol.* **2009,** 61, (3), 311-321.
83. Kunwar, A.; Barik, A.; Pandey, R.; Priyadarsini, K. I., Transport of liposomal and albumin loaded curcumin to living cells: An absorption and fluorescence spectroscopic study. *Biochim. Biophys. Acta-Gen. Subj.* **2006,** 1760, (10), 1513-1520.
84. Mandeville, J. S.; Froehlich, E.; Tajmir-Riahi, H. A., Study of curcumin and genistein interactions with human serum albumin. *Journal of Pharmaceutical and Biomedical Analysis* **2009,** 49, (2), 468-474.

85. Barik, A.; Mishra, B.; Kunwar, A.; Priyadarsini, K. I., Interaction of curcumin with human serum albumin: Thermodynamic properties, fluorescence energy transfer and denaturation effects. *Chem. Phys. Lett.* **2007,** 436, (1-3), 239-243.
86. Reddy, A. C. P.; Sudharshan, E.; Rao, A. G. A.; Lokesh, B. R., Interaction of curcumin with human serum albumin - A spectroscopic study. *Lipids* **1999,** 34, (10), 1025-1029.
87. Sahu, A.; Kasoju, N.; Bora, U., Fluorescence Study of the Curcumin-Casein Micelle Complexation and Its Application as a Drug Nanocarrier to Cancer Cells. *Biomacromolecules* **2008,** 9, (10), 2905-2912.
88. Leung, M. H. M.; Kee, T. W., Effective Stabilization of Curcumin by Association to Plasma Proteins: Human Serum Albumin and Fibrinogen. *Langmuir* **2009,** 25, (10), 5773-5777.
89. Fathima, N. N.; Devi, R. S.; Rekha, K. B.; Dhathathreyan, A., Collagen-curcumin interaction - A physico-chemical study. *Journal of Chemical Sciences* **2009,** 121, (4), 509-514.
90. Sneharani, A. H.; Singh, S. A.; Appu Rao, A. G., Interaction of αS1-Casein with Curcumin and Its Biological Implications. *J. Agric. Food Chem.* **2009,** 57, (21), 10386-10391.
91. Tang, B.; Ma, L.; Wang, H. Y.; Zhang, G. Y., Study on the supramolecular interaction of curcumin and beta-cyclodextrin by spectrophotometry and its analytical application. *J. Agric. Food Chem.* **2002,** 50, (6), 1355-1361.
92. Tomren, M. A.; Masson, M.; Loftsson, T.; Tonnesen, H. H., Studies on curcumin and curcuminoids XXXI. Symmetric and asymmetric curcuminoids: Stability, activity and complexation with cyclodextrin. *International Journal of Pharmaceutics* **2007,** 338, (1-2), 27-34.
93. Kurien, B. T.; Singh, A.; Matsumoto, H.; Scofield, R. H., Improving the solubility and pharmacological efficacy of curcumin by heat treatment. *Assay and Drug Development Technologies* **2007,** 5, (4), 567-576.
94. Tonnesen, H. H.; Masson, M.; Loftsson, T., Studies of curcumin and curcuminoids. XXVII. Cyclodextrin complexation: solubility, chemical and photochemical stability. *International Journal of Pharmaceutics* **2002,** 244, (1-2), 127-135.
95. Hegge, A. B.; Masson, M.; Kristensen, S.; Tonnesen, H. H., Investigation of curcumin-cyclodextrin inclusion complexation in aqueous solutions containing various alcoholic co-solvents and alginates using an UV-VIS titration method. *Pharmazie* **2009,** 64, (6), 382-389.
96. Hegge, A. B.; Schuller, R. B.; Kristensen, S.; Tonnesen, H. H., In vitro release of curcumin from vehicles containing alginate and cyclodextrin. Studies of curcumin and curcuminoides. XXXIII. *Pharmazie* **2008,** 63, (8), 585-592.
97. Began, G.; Sudharshan, E.; Sankar, K. U.; Rao, A. G. A., Interaction of curcumin with phosphatidylcholine: A spectrofluorometric study. *J. Agric. Food Chem.* **1999,** 47, (12), 4992-4997.
98. Maiti, K.; Mukherjee, K.; Gantait, A.; Saha, B. P.; Mukherjee, P. K., Curcumin-phospholipid complex: Preparation, therapeutic evaluation and pharmacokinetic study in rats. *International Journal of Pharmaceutics* **2007,** 330, (1-2), 155-163.

99. Marczylo, T. H.; Verschoyle, R. D.; Cooke, D. N.; Morazzoni, P.; Steward, W. P.; Gescher, A. J., Comparison of systemic availability of curcumin with that of curcumin formulated with phosphatidylcholine. *Cancer Chemotherapy and Pharmacology* **2007,** 60, (2), 171-177.
100. Merrell, J. G.; McLaughlin, S. W.; Tie, L.; Laurencin, C. T.; Chen, A. F.; Nair, L. S., Curcumin-loaded poly(epsilon-caprolactone) nanofibres: Diabetic wound dressing with anti-oxidant and anti-inflammatory properties. *Clinical and Experimental Pharmacology and Physiology* **2009,** 36, (12), 1149-1156.
101. Li, L.; Ahmed, B.; Mehta, K.; Kurzrock, R., Liposomal curcumin with and without oxaliplatin: effects on cell growth, apoptosis, and angiogenesis in colorectal cancer. . *Molecular Cancer Therapeutics* **2007,** 6, (4), 1276–82.
102. Liu, R. H.; Finley, J., Potential Cell Culture Models for Antioxidant Research. *Journal of Agricultural and Food Chemistry* **2005,** 53, (10), 4311-4314.
103. Takahashi, M.; Uechi, S.; Takara, K.; Asikin, Y.; Wada, K., Evaluation of an Oral Carrier System in Rats: Bioavailability and Antioxidant Properties of Liposome-Encapsulated Curcumin. *Journal of Agricultural and Food Chemistry* **2009,** 57, (19), 9141-9146.
104. Thangapazham, R. L.; Puri, A.; Tele, S.; Blumenthal, R.; Maheshwari, R. K., Evaluation of a nanotechnology-based carrier for delivery of curcumin in prostate cancer cells. *Int. J. Oncol.* **2008,** 32, (5), 1119-1123.
105. Anand, P.; Nair, H. B.; Sung, B.; Kunnumakkara, A. B.; Yadav, V. R.; Tekmal, R. R.; Aggarwal, B. B., Design of curcumin-loaded PLGA nanoparticles formulation with enhanced cellular uptake, and increased bioactivity in vitro and superior bioavailability in vivo. *Biochemical Pharmacology* **2010,** 79, (3), 330-338.
106. Costache, A. D.; Sheihet, L.; Zaveri, K.; Knight, D. D.; Kohn, J., Polymer-Drug Interactions in Tyrosine-Derived Triblock Copolymer Nanospheres: A Computational Modeling Approach. *Molecular Pharmaceutics* **2009,** 6, (5), 1620-1627.
107. Mukerjee, A.; Vishwanatha, J. K., Formulation, Characterization and Evaluation of Curcumin-loaded PLGA Nanospheres for Cancer Therapy. *Anticancer Res.* **2009,** 29, (10), 3867-3875.
108. Nam, S. H.; Nam, H. Y.; Joo, J. R.; Back, I. S.; Park, J. S., Curcumin-loaded PLGA nanoparticles coating onto metal stent by electrophoretic deposition techniques. *Bulletin of the Korean Chemical Society* **2007,** 28, (3), 397-402.
109. Prajakta, D.; Ratnesh, J.; Chandan, K.; Suresh, S.; Grace, S.; Meera, V.; Vandana, P., Curcumin Loaded pH-Sensitive Nanoparticles for the Treatment of Colon Cancer. *J. Biomed. Nanotechnol.* **2009,** 5, (5), 445-455.
110. Ratul Kumar, D.; Naresh, K.; Utpal, B., Encapsulation of Curcumin in Alginate-Chitosan-Pluronic Composite Nanoparticles for Delivery to Cancer cells. *Nanomedicine : the official journal of the American Academy of Nanomedicine* **2009**.
111. Salaun, F.; Vroman, I., Curcumin-Loaded Nanocapsules: Formulation and Influence of the Nanoencapsulation Processes Variables on the Physico-Chemical Characteristics of the Particles. *Int. J. Chem. React. Eng.* **2009,** 7, 28.
112. Shaikh, J.; Ankola, D. D.; Beniwal, V.; Singh, D.; Kumar, M., Nanoparticle encapsulation improves oral bioavailability of curcumin by at least 9-fold when compared to curcumin administered with piperine as absorption enhancer. *European Journal of Pharmaceutical Sciences* **2009,** 37, (3-4), 223-230.

113. Suwantong, O.; Opanasopit, P.; Ruktanonchal, U.; Supaphol, P., Electrospun cellulose acetate fiber mats containing curcumin and release characteristic of the herbal substance. *Polymer* **2007,** 48, (26), 7546-7557.
114. Dubey, S. K.; Sharma, A. K.; Narain, U.; Misra, K.; Pati, U., Design, synthesis and characterization of some bioactive conjugates of curcumin with glycine, glutamic acid, valine and demethylenated piperic acid and study of their antimicrobial and antiproliferative properties. *European Journal of Medicinal Chemistry* **2008,** 43, (9), 1837-1846.
115. Safavy, A.; Raisch, K. P.; Mantena, S.; Sanford, L. L.; Sham, S. W.; Krishna, N. R.; Bonner, J. A., Design and Development of Water-Soluble Curcumin Conjugates as Potential Anticancer Agents. *J. Med. Chem.* **2007,** 50, (24), 6284-6288.
116. Shi, W.; Dolai, S.; Rizk, S.; Hussain, A.; Tariq, H.; Averick, S.; L'Amoreaux, W.; El Ldrissi, A.; Banerjee, P.; Raja, K., Synthesis of monofunctional curcumin derivatives, clicked curcumin dimer, and a PAMAM dendrimer curcumin conjugate for therapeutic applications. *Org. Lett.* **2007,** 9, (26), 5461-5464.
117. Evans, A. M., Influence of dietary components on the gastrointestinal metabolism and transport of drugs. *Ther. Drug Monit.* **2000,** 22, (1), 131-136.
118. WalterSack, I.; Klotz, U., Influence of diet and nutritional status on drug metabolism. *Clin. Pharmacokinet.* **1996,** 31, (1), 47-64.
119. Kakkar, V.; Singh, S.; Singla, D.; Kaur, I. P., Exploring solid lipid nanoparticles to enhance the oral bioavailability of curcumin. *Molecular Nutrition & Food Research* **2011,** 55, (3), 495-503.
120. Tsai, Y. M.; Jan, W. C.; Chien, C. F.; Lee, W. C.; Lin, L. C.; Tsai, T. H., Optimised nano-formulation on the bioavailability of hydrophobic polyphenol, curcumin, in freely-moving rats. *Food Chem.* **2011,** 127, (3), 918-925.
121. Shaikh, J.; Bhosale, R.; Singhal, R., Microencapsulation of black pepper oleoresin. *Food Chemistry* **2006,** 94, (1), 105-110.
122. Krishnan, S.; Bhosale, R.; Singhal, R. S., Microencapsulation of cardamom oleoresin: Evaluation of blends of gum arabic, maltodextrin and a modified starch as wall materials. *Carbohydrate Polymers* **2005,** 61, (1), 95-102.
123. Soottitantawat, A.; Bigeard, F.; Yoshii, H.; Furuta, T.; Ohkawara, M.; Linko, P., Influence of emulsion and powder size on the stability of encapsulated d-limonene by spray drying. *Innovative Food Science & Emerging Technologies* **2005,** 6, (1), 107-114.
124. Soottitantawat, A.; Takayama, K.; Okamura, K.; Muranaka, D.; Yoshii, H.; Furuta, T.; Ohkawara, M.; Linko, P., Microencapsulation of l-menthol by spray drying and its release characteristics. *Innovative Food Science & Emerging Technologies* **2005,** 6, (2), 163-170.
125. Xie, Y. L.; Zhou, H. M.; Zhang, Z. R., Effect of relative humidity on retention and stability of vitamin A microencapsulated by spray drying. *Journal of Food Biochemistry* **2007,** 31, (1), 68-80.
126. Shih, I. L.; Shen, M. H.; Van, Y. T., Microbial synthesis of poly(epsilon-lysine) and its various applications. *Bioresour. Technol.* **2006,** 97, (9), 1148-1159.
127. Hirohara, H.; Takehara, M.; Saimura, M.; Masayuki, A.; Miyamoto, M., Biosynthesis of poly(epsilon-L-lysine)s in two newly isolated strains of Streptomyces sp. *Appl. Microbiol. Biotechnol.* **2006,** 73, (2), 321-331.

128. Saimura, M.; Takehara, M.; Mizukami, S.; Kataoka, K.; Hirohara, H., Biosynthesis of nearly monodispersed poly(epsilon-L-lysine) in Streptomyces species. *Biotechnol. Lett.* **2008,** 30, (3), 377-385.
129. Shima, S.; Matsuoka, H.; Iwamoto, T.; Sakai, H., Antimicrobial action of epsilon-poly-L-lysine. *The Journal of Antibiotics* **1984,** 37, (11), 1449-1455.
130. Geornaras, I.; Sofos, J. N., Activity of epsilon-polylysine against Escherichia coli O157 : H7, Salmonella Typhimurium, and Listeria monocytogenes. *J. Food Sci.* **2005,** 70, (9), M404-M408.
131. Neda, K.; Sakurai, T.; Takahashi, M.; Aiuchi, M.; Ohgushi, M., Two-generation reproduction study with teratology test of ?-poly-L-lysine by dietary administration in rats. *Japanese Pharmacology and Therapeutics* **1999,** 27, (7), 28-29.
132. Hiraki, J.; Ichikawa, T.; Ninomiya, S.; Seki, H.; Uohama, K.; Kimura, S.; Yanagimoto, Y.; Barnett, J. W., Use of ADME studies to confirm the safety of epsilon-polylysine as a preservative in food. *Regul. Toxicol. Pharmacol.* **2003,** 37, (2), 328-340.
133. USFDA, Agency Response Letter GRAS Notice No. GRN 000135. In *GRAS Notice No. GRN 000135*, Administration, U. S. F. a. D., Ed. Washington, D.C., 2004.
134. Kido, Y.; Hiramoto, S.; Murao, M.; Horio, Y.; Miyazaki, T.; Kodama, T.; Nakabou, Y., epsilon-Polylysine inhibits pancreatic lipase activity and suppresses postprandial hypertriacylglyceridemia in rats. *J. Nutr.* **2003,** 133, (6), 1887-1891.
135. Ho, Y. T.; Ishizaki, S.; Takaichi, H., Effect of the Maillard reaction on the bactericidal activity of epsilon-polylysine. *Journal of Tokyo University of Fisheries* **1997,** 84, (2), 25-30.
136. Ho, Y. T.; Ishizaki, S.; Tanaka, M., Improving emulsifying activity of epsilon-polylysine by conjugation with dextran through the Maillard reaction. *Food Chem.* **2000,** 68, (4), 449-455.
137. Porter, C. J. H.; Charman, W. N., In vitro assessment of oral lipid based formulations. *Advanced Drug Delivery Reviews* **2001,** 50, (Supplement 1), S127-S147.
138. Porter, C. J. H.; Pouton, C. W.; Cuine, J. F.; Charman, W. N., Enhancing intestinal drug solubilisation using lipid-based delivery systems. *Advanced Drug Delivery Reviews* **2008,** 60, (6), 673-691.
139. Porter, C. J. H.; Trevaskis, N. L.; Charman, W. N., Lipids and lipid-based formulations: optimizing the oral delivery of lipophilic drugs. *Nat. Rev. Drug Discov.* **2007,** 6, (3), 231-248.
140. Trevaskis, N. L.; Charman, W. N.; Porter, C. J. H., Lipid-based delivery systems and intestinal lymphatic drug transport: A mechanistic update. *Advanced Drug Delivery Reviews* **2008,** 60, (6), 702-716.
141. Christopher, J. H. P.; Ann Marie, K.; Agnes, T.-B.; Ben, J. B.; Jacquelyn, M. O. C.; Glenn, A. E.; William, N. C., Use of in vitro lipid digestion data to explain the <I>in vivo</I> performance of triglyceride-based oral lipid formulations of poorly water-soluble drugs: Studies with halofantrine. *Journal of Pharmaceutical Sciences* **2004,** 93, (5), 1110-1121.
142. Dahan, A.; Hoffman, A., Use of a Dynamic in Vitro Lipolysis Model to Rationalize Oral Formulation Development for Poor Water Soluble Drugs: Correlation with in Vivo Data and the Relationship to Intra-Enterocyte Processes in Rats. *Pharmaceutical Research* **2006,** 23, (9), 2165-2174.

143. White, D. A.; Fisk, I. D.; Makkhun, S.; Gray, D. A., In Vitro Assessment of the Bioaccessibility of Tocopherol and Fatty Acids from Sunflower Seed Oil Bodies. *J. Agric. Food Chem.* **2009,** 57, (13), 5720-5726.
144. Christensen, J. 獺.; Schultz, K.; Mollgaard, B.; Kristensen, H. G.; Mullertz, A., Solubilisation of poorly water-soluble drugs during in vitro lipolysis of medium- and long-chain triacylglycerols. *European Journal of Pharmaceutical Sciences* **2004,** 23, (3), 287-296.
145. Reis, P. M.; Raab, T. W.; Chuat, J. Y.; Leser, M. E.; Miller, R.; Watzke, H. J.; Holmberg, K., Influence of Surfactants on Lipase Fat Digestion in a Model Gastro-intestinal System. *Food Biophys.* **2008,** 3, (4), 370-381.
146. Pasquier, B.; Armand, M.; Guillon, F.; Castelain, C.; Borel, P.; Barry, J. L.; Pieroni, G.; Lairon, D., Viscous soluble dietary fibers alter emulsification and lipolysis of triacylglycerols in duodenal medium in vitro. *J. Nutr. Biochem.* **1996,** 7, (5), 293-302.
147. O'Connor, C. J.; Sun, D.; Smith, B. G.; Melton, L. D., Effect of soluble dietary fibers on lipase-catalyzed hydrolysis of tributyrin. *J. Food Sci.* **2003,** 68, (3), 1093-1099.
148. Juhel, C.; Armand, M.; Pafumi, Y.; Rosier, C.; Vandermander, J.; Lairon, D., Green tea extract (AR25 (R)) inhibits lipolysis of triglycerides in gastric and duodenal medium in vitro. *J. Nutr. Biochem.* **2000,** 11, (1), 45-51.
149. Mun, S.; Decker, E. A.; Park, Y.; Weiss, J.; McClements, D. J., Influence of interfacial composition on in vitro digestibility of emulsified lipids: Potential mechanism for chitosan's ability to inhibit fat digestion. *Food Biophys.* **2006,** 1, (1), 21-29.
150. Zhao, C. L.; Winnik, M. A.; Riess, G.; Croucher, M. D., Fluorescence probe techniques used to study micelle formation in water-soluble block copolymers. *Langmuir* **1990,** 6, (2), 514-516.
151. Cao, J.; Jia, L.; Zhou, H. M.; Liu, Y.; Zhong, L. F., Mitochondrial and nuclear DNA damage induced by curcumin in human hepatoma G2 cells. *Toxicol. Sci.* **2006,** 91, (2), 476-483.
152. Bhosale, R.; Singhal, R., Process optimization for the synthesis of octenyl succinyl derivative of waxy corn and amaranth starches. *Carbohydrate Polymers* **2006,** 66, (4), 521-527.
153. Wilhelm, M.; Zhao, C. L.; Wang, Y.; Xu, R.; Winnik, M. A.; Mura, J. L.; Riess, G.; Croucher, M. D., Poly(styrene-ethylene oxide) block copolymer micelle formation in water: a fluorescence probe study. *Macromolecules* **1991,** 24, (5), 1033-1040.
154. Astafieva, I.; Zhong, X. F.; Eisenberg, A., Critical micellization phenomena in block polyelectrolyte solutions. *Macromolecules* **1993,** 26, (26), 7339-7352.
155. Cao, Y.; Shen, X.; Chen, Y.; Guo, J.; Chen, Q.; Jiang, X., pH-Induced Self-Assembly and Capsules of Sodium Alginate. *Biomacromolecules* **2005,** 6, (4), 2189-2196.
156. Hancock, R. E. W. Hancock Laboratory Methods: MIC Determination by microtitre broth dilution method. http://cmdr.ubc.ca/bobh/methods/MICDETERMINATIONBYMICROTITREBROTHDILUTIONMETHOD.htm (May 1, 2009),
157. Mosmann, T., Rapid colorimetric assay for cellular growth and survival: Application to proliferation and cytotoxicity assays. *Journal of Immunological Methods* **1983,** 65, (1-2), 55-63.

158. Yu, H.; Huang, Y.; Huang, Q., Synthesis and Characterization of Novel Antimicrobial Emulsifiers from ε-Polylysine. *J. Agric. Food. Chem.* **2010,** 58, (2), 1290-1295.
159. Bao, J.; Xing, J.; Phillips, D. L.; Corke, H., Physical Properties of Octenyl Succinic Anhydride Modified Rice, Wheat, and Potato Starches. *Journal of Agricultural and Food Chemistry* **2003,** 51, (8), 2283-2287.
160. He, J.; Liu, J.; Zhang, G., Slowly Digestible Waxy Maize Starch Prepared by Octenyl Succinic Anhydride Esterification and Heat−Moisture Treatment: Glycemic Response and Mechanism. *Biomacromolecules* **2008,** 9, (1), 175-184.
161. Liu, Z.; Li, Y.; Cui, F.; Ping, L.; Song, J.; Ravee, Y.; Jin, L.; Xue, Y.; Xu, J.; Li, G.; Wang, Y.; Zheng, Y., Production of Octenyl Succinic Anhydride-Modified Waxy Corn Starch and Its Characterization. *Journal of Agricultural and Food Chemistry* **2008,** 56, (23), 11499-11506.
162. Yang, B. Y.; Ding, Q.; Montgomery, R., Preparation and physical properties of chitin fatty acids esters. *Carbohydrate Research* **2009,** 344, (3), 336-342.
163. Jones, M. C.; Leroux, J. C., Polymeric micelles - a new generation of colloidal drug carriers. *European Journal of Pharmaceutics and Biopharmaceutics* **1999,** 48, (2), 101-111.
164. Mahmud, A.; Xiong, X. B.; Aliabadi, H. M.; Lavasanifar, A., Polymeric micelles for drug targeting. *J. Drug Target.* **2007,** 15, (9), 553-584.
165. Arechabala, B.; Coiffard, C.; Rivalland, P.; Coiffard, L. J. M.; Roeck-Holtzhauer, Y. D., Comparison of cytotoxicity of various surfactants tested on normal human fibroblast cultures using the neutral red test, MTT assay and LDH release. *Journal of Applied Toxicology* **1999,** 19, (3), 163-165.
166. Schipper, N. G. M.; Vårum, K. M.; Artursson, P., Chitosans as Absorption Enhancers for Poorly Absorbable Drugs. 1: Influence of Molecular Weight and Degree of Acetylation on Drug Transport Across Human Intestinal Epithelial (Caco-2) Cells. *Pharm. Res.* **1996,** 13, (11), 1686-1692.
167. Schipper, N. G. M.; Olsson, S.; Hoogstraate, J. A.; deBoer, A. G.; Varum, K. M.; Artursson, P., Chitosans as absorption enhancers for poorly absorbable drugs .2. Mechanism of absorption enhancement. *Pharm. Res.* **1997,** 14, (7), 923-929.
168. Rossi, S.; Ferrari, F.; Bonferoni, M. C.; Caramella, C., Characterization of chitosan hydrochloride-mucin interaction by means of viscosimetric and turbidimetric measurements. *European Journal of Pharmaceutical Sciences* **2000,** 10, (4), 251-257.
169. Thanou, M.; Nihot, M. T.; Jansen, M.; Verhoef, J. C.; Junginger, H. E., Mono-N-carboxymethyl chitosan (MCC), a polyampholytic chitosan derivative, enhances the intestinal absorption of low molecular weight heparin across intestinal epithelia in vitro and in vivo. *Journal of Pharmaceutical Sciences* **2001,** 90, (1), 38-46.
170. Ranaldi, G.; Marigliano, I.; Vespignani, I.; Perozzi, G.; Sambuy, Y., The effect of chitosan and other polycations on tight junction permeability in the human intestinal Caco-2 cell line. *The Journal of Nutritional Biochemistry* **2002,** 13, (3), 157-167.
171. Prego, C.; Torres, D.; Fernandez-Megia, E.; Novoa-Carballal, R.; Qui 駉, E.; Alonso, M. J., Chitosan-PEG nanocapsules as new carriers for oral peptide delivery: Effect of chitosan pegylation degree. *J. Control. Release* **2006,** 111, (3), 299-308.

172. Yu, H.; Huang, Q., Enhanced in vitro anti-cancer activity of curcumin encapsulated in hydrophobically modified starch. *Food Chemistry* **2010,** 119, (2), 669-674.
173. Wolfe, K. L.; Kang, X. M.; He, X. J.; Dong, M.; Zhang, Q. Y.; Liu, R. H., Cellular antioxidant activity of common fruits. *Journal of Agricultural and Food Chemistry* **2008,** 56, (18), 8418-8426.
174. Ilavsky, J.; Jemian, P. R., Irena: tool suite for modeling and analysis of small-angle scattering. *J. Appl. Crystallogr.* **2009,** 42, (2), 347-353.
175. Svergun, D., Determination of the regularization parameter in indirect-transform methods using perceptual criteria. *J. Appl. Crystallogr.* **1992,** 25, (4), 495-503.
176. Huang, Y.; Yu, H.; Guo, L.; Huang, Q., Structure and Self-Assembly Properties of a New Chitosan-Based Amphiphile. *The Journal of Physical Chemistry B* **2010,** 114, (23), 7719-7726.
177. Jones, M.-C.; Leroux, J.-C., Polymeric micelles - a new generation of colloidal drug carriers. *European Journal of Pharmaceutics and Biopharmaceutics* **1999,** 48, (2), 101-111.
178. Peret-Almeida, L.; Cherubino, A. P. F.; Alves, R. J.; Dufoss, L.; Gloria, M. B. A., Separation and determination of the physico-chemical characteristics of curcumin, demethoxycurcumin and bisdemethoxycurcumin. *Food Research International* **2005,** 38, (8-9), 1039-1044.
179. Tonnesen, H. H., Solubility, chemical and photochemical stability of curcumin in surfactant solutions - Studies of curcumin and curcuminolds, XXVIII. *Pharmazie* **2002,** 57, (12), 820-824.
180. Leung, M. H. M.; Colangelo, H.; Kee, T. W., Encapsulation of Curcumin in Cationic Micelles Suppresses Alkaline Hydrolysis. *Langmuir* **2008,** 24, (11), 5672-5675.
181. Wang, Z.; Leung, M. H. M.; Kee, T. W.; English, D. S., The Role of Charge in the Surfactant-Assisted Stabilization of the Natural Product Curcumin. *Langmuir* **2009,** 26, (8), 5520-5526.
182. Wolfe, K. L.; Liu, R. H., Cellular antioxidant activity (CAA) assay for assessing antioxidants, foods, and dietary supplements. *Journal of Agricultural and Food Chemistry* **2007,** 55, (22), 8896-8907.
183. Pernetti, M.; van Malssen, K. F.; Floter, E.; Bot, A., Structuring of edible oils by alternatives to crystalline fat. *Curr. Opin. Colloid Interface Sci.* **2007,** 12, (4-5), 221-231.
184. Sek, L.; Porter, C. J. H.; Charman, W. N., Characterisation and quantification of medium chain and long chain triglycerides and their in vitro digestion products, by HPTLC coupled with in situ densitometric analysis. *Journal of Pharmaceutical and Biomedical Analysis* **2001,** 25, (3-4), 651-661.
185. Yu, H.; Li, J.; Shi, K.; Huang, Q., Structure of Modified ε-Polylysine Micelles and Their Application in Improving Cellular Antioxidant Activity of Curcuminoids. *Food and Function* **2011,** DOI: 10.1039/c1fo10053j.
186. Sek, L.; Porter, C. J. H.; Kaukonen, A. M.; Charman, W. N., Evaluation of the in-vitro digestion profiles of long and medium chain glycerides and the phase behaviour of their lipolytic products. *J. Pharm. Pharmacol.* **2002,** 54, (1), 29-41.
187. Marangoni, A.; Idziak, S.; Rush, J., Controlled Release of Food Lipids Using Monoglyceride Gel Phases Regulates Lipid and Insulin Metabolism in Humans. *Food Biophysics* **2008,** 3, (2), 241-245.

188. Yu, H.; Shi, K.; Liu, D.; Huang, Q., Development of curcumin organogel with high in vitro bioaccessibility and loading of curcumin. *Food Chem* **submitted**.
189. Yu, H.; Huang, Q., Permeation of curcumin through Caco-2 cell monolayers via passive diffusion. *J. Agric. Food Chem.* **(revison submitted)**.
190. Heath, D. D.; Pruitt, M. A.; Brenner, D. E.; Rock, C. L., Curcumin in plasma and urine: quantitation by high-performance liquid chromatography. *J Chromatogr B* **2003,** 783, (1), 287-295.
191. Yu, H.; Li, J.; Shi, K.; Huang, Q., Structure of modified epsilon-polylysine micelles and their application in improving cellular antioxidant activity of curcuminoids. *Food & Function* **2011**.
192. Li, Y.; McClements, D. J., New Mathematical Model for Interpreting pH-Stat Digestion Profiles: Impact of Lipid Droplet Characteristics on in Vitro Digestibility. *J. Agric. Food Chem.* **2010,** 58, (13), 8085-8092.
193. Rabinow, B. E., Nanosuspensions in drug delivery. *Nat Rev Drug Discov* **2004,** 3, (9), 785-796.
194. Hatanaka, J.; Chikamori, H.; Sato, H.; Uchida, S.; Debari, K.; Onoue, S.; Yamada, S., Physicochemical and pharmacological characterization of [alpha]-tocopherol-loaded nano-emulsion system. *International Journal of Pharmaceutics* **2010,** 396, (1-2), 188-193.
195. Bai, Y.; Zhang, Y.; Zhang, J.; Mu, Q.; Zhang, W.; Butch, E. R.; Snyder, S. E.; Yan, B., Repeated administrations of carbon nanotubes in male mice cause reversible testis damage without affecting fertility. *Nat Nano* **2010,** 5, (9), 683-689.
196. Yamashita, K.; Yoshioka, Y.; Higashisaka, K.; Mimura, K.; Morishita, Y.; Nozaki, M.; Yoshida, T.; Ogura, T.; Nabeshi, H.; Nagano, K.; Abe, Y.; Kamada, H.; Monobe, Y.; Imazawa, T.; Aoshima, H.; Shishido, K.; Kawai, Y.; Mayumi, T.; Tsunoda, S.-i.; Itoh, N.; Yoshikawa, T.; Yanagihara, I.; Saito, S.; Tsutsumi, Y., Silica and titanium dioxide nanoparticles cause pregnancy complications in mice. *Nat Nano* **2011,** 6, (5), 321-328.
197. Bhabra, G.; Sood, A.; Fisher, B.; Cartwright, L.; Saunders, M.; Evans, W. H.; Surprenant, A.; Lopez-Castejon, G.; Mann, S.; Davis, S. A.; Hails, L. A.; Ingham, E.; Verkade, P.; Lane, J.; Heesom, K.; Newson, R.; Case, C. P., Nanoparticles can cause DNA damage across a cellular barrier. *Nat Nano* **2009,** 4, (12), 876-883.
198. Hidalgo, I. J.; Raub, T. J.; Borchardt, R. T., Characterization of the human colon carcinoma cell line (Caco-2) as a model system for intestinal epithelial permeability. *Gastroenterology* **1989,** 96, (3), 736-49.
199. Bort, R.; Ponsoda, X.; Jover, R.; Gomez-Lechon, M. J.; Castell, J. V., Diclofenac toxicity to hepatocytes: A role for drug metabolism in cell toxicity. *J. Pharmacol. Exp. Ther.* **1999,** 288, (1), 65-72.
200. Lu, Y. K.; Cederbaum, A. I., Cisplatin-induced hepatotoxicity is enhanced by elevated expression of cytochrome P450 2E1. *Toxicol. Sci.* **2006,** 89, (2), 515-523.
201. Yamashita, S.; Furubayashi, T.; Kataoka, M.; Sakane, T.; Sezaki, H.; Tokuda, H., Optimized conditions for prediction of intestinal drug permeability using Caco-2 cells. *European Journal of Pharmaceutical Sciences* **2000,** 10, (3), 195-204.
202. Ohno, Y.; Naganuma, T.; Ogawa, T.; Muramoto, K., Effect of Lectins on the Transport of Food Factors in Caco-2 Cell Monolayers. *Journal of Agricultural and Food Chemistry* **2006,** 54, (2), 548-553.
203. Clift, M. J. D.; Rothen-Rutishauser, B.; Brown, D. M.; Duffin, R.; Donaldson, K.; Proudfoot, L.; Guy, K.; Stone, V., The impact of different nanoparticle surface chemistry

and size on uptake and toxicity in a murine macrophage cell line. *Toxicology and Applied Pharmacology* **2008,** 232, (3), 418-427.
204. Tsutsumi, Y.; Onda, M.; Nagata, S.; Lee, B.; Kreitman, R. J.; Pastan, I., Site-specific chemical modification with polyethylene glycol of recombinant immunotoxin anti-Tac(Fv)-PE38 (LMB-2) improves antitumor activity and reduces animal toxicity and immunogenicity. *Proceedings of the National Academy of Sciences* **2000,** 97, (15), 8548-8553.
205. Huang, Q.; Yu, H.; Ru, Q., Bioavailability and Delivery of Nutraceuticals Using Nanotechnology. *Journal of Food Science* **2010,** 75, (1), R50-R57.
206. McClements, D. J.; Rao, J., Food-Grade Nanoemulsions: Formulation, Fabrication, Properties, Performance, Biological Fate, and Potential Toxicity. *Crit. Rev. Food Sci. Nutr.* **2011,** 51, (4), 285-330.

CURRICULUM VITA
Hailong Yu

EDUCATION

Ph.D. Food Science, Rutgers, the State University of New Jersey (May 2012)
M.S. Molecular Genetics, Microbiology and Immunology, University of Medicine and Dentistry of New Jersey and Rutgers, the State University of New Jersey (December 2008)
B.S. Biotechnology, Nanjing University, China (June 2004)

PUBLICATION

1. **Yu, H**.; Huang, Q. Investigation of the Absorption Mechanism of Solubilized Curcumin using Caco-2 Cell Monolayers. Journal of Agriculture and Food Chemistry 2011, 59 (17), 9120–9126

2. **Yu, H**.; Li, J.; Shi, K.; Huang, Q. Structure of modified ε-polylysine micelles and their application in improving cellular antioxidant activity of curcuminoids. Food and Function 2011, **2**, 373-380

3. **Yu, H**.; Shi, K.; Liu, D.; Huang, Q. Development of a food-grade organogel with high bioaccessibility and loading of curcuminoids. Food Chemistry 2012 131 (1), 48–54

4. Shi, K., Huang, Y., **Yu, H**., Lee, T-C.; Huang, Q. Reducing the brittleness of zein films through chemical modification. Journal of Agriculture and Food Chemistry, 2011, 59 (1), 56–61

5. Ru, Q., **Yu, H**., Huang, Q. Encapsulation of epigallocatechin-3-gallate (EGCG) using O/W sub-micrometer emulsions stabilized by ι-carrageenan and β-lactoglobulin. Journal of Agriculture and Food Chemistry, 2010, 58(19), 10373-81.

6. Huang, Y., **Yu, H**., Guo L., and Huang Q. Structure and Self-Assembly Properties of a New Chitosan-Based Amphiphile. Journal of Physical Chemistry B, 2010, 114 (23), 7719–7726.

7. **Yu, H**., Huang, Y.; Huang, Q. Synthesis and Characterization of Novel Antimicrobial Emulsifiers from ε-Polylysine. Journal of Agriculture and Food Chemistry, 2010, 58 (2), 1290–1295.

8. **Yu, H**., Huang Q. Enhanced in vitro anti-cancer activity of curcumin encapsulated in hydrophobically modified starch. Food Chemistry, 2010, 119, 669-674.

9. Huang, Q., **Yu, H**., and Ru, Q. Bioavailability and Delivery of Nutraceuticals using Nanotechnology. Journal of Food Science, 2010, 75, (1), R50-R57.

10. Kuo Y., Wang Q., Ruengruglikit C., **Yu H**., Huang Q. Antibody-Conjugated CdTe quantum dots for Escherichia coli detection. Journal of Physical Chemistry C. 2008, 112, 4818–4824

11. Wang, X., Kruithof-de Julio M., Economides, K.D.,Walker D., **Yu, H**., Halili, V.M., Hu Y.-P., Price S.M., Abate-Shen, C., Shen, M.M. A luminal epithelial stem cell that is a cell of origin for prostate cancer. Nature, 2009, 461, 495-500

CONFERENCE PRESENTATION

1. **Yu, H**.; Liu, D; Huang, Q. In vitro lipolysis of curcumin in basic lipid-based formulations. Institute of Food Technologists annual meeting, New Orleans, LA, 2011

2. **Yu, H**.; Huang, Q. Improvement of the oral bioavailability of curcumin using polymer micelle- and lipid-based delivery systems. Poster presentation, 241th American Chemical Society national meeting, Anaheim, California, 2011

3. **Yu, H**.; Huang, Q. Encapsulation of curcumin in micelles formed by hydrophobically modified epsilon polylysine. Poster presentation, Institute of Food Technologists annual meeting, Chicago, IL., 2010

4. **Yu, H**.; Huang, Y., and Huang, Q. Synthesis and characterization of hydrophobically modified epsilon polylysine. Oral presentation, 238th American Chemistry Society national meeting, Washington D.C., 2009

5. **Yu, H**., Huang Q. Enhanced in vitro anti-cancer activity of curcumin encapsulated in hydrophobically modified starch. Poster Competition of Institute of Food Technologists, New York Section, New Brunswick, NJ, 2009

6. **Yu, H** .; Leng, Y.; Lee, T.C.; Huang, Q. Physicochemical conditions for optimum activity of extracellular ice nucleating proteins from *Erwinia herbicola.* Poster Competition of Institute of Food Technology, New York Section, New Brunswick, NJ, 2008

7. **Yu, H**.; Huang, Q. Increasing curcumin water solubility by chemically modified starch. Oral Presentation, 236th American Chemistry Society national meeting, Philadelphia, PA, 2008

EMPLOYMENT

Laboratory Instructor, General Biology Laboratory, Rutgers University, 09/2009 – 05/2012

Associate Scientist GenScript Corporation, Piscataway, NJ 05/2008 - 12/2008